Role of Endothelin-1 in the Brown Adipose Tissue

Dissertation zur

Erlangung des Doktorgrades (Dr. rer. nat.)

der

Mathematisch-Naturwissenschaftlichen Fakultät

der

Rheinischen Friedrich-Wilhelms-Universität Bonn

vorgelegt von

Stefan Michael Jan Löffler geb. Juhas

aus

München

Bonn 2021

Angefertigt mit der Genehmigung der Mathematisch-Naturwissenschaftlichen Fakultät der Rheinischen Friedrich-Wilhelms-Universität Bonn

1. Gutachter: Prof. Dr. Alexander Pfeifer

2. Gutachter: Prof. Dr. Günther Weindl

Tag der Promotion: 21.05.2021

Erscheinungsjahr: 2021

Acknowledgements

I am grateful to Prof. Pfeifer and Dr. Hildebrand for supervision and guidance throughout the projects. Many thanks to Dr. Gnad and Dr. Reverte-Salisia for kindly providing tissue samples of acutely cold exposed mice and the Epac-KO cell line. I would like to extend my warmest thanks to Ms. Lamby and Mr. Niu for extensive help with animal experiments, without whom continued execution of experiments during the Covid-19 pandemic would not have been possible. Similarly, Ms. Yang, Ms. Niemann and Ms. Zurkovic kindly provided help with animal experimentation at crucial time-points during the project for which I am very grateful. I would further like to thank, Dr. Copperi and Mr. Freyter, Dr. de Coninck, Dr. Malfacini, Mr. Mikhael, Dr. Garg, Dr. Götz-Miroschnikow, Dr. Hildebrand and Dr. Sanyal, for fruitful discussions and experimental expertise.

Table of Contents

Abbreviations

ActD	Actinomycin D
ANCOVA	Analysis of co-variance
ANOVA	Analysis of variance
AREs	Adenine and uracil-rich elements
AT	Adipose tissue
AT-MEC	Adipose tissue derived microvascular endothelial cells
BA	Brown adipocytes
BAPTA AM	acetyloxymethyl 2-[N-[2-(acetyloxymethoxy)-2-oxoethyl]-2-[2-[2-[bis[2-(acetyloxymethoxy)-2-oxoethyl]amino] phenoxy]ethoxy]anilino]acetate
BAT	Brown adipose tissue
BSA	Bovine serum albumin
cAMP	cyclic adenosine monophosphate
cDNA	Complementary deoxyribonucleic acid
DAPI	4',6-Diamidino-2-Phenylindole
DETA-NONOate	3,3-Bis(2-aminoethyl)-1-hydroxy-1-triazene 2-oxide
DIO	Diet-induced obesity
DMEM	Dulbecco's Modified Eagle Medium
DMSO	Dimethyl sulfoxide
EC	Endothelial cell
ECE	Endothelin converting enzyme
Ednra	Endothelin-1 Receptor A gene symbol
Ednrb	Endothelin-1 Receptor B gene symbol
Edn1	Endothelin-1 gene symbol

ETA	Endothelin-1 Receptor A
ETB	Endothelin-1 Receptor B
ET-1	Endothelin-1
Epac	Exchange factor directly activated by cAMP 1
FACS	Fluorescence-activated cell sorting
HDAC	Histone deacetylase
HFD	High fat diet
Hif-1	Hypoxia inducible factor-1
Hprt	Hypoxanthine-guanine phosphoribosyltransferase
HRP	horseradish peroxidase
HuR	Human antigen R
H89	*N*-[2-[[3-(4-Bromophenyl)-2-propenyl]amino]ethyl]-5-isoquinolinesulfonamide
KO	Knock-out
L-NAME	NG-Nitro-L-arginine methyl ester
MACS	Magnetic-activated cell sorting
NE	Norepinephrine
NO	Nitric oxide
NOS	Nitric oxide synthase
PFA	Para formaldehyde
PKA	Protein kinase A
Pparγ	Peroxisome proliferator-activated receptor gamma
preBA	Brown adipocyte precursor
RT	Room temperature
RT-qPCR	Real-time quantitative polymerase chain reaction

SVF	Stromal vascular fraction
TSA	Trichostatin A
TTP	Tristetraprolin
Ucp1	Uncoupling protein 1 gene symbol
UCP1	Uncoupling protein 1
WA	White adipocytes
WAT	White adipose tissue
WATi	Inguinal white adipose tissue
WATg	Gonadal white adipose tissue
WT	Wildtype
8Br-cAMP	8-Bromoadenosine 3',5'-cyclic monophosphate

1 | Introduction

1.1 | Microvasculature in the adipose tissue

There are different types of adipose tissue (AT). White adipose tissue (WAT) is composed of single lipid bearing white adipocytes (WA). Their function is to store excess energy in form of triglycerides. This tissue-type can be further characterized by its localization: In humans, one may distinguish subcutaneous and visceral fat, whereas in rodents inguinal (WATi) and perigonadal fat tissue (WATg) exist.

In contrast to WAT, brown adipose tissue (BAT) does not store, but dissipates energy in the form of heat. Its brown color is derived from the high content of mitochondria which have iron-containing cytochrome molecules. Initially it was thought to be present in newborns and hibernating mammals only (as reviewed by Lee et al., 2013).Within the last 10 years it became clear that functional BAT is retained beyond infancy (Virtanen et al., 2009) and – given targeted pharmacological stimulation – could prove a novel approach in the treatment regime of obesity (Kuryłowicz & Puzianowska-Kuźnicka, 2020; Lee et al., 2013; Lidell et al., 2014; Trayhurn, 2018; Q. A. Wang et al., 2014).

Besides classical BAT and WAT another type of AT is described. This tissue type emerges within WAT but exhibits BAT-like features, such as elevated mitochondria content and heat-dissipation. Cold-exposure and adrenergic innervation are factors which trigger the formation of cells with BAT-like features in white (brite). These emerging cells are called beige cells and the process of their formation in WAT is called browning (reviewed by Pfeifer & Hoffmann, 2015).

AT browning is accompanied by an increase in blood vessel networks (Lim et al., 2012). In general, blood vessels have different shapes and sizes and thus have different functionality. Macrovascular vessels have a large diameter and contain an encircling ring of smooth vasculature to control its tone, while microvascular vessels are very small, sometimes do not have a smooth vascular ring and provide nutrients rather than regulate blood pressure. The inner lining of the vessels is made of endothelial cells (ECs). This cell-type is in direct contact with the luminar blood flow and governs a range of different functions. ECs provide nutrients, oxygen and growth factors to the adjacent cells. The tightness of the layer regulates

the flux of water and immune cells into the tissue and thus tissue inflammation. Angiogenesis, the process of forming new vasculature is a decisive factor in tissue formation and remodeling. Here, proliferating ECs invade the tissue and start to form new blood vessels (Aird, 2007a, 2007b; as reviewd by Cahill & Redmond, 2016; Scalia, 2013).

In the adipose tissue, the supply with oxygen and nutrients is mainly provided by a mesh of microvascular vessels and its endothelial lining. In general, the highest vascularization can be seen in the BAT and the tip region of WATi (as reviewed by Rutkowski et al., 2009), which is the most dorsal part of WATi. In BAT, vasculature is mostly composed of small (<220 µm) micro vessels (Mrzilkova et al., 2020). For the adipose tissue to fulfil its function as energy storage, it is dependent on its transport of lipids through the endothelial layer. All lipids in the blood are transported through the endothelium to be stored in the adipocytes. In times of starvation, lipids take the opposite route through EC after mobilization from adipocytes. Emerging evidence suggests that the endothelium buffers nutrient-derived lipids by temporarily storing them in intracellular lipid droplets, before passing them on to the adipocytes (as reviewed by Ibrahim & Arany, 2017). Therefore, tissue expansion by hypertrophic growth of adipocytes is dependent on the supply through ECs (as reviewed by Ibrahim & Arany, 2017; Zhang et al., 2018).

Interestingly, some endocrine factors are not transported via the blood circulation into the target tissue but are produced in EC directly. A group of soluble factors were identified to be produced by microvasculature EC directly in the adipose tissue (AT-MEC) (Hocking et al., 2010). For example, several factors like endogenous Peroxisome proliferator-acitvated receptor gamma (Pparγ) ligands (Gogg et al., 2019) shape the development and alter functions of adipose tissue. Moreover, obesity has been shown to influence the secretion profile of AT-MECs. Cultured AT-MEC derived from obese subjects, produced more of the proinflammatory cytokines Il6 and Il1 and reduced lipolytic activity of co-cultured adipocytes (Pellegrinelli et al., 2014).

1.2 | Endothelin-1 signaling in the adipose tissue

Another factor commonly secreted by ECs is Endothelin-1 (ET-1). Its gene symbol is Edn1. ET-1 is a peptide built of 21 amino acids, which was first discovered by Hickey et al., 1985 and later isolated, named and characterized (Yanagisawa et al., 1988). The precursor peptide Prepro-endothelin is processed via endothelin-converting enzyme 1 and 2 (ECE1 and 2) to its final product. ET-1 is most often liberated on the basolateral side of ECs, thus signaling to the vascular smooth muscles cells and other underlying cell-types in the tissue enclosing the blood vessel.

ET-1 is the most powerful vasoconstrictive factor known in humans and its physiological functions to regulate vascular tone and blood flow. ET-1 has two receptors: Endothelin-1 receptor A and B (ETA and ETB). Their gene symbols are Ednra and Ednrb. ETA is highly expressed in the vascular medial layer, which is mainly composed of vascular smooth muscle cells and mediates its long-lasting vasoconstrictive properties. ETB is mainly expressed in airway smooth muscle cells and mediates the corresponding bronchoconstriction (as reviewed by Davenport et al., 2016). ET-1 enhances inflammatory processes in the vascular wall. This is due to the induction of other pro-inflammatory cytokines like Tumor necrosis factor α, interleukin-1 and 6 in response to ET-1. ET-1 liberation is triggered by external stimuli like endotoxins, hypoxia and low shear stress (as reviewed by Kowalczyk et al., 2015).

ET-1 is well investigated in the context of several diseases. For example, these are pulmonary arterial hypertension (as reviewed by Chester & Yacoub, 2014), chronic kidney disease (as reviewed by Barton & Sorokin, 2015 and Kohan & Barton, 2014), prostate cancer (as reviewed by Kopetz et al., 2002), obstructive sleep apnea (as reviewed by Karkoulias K et al., 2010), diabetic retinopathies (as reviewed by Ergul, 2011) and obesity. It is well known that ET-1 plasma levels are positively correlated with obesity in humans (Carratù et al., 2016; Ferri et al., 1995) and are induced in rodents upon high-fat diets (Adiarto et al., 2007).

Additionally, cold exposure induces an upregulation of ET-1 in the rodent's heart (G.-F. Chen & Sun, 2006).

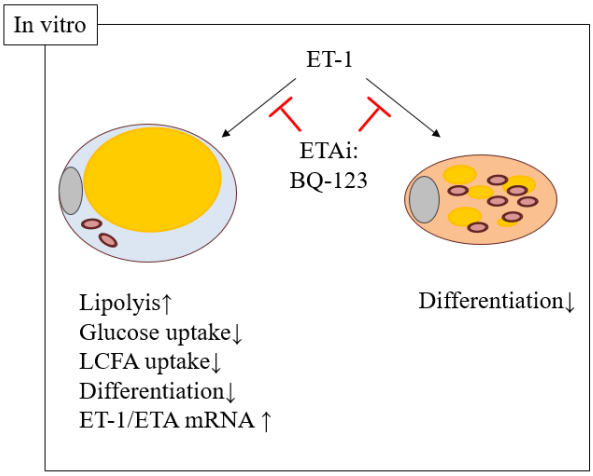

Figure 1 Scheme of in vitro effects of Endothelin-1 on metabolism of white (left) and brown adipocytes (right).

Adapted from Juan et al., 2005, Chien et al., 2011, Lien et al., 2016 and Klepac et al., 2016.

ET-1: Endothelin-1, ETA: Endothelin-1 receptor A, ETAi: ETA inhibitor, LCFA: Long-chain fatty acid

In vitro evidence indicates a role of ET-1 in WAT metabolism and adipogenesis. ET-1 induces lipolysis (Juan et al., 2005) and reduces uptake of long chain fatty acids via the ETA-extracellular-regulated kinase pathway in cell line 3T3L1 (Chien et al., 2011). In addition, ET-1 inhibits adipogenesis in 3T3L1 via ETA. The exact mechanism of inhibition remains unclear. The authors observed an induction of proliferation during the mitotic clonal expansion phase upon ET-1 treatment but disproved it to be the causative factor for inhibition of differentiation induced by ET-1 (Lien et al., 2016). A graphical summary of the paragraph can be found in Figure 1.

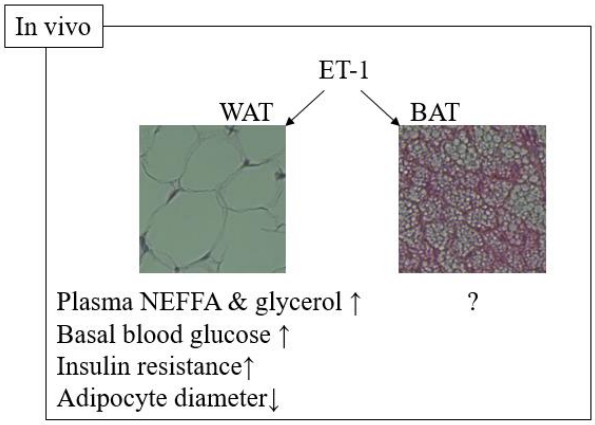

Figure 2 Scheme of long-term effects of Endothelin-1 on the metabolism of white adipose tissue (left) and brown adipose tissue (right).
Adapted from Wilkes et al., 2003 and Lien et al., 2016.

ET-1: Endothelin-1, BAT: brown adipose tissue, WAT: white adipose tissue, NEFFA: Non-esterified free fatty acids

Subcutaneous injections of ET-1 inflict pain-like behavior in rodents by excitation of nociceptive fibers (Fareed et al., 2000; Gokin et al., 2001), thus limiting its use in short-term application to characterize metabolic changes in vivo. Long-term infusion of ET-1 over the duration of 5 days induced insulin resistance in rats (Wilkes et al., 2003). Another study reported reduced WA-diameter in WAT, increased plasma-free fatty acid, glucose, insulin and glycerol levels after a 4-week infusion of ET-1 (10 ng/kg/min) in rats (Lien et al., 2016). It is thus reasonable to assume that ET-1 induces lipolysis and/or reduces lipogenesis in vivo. However the role of ET-1 in BAT is not resolved. ET-1 was shown to inhibit adipogenesis in murine mesenchymal stem cells derived from new-born BAT in vitro (Klepac et al., 2016). The information of this paragraph are graphically summarized in Figure 2.

Complementing metabolic studies on the antagonism of the effect of ET-1 are summarized in the following paragraph. Antagonism of ETB (Antagonist of ETB: BQ-788), but not ETA (Antagonist of ETA: BQ-123), ameliorated insulin-sensitivity in a mouse model of intermittent hypoxia, which naturally exhibits elevated levels of ET-1. Antagonism by BQ-123 even worsened insulin-sensitivity (Polak et al., 2018). An antagonist with a mixed receptor profile (Mixed antagonist ETA>ETB: Bosentan) induced weight loss and ameliorated Glucose-intolerance in mice after 9 weeks of high fat diet (HFD) (Jurrissen et al., 2019). A first report of adipocyte-specific depletion of ETA in vivo produced an increase

of adiposity by 3 % (total body fat) in mice (Rivera-Gonzalez & Speed, 2020). This is surprising, since it does not reflect the observations made *in vitro* or other studies in vivo using ETA-antagonistic treatments. Nevertheless, several genes involved in lipid-handling are reported to be differentially regulated upon deletion of ETA in adipocytes (Rivera-Gonzalez & Speed, 2020). Lastly, a first study with implications for ETA-receptors in the treatment of diabetes and obesity in humans was provided by Farrah et al., 2019. Selective ETA-antagonism reduced plasma free fatty acid and cholesterol levels and beneficially impacted lipoprotein-mass ratios in patients with chronic kidney disease.

1.3 | Molecular regulation of Endothelin-1 expression

ET-1-encoding mRNA has a short half-life of about 15 min (Inoue et al., 1989) which implies the strong regulation of resulting peptide product by the abundance of its transcripts. ET-1 mRNA is regulated by extensive signaling networks on transcriptional and non-transcriptional levels (as reviewed by Stow et al., 2011) and underlies a tissue-specific circadian rhythm (Richards et al., 2014).

Besides classical regulation by transcription factors such as activator protein-1, forkhead-box O1, hypoxia inducible factor-1 (Hif-1), vascular endothelial zinc finger protein f1 and GATA transcription factor (as reviewed by Stow et al., 2011), other factors shape transcriptional regulation. Epigenetic factors, such as DNA methylation, regulate ET-1 mRNA transcription shown in microvascular ECs (as reviewed by Biswas et al., 2018). Furthermore, ET-1-transcription is known to be extensively regulated by mi-RNA (as reviewed by Jacobs et al., 2013). A very recent report highlights the role of a long non-coding antisense RNA species in human kidney cells. Its genetic ablation effectively increases ET-1 mRNA levels (Douma et al., 2020).

With further understanding of post-transcriptional regulation of mRNA, ET-1 mRNA was identified to be regulated by adenine and uracil-rich elements (AREs) in its 3'untranslating region (Reimunde et al., 2005). AREs are protein-binding motifs, which regulate mRNA-stability and most often accelerate degradation of the corresponding transcript. Besides known inter-actors like glycerol aldehyde dehydrogenase (Rodriguez-Pascual et al., 2008), several effector proteins of the 3'untranslating region -driven RNA degradation machinery belong to the human antigen R (HuR) and tristetraprolin family (TTPs). Several members in these families are known to be activated by cyclic adenosine monophosphate (cAMP) (Klöss et al., 2004; Rataj et al., 2016).

It was discovered that elevated levels of intracellular cAMP downregulate ET-1 mRNA. This incidental observation was made in search for an intracellular response element for shear stress in ECs. (Malek et al., 1993). Subsequent studies could reproduce the effect and revealed that addition of a Protein kinase A (PKA) inhibitor KT5720 could reverse the effect (Stewart et al., 1994).

2 | Objectives

The aim of the doctoral research project was to elucidate the role (source, regulation and physiological relevance) of ET-1 and its effect mediated through ETA in BAT. The following questions will be addressed:

1. What is the molecular mechanism of ET-1 regulation in EC and brown adipocytes (BA) upon activation in vitro?
2. What is the transcriptomic response of AT-MEC in cold-activated BAT in vivo?
3. What is the effect of pharmacological antagonism of ETA on whole-body metabolism during cold-activation or diet-induced obesity (DIO)?
4. What is the effect of AT specific depletion of ETA on whole-body metabolism during cold-activation or DIO?

RNA-sequencing of AT-MEC was employed to learn about the regulation or ET-1 production within the AT and further investigated in vitro. To elucidate the effect of ET-1 mediated through the ETA in vivo a dual approach was chosen: A pharmacological approach was chosen using a specific antagonist of ETA. In parallel, a genetic approach was employed based on depletion of ETA in the AT (Ednra AT-KO).

3 | Materials and methods

3.1 | Common materials and equipment

- 96-well plates (Sarstedt, Cat. No. 83.3924)
- Acetic acid (Carl Roth, Cat. No. KK62)
- Autoclave, Varioklav 135 T (Faust)
- BAPTA AM (Tocris, Cat. No. 2787)
- Beads, Zirconium oxide 0.5 mm (Next Advance, Cat. No. ZROB05)
- Beads, Zirconium oxide 1 mm (Next Advance, Cat. No. ZROB10)
- Beads, Zirconium oxide 2 mm (Next Advance, Cat. No. ZROB20)
- Bovine Serum Albumin, (Carl Roth, Cat. No. 8076)
- Bullet blender 24 Biostep (Next Advance)
- BQ-123 in vitro experiments (Tocris, Cat. No. 1188)
- BQ-123 sodium salt for in vivo experiments (Alomone Labs, Cat. No. B-185)
- BQ-788 (Tocris, Cat. No. 1500)
- Calcium chloride, $CaCl_2$ (Carl Roth, Cat. No. A119)
- Centrifuge (Eppendorf, Cat. No. 5415R)
- Chloroform (Carl Roth, Cat. No. Y015)
- Conical tubes, 15 ml and 50 ml volume (Sarstedt, Cat. No. 62.554.502, 62.547.254)
- Confocal microscope LSM 700 (Zeiss)
- D-(+)-Glucose (Sigma Aldrich, Cat. No. G8270)
- DETA NONOate (Tocris, Cat. No. 6077)
- Dimethyl sulfoxide, DMSO (Carl Roth, Cat. No. 7029)
- Disodium phosphate, Na_2HPO_4 (Carl Roth, Cat. No. P030)
- EnSpire Multimode Plate Reader (Perkin Elmer)
- Ethanol, EtOH (Carl Roth, Cat. No. 9065)
- Ethylenediaminetetraacetic acid, EDTA (Carl Roth, Cat. No. 8040)
- EVOS FL Cell Imaging System (Thermo Fisher Scientific)
- Glycerol (Sigma Aldrich, Cat. No. G5516)
- Glycine (Carl Roth, Cat. No. 3908)

- HEPES (Sigma Aldrich, Cat. No. PHG0001)
- Hydrogen peroxide 30 % (Carl Roth, Cat. No. 8070.1)
- H89 dihydrochloride, *N*-[2-[[3-(4-Bromophenyl)-2-propenyl]amino]ethyl]-5-isoquinolinesulfonamide (Tocris, Cat. No. 2910/1)
- Incubator, HERAcell 150 (Heraeus)
- Isopropyl alcohol, Propan-2-ol (Carl Roth, Cat. No. AE73)
- Laminar air flow, Herasafe (Heraeus)
- Magnesium chloride, $MgCl_2$ (Carl Roth, Cat. No. KK36)
- Methanol (Carl Roth, Cat. No. 0082)
- Minispin centrifuge (Sigma Aldrich, Cat. No. Z606235)
- Monopotassium phosphate, KH_2PO_4 (Carl Roth, Cat. No. 3904)
- Monosodium citrate (Carl Roth, Cat. No. HN13.3)
- NaCl 0.9% saline solution (B. Braun)
- NG-Nitro-L-arginine methyl ester hydrochloride, L-NAME (Tocris, Cat. No. 0665)
- Nonidet P 40 Substitute, NP-40 (Sigma Aldrich, Cat. No. 74385)
- Paraformaldehyde, PFA (Carl Roth, Cat. No. 0964)
- Pipetboy acu 2 (Integra)
- Potassium chloride, KCl (Carl Roth, Cat. No. 6781)
- Potassium hydroxide, KOH (Carl Roth, Cat. No. 7986)
- Reaction tube PP 1.5 mL (Sarstedt, Cat. No. 72706)
- Rp-cAMPs triethylammonium salt (Tocris, Cat. No. 1337)
- Scissors, forceps (Fine science tools)
- Serological pipettes 5 ml, 10 ml, 25 ml (Sarstedt, Cat. No. 86.1253.001, 86.1254.001, 86.1685.001)
- Sodium chloride, NaCl (Carl Roth, Cat. No. 3953)
- Sodium dodecyl sulfate, SDS (Carl Roth, Cat. No. 0183)
- Thermomixer comfort (Eppendorf, Cat. No. 2050-120-04)
- Trichostatin A (Tocris, Cat. No. 1406)
- Tris-HCl (Carl Roth, Cat. No. 9090)
- Triton X100 (Carl Roth, Cat. No. 3051)

- Xylol (Carl Roth, Cat. No. 9713)

3.2 | Isolation and culture of eukaryotic cells

Materials and equipment

- 10 cm^2 tissue culture dishes, Standard (Sarstedt, Cat. No. 83.3902)
- 12-well tissue culture plates, Standard (Sarstedt, Cat. No. 83.3921)
- 3,3′,5-Triiodo-L-thyronine sodium salt (Sigma Aldrich, Cat. No. T6397)
- 30 µm and 100 µm nylon meshes (Millipore, Cat. No. NY3002500, NY1H00010)
- 3-Isobutyl-1-methylxanthine, IBMX (Sigma Aldrich, Cat. No. I5879)
- 6-well tissue culture plates (Sarstedt, Cat. No. 83.3920)
- Cannulas (Braun, Sterican 0,90 x 40 mm, Cat. No. 4657519)
- Collagenase, Type II (Worthington, Cat. No. CLS2)
- Countess Automated Cell Counter (Invitrogen, Cat. No. C10227)
- Cryogenic vials (Sarstedt, Cat. No. 72.379.992)
- Dexamethasone (Sigma Aldrich, Cat. No. D4902)
- DMEM, high glucose, GlutaMAX (Gibco, Cat. No. 61965)
- Fetal Bovine Serum, FBS (Biochrom, Cat. No. S0015)
- Insulin solution human (Sigma Aldrich, Cat. No. I9278)
- Mr Frosty freezing device (Thermo Fisher, Cat. No. 5100-0001)
- Penicillin/streptomycin (Merck, Cat. No. A2213)
- Sodium ascorbate (Carl Roth, Cat. No. 3149)
- Syringe filter 0.22 µm cut-off (VWR, Cat. No. 514-0061)
- Syringes 5 ml (BD Discardit II, Cat. No. 309050)
- T75 tissue culture flasks (Sarstedt, Cat. No. 50-809-261)
- T175 tissue culture flasks (Sarstedt, Cat. No. 83.3912.002)
- Trypan Blue Stain (Gibco, Cat. No. 15250)
- Trypsin-EDTA (0.05 %), phenol red (Gibco, Cat. No. 25300054)

3.2.1 | Isolation and culture of BAT derived MSCs

BAT derived MSC isolation

Table 1 Buffers and culture medium for isolation and initial culture of primary BAT derived mesenchymal stem cells

Isolation buffer	
$CaCl_2$	1.3 mM
Glucose	5 mM
HEPES	100 mM
KCl	5 mM
NaCl	123 mM
H_2O	
pH was adjusted to 7.4 and sterile filtered	
Digestion buffer	
Bovine serum albumin (BSA)	1.5 %
Collagenase II	2 mg/ml
BSA and Collagenase II were dissolved in isolation buffer and sterile filtered	
BA isolation culture medium	
Fetal bovine serum	10 %
HEPES	10 nM
Insulin	4 nM
Penicillin/streptomycin	1 %
Sodium Ascorbate	25 µg/ml
Tri-iodo-thyronine	4 nM
All substances were added toDulbecco's Modified Eagle Medium (DMEM), high glucose, GlutaMAX (Gibco, Cat. No. 61965)	

Extracted interscapular BAT from newborn mice was chopped into small pieces using surgical scissors. The animal's tails were collected and used for extraction of genomic DNA

and genotyping. The minced tissue was digested in 3 ml of digestion buffer at 37 °C for 30 min. Every 5 min, the container was shaken vigorously to ensure complete digestion of the tissue. Once digested, the tissue was filtered through a 100 μm nylon-mesh and incubated on ice for 30 min. Using a syringe with a blunt needle, the middle-phase was collected and filtered a second time using a 30 μm nylon-mesh. The obtained samples were centrifuged at 700 rcf for 10 min. After centrifugation, the pellet was re-suspended in 2 ml of BA isolation culture medium and plated in a 6-well TC plate and cultured at 37 °C, 5 % CO_2 for 24 h.

Immortalization of the obtained mesenchymal stem cells (preadipocytes) was achieved by using Simian Virus 40 (SV40) large T-antigen under the control of phosphoglycerate kinase (PGK) promoter.

Expansion of immortalized BAT MSCs

Table 2 Phosphate buffered saline buffer preparation for use in eukaryotic cell-culture

PBS	
KH_2PO_4	1.4 mM
KCl	2.7 mM
NaCl	137 mM
Na_2HPO_4	8 mM
All substances were dissolved in H_2O, the pH adjusted to 7.4 and the solution autoclaved.	

Immortalized cells were maintained in BA growth medium until reaching 80-90 % confluency. Cultured cells were washed with PBS and detached from the well by adding Trypsin/EDTA and incubated at 37 °C until complete detachment. Trypsin was inactivated by adding BA growth medium. The obtained cell suspension was centrifuged at 250 rcf for 5 min. After resuspending the pellet in BA growth medium, cells from three mice of the same genotype were pooled and reseeded in three 10 cm^2 tissue culture plates (passage 1). Cells were further expanded in a 1:10 ratio following the same procedure until passage 4. Storage of cells in cryogenic vials in BA growth medium containing 10 % ‘Dimethyl sulfoxide (DMSO) was performed at passage 2 ($1 \cdot 10^6$ cells/vial) and passage 4 (1 to $3 \cdot 10^6$ cells/vial). Cells were counted before freezing using Trypan Blue Stain and Countess Automated Cell

Counter. Cells were frozen at -1 °C/min in Mr. Frosty containers overnight to -70 °C. The cryogenic vials were stored for few weeks at -70°C and in liquid nitrogen vapor for longer-term storage.

Differentiation of BA

Table 3 Media for maintenance and differentiation of adipose derived mesenchymal stem cells

BA growth medium	
Fetal bovine serum	10 %
Penicillin/streptomycin	1 %
BA differentiation medium	
Fetal bovine serum	10 %
Penicillin/streptomycin	1 %
Insulin	1 nM
Tri-iodo-thyronine	20 nM
BA induction medium	
Fetal bovine serum	10 %
Penicillin/streptomycin	1 %
Insulin	1 nM
Tri-iodo-thyronine	20 nM
Dexamethasone	1 µM
IBMX	0.5 mM
All substances were added to DMEM, high glucose, GlutaMAX (Gibco, Cat. No. 61965)	

Preadipocytes (preBA) were seeded (day -4) in BA growth medium in a density of $1 \cdot 10^6$ cells/plate, in 6-well or 12-well plates and maintained at 37°C, 5 % CO_2. After two days, medium was changed to BA differentiation medium (day -2). After another two days, induction of adipogenesis was started by changing the medium to BA induction medium (day 0). Differentiating adipocytes were maintained in BA Differentiation medium with medium change every other day until day 7. Mature BA were analyzed at day 7. PreBA were analyzed at day -2. Chronic stimulation was performed from day -2 to day 7, if not otherwise stated.

3.2.2 | Isolation of AT-MECs

Materials and equipment

- BD FACSAria III Cell Sorter (BD biosciences)
- Blocking antibody Fc Block (BD biosciences, Cat. No. 564219)
- Centrifuge tubes Nunc 5 ml (Thermo Fisher, Cat. No. 341661)
- CD31 Micro beads, mouse (Miltenyi Biotec, Cat. No. 130-097-418)
- CD31-PECAM PerCP/Cy5.5 (Biolegend, Cat. No. 102420)
- CD45-LCA clone 30-F11 APC/Cy7 (Biolegend, Cat. No. 103116)
- CD102-ICAM2 clone 3C4 PE (Thermo Fisher, Cat. No. A15451)
- CD144-cadherin clone eBioBV13 AF488 (Thermo Fisher, Cat. No. 53-1441-82)
- CD146-MCAM clone ME-9F1 BV605 (BD biosciences, Cat. No. 740434)
- 4',6-Diamidino-2-Phenylindole, DAPI (Thermo Fisher, Cat. No. D1306)
- LS columns (Miltenyi Biotec, Cat. No. 130-042-401)
- QuadroMACS separator (Miltenyi Biotec, Cat. No. 130-090-976)

Digestion and MACS separation

Table 4 Resuspension buffer for magnetic activated cell sorting

MACS buffer	
Fatty acid free BSA	2 %
Penicillin/streptomycin	1 %
EDTA	2 mM
All substances were added to PBS and filtered sterile	

ATs of the same type of two mice were pooled, digested in 7 ml digestion buffer filtered through a 100 µm mesh and centrifuged at 700 rcf for 10 min (see section 3.2.1 for digestion buffer). After centrifugation, the pellet was resuspended in 5 ml ice-cold MACS-buffer and filtered through a 30 µm mesh. Afterwards, the number of the cells suspended in solution was determined using Trypan Blue Stain and Countess Automated Cell Counter. This cell-solution was centrifuged at 300 rcf for 10 min and resuspended in 100 µl MACS buffer. 10 µl

of CD31 micro bead solution were added per $1 \cdot 10^7$ cells. Typically, 30 µl of beads were added to 170 µl of MACS buffer and applied to the samples in a master mix. MACS separation was performed according to the manufacturer's instructions using ice-cold solutions and pre-cooled appliances. The elution fraction was collected in 5 ml centrifuge tubes centrifuged at 300 rcf for 10 min.

Cell labelling and sorting

Table 5 Cell labelling solution of isolated cells for subsequent fluorescent activated cell sorting

Cell labelling solution	
CD31 AB	1:200 (v/v)
CD45 AB	1:200 (v/v)
CD102 AB	1:200 (v/v)
CD144 AB	1:200 (v/v)
CD146 AB	1:200 (v/v)
Blocking AB	1:250 (v/v)
All antibodies were added to ice-cold MACS buffer	

The pellet was re-suspended in 300 µl cell labelling solution and incubated for 20 min at room temperature (RT). Afterwards, 5 µl of 4',6-Diamidino-2-Phenylindole (DAPI) 1 mM was added to the mixture and incubated for 10 min. The samples were centrifuged 10 min 300 rcf, re-suspended in the last remaining drop, filtered through a 100 µm nylon mesh and subsequently sorted in MACS buffer using a FACSAria III Cell Sorter equipped with a 100 µm nozzle.

Fractions were collected in 1.5 ml reaction tubes on ice and centrifuged at 300 rcf for 10 min. The supernatant was subsequently discarded and innuSOLV RNA Reagent added. Samples were stored at -70 C until further use in RNA isolation.

3.2.3 | Cell culture of HUVECs

Materials and equipment

- HUVEC 2 (Promocell, Cat. No. C-12209)
- Endothelial Cell Growth Medium 2, EGM2 (Promocell, Cat. No. C-22111)

HUVEC passage 2 were seeded $1 \cdot 10^6$ cells/T75 flasks and were maintained with EGM2 1 % Penicllin/streptomycin and passaged until passage 5 for use in experiments. To detach, cells were washed twice with PBS and incubated at 37 °C in Trypsin/EDTA 0.05 % for up to 3 min. Detached cells were resuspended in EGM2 10 % DMSO at a concentration of $1 \cdot 10^6$ cells/ml, aliquoted into cryogenic vials, transferred to -70 °C in Mr. Frosty containers and kept in liquid nitrogen vapor for long term storage.

3.2.4 | Cell culture of MuMECs

Materials and equipment

- CI-MuMEC (inSCREENeX, Cat. No. INS-CI-1004)
- MuMEC medium (inSCREENeX, Cat. No. INS-ME-1004)
- Gelatin solution 2 % (inSCREENeX, Cat. No. INS-SU-1015)
- Feezing medium (inSCREENeX, Cat. No. INS-SU-1004)

Gelatin solution was diluted to 0.5 % final concentration in PBS and supplemented with 1 % Penicillin/streptomycin. This working solution was used to coat plastic ware at 1 ml/10 cm^2 for 1 h at 37 °C prior to seeding of cells. MuMEC passage 22 were seeded in MuMEC-medium at a density of $5 \cdot 10^5$ cells/T75 flasks. To detach, cells were washed twice with PBS and incubated in Trypsin/EDTA 0.05 % at 37 °C for 3 min. Detached cells were re-suspended in freezing medium at a concentration of $1 \cdot 10^6$ cells/ml, aliquoted into cryogenic vials, transferred to -70 °C in Mr. Frosty containers and kept in liquid nitrogen vapor for long term storage. Following the manufacturer's recommendation, split ratio was 1:2 until passage 25 and 1:4 therefrom until passage 30. For experiments conducted on the next day, cells were seeded at a density of $2 \cdot 10^5$/well on pre-coated 6-well plates.

3.3 | RNA analysis

Materials and equipment

- Diethyl pyrocarbonate, DEPC (Carl Roth, Cat. No. K028.1)
- InnuSOLV RNA Reagent (Analytik Jena AG, Cat. No. 845-SB-2090100)
- LightCycler 480 SYBR Green I Master (Roche, Cat. No. 04707516001)
- Nanodrop200 Spectrophotometer (Thermo Fisher Scientific)
- ProtoScript II First Strand cDNA Synthesis Kit (New England Biolabs, Cat. No. E6560S)
- Reaction tube PP 1.5 ml RNAase-free (Sarstedt, Cat. No. 72706.400)
- Real-time PCR machine, HT7900 (Applied Biosystems)
- SpeedVac Concentrator, 5301 (Eppendorf)
- SYBR-Green PCR master mix (Applied Biosystems, Cat. No. 4309155)

3.3.1 | RNA isolation

Isolation of RNA from cells or tissues was performed the classical method of guanidinium thiocyanate-phenol-chloroform extraction (Chomczynski & Sacchi, 2006). 1 ml of ice-cold InnuSOLV RNA reagent was added directly to the wells. The cell lysate was transferred into a clean RNAase-free 1.5 ml reaction tube and combined with 0.2 ml of chloroform. Subsequently, the samples were shaken by hand for 15 s and incubated for 5 min at RT. To achieve separation, the samples were centrifuged for 10 min at 13,000 rpm and 4° C. The clear aqueous phase of about 500 µl, layered on top was carefully collected and transferred to a new 1.5 ml reaction tube. By adding 0.5 ml isopropyl alcohol, the RNA was precipitated. The precipitate was collected by centrifugation for 10 min, 13,000 rpm at 4°C and washed three times in 1 ml 75 % ethanol in DEPC-water followed by centrifugation step (5 min, 4 °C, 13,000 rpm) each. Any remaining liquid was removed and the pellet was left to dry for up to 45 min at RT. The pellet was dissolved in DEPC water or nuclease free water H_2O at 55 °C for 10 min. Samples were stored at -70 °C, if not processed immediately.

For isolation of whole tissue samples with high-fat content after HFD feeding, a modified protocol was used. Approx. 50 mg of fat tissue was homogenized in 0.5 ml InnuSOLV RNA reagent using zirconium oxide beads and a bullet blender (Next advance) with 2 ml reaction

tubes. Another 1 mL of InnuSOLV RNA reagent was added, mixed and centrifuged 10 min, 13,000 rpm at 4 °C. A fat layer formed on top. The clear layer underneath (approx. 1.5 ml) was collected and transferred into a fresh RNAase-free 2 ml reaction tube. 300 µl of chloroform was added, mixed, incubated 5 min at RT and centrifuged 10 min at 13,000 rpm and 4 C. The newly formed clear layer on top (approx. 700 µl) was transferred into a fresh 1.5 ml reaction tube and extracted a second time with chloroform: 200 µl was added, mixed, incubated 5 min at RT and centrifuged 25 min at 13,000 rpm and 4 C. The clear aqueous phase of approx. 500 µl was collected and further processed as stated above.

3.3.2 | Synthesis of complementary DNA

The resulting concentration of RNA was quantified using a Nanodrop Spectrophotometer. Following the manufacturer's instructions, up to 1 µg of RNA were transcribed using a First Strand cDNA Synthesis Kit as shown in Figure 3.

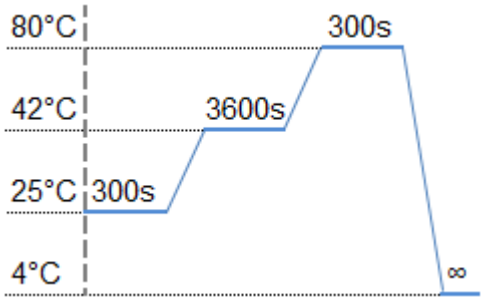

Figure 3 Temperature profile of the utilized reverse transcription polymerase chain reaction.

The complimentary DNA (cDNA) was diluted in tissue culture grade water to a final concentration of 2.5 ng/µl.

3.3.3 | Real-time quantitative PCR

Real-time quantitative PCR (RT-qPCR) was performed using a HT7900 or Step One Plus Thermo cycler instrument, the fluorescent dye SYBR-Green in a 10 µl reaction volume and the program shown in Figure 4.

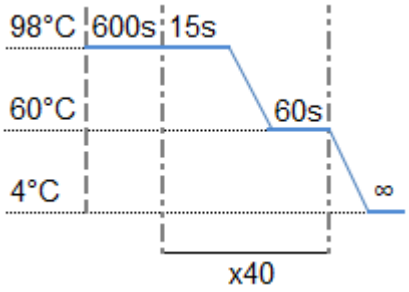

Figure 4 Temperature profile of the utilized two-step quantitative polymerase chain reaction program

Relative quantification of mRNA levels was performed based on the $2^{-\Delta\Delta C}{}_T$-method (Livak & Schmittgen, 2001). The Gene Hypoxanthine-guanine phosphoribosyltransferase (Hprt) was used an internal control if not stated otherwise. The primer sequences used to amplify the target genes are shown in Table 6.

Table 6 List of oligonucleotides utilized to perform quantitative polymerase chain reaction analysis

Name	**Primer sequence (5'->3')**	**Species**
β-ACT for	CCTCTATGCCAACACAGTGC	human
β-ACT rev	CATCGTACTCCTGCTTGCTG	human
Ccl2 for	TGGAGCATCCACGTGTTGG	mouse
Ccl2 rev	GCTGGTGAATGAGTAGCAGCA	mouse
Edn1 forward	GTGTCTACTTCTGCCACCTG	mouse
Edn1 reverse	CACTGACATCTAACTGCCTGG	mouse
EDN1 for	AAGCCCTCCAGAGAGCGTTAT	human
EDN1 rev	CCGAAGGTCTGTCTGTCACCAATGT	human
Ednra forward	GCTGGTTCCCTCTTCACTTAAGC	mouse
Ednra reverse	TCATGGTTGCCAGGTTAATGC	mouse
Ednrb forward	TGTGCTCTAAGTATTGAC	mouse
Ednrb reverse	GGCTGTCTTGTAAAACTGCATGA	mouse
Fabp4 for	GCGTGGAATTCGATGAAATCA	mouse
Fabp4 rev	CCCGCCATCTAGGGTTATGA	mouse
Hprt forward	GTCCCAGCGTCGTGATTAGC	mouse
Hprt reverse	TCATGACATCTCGAGCAAGTCTTT	mouse
Il1b for	TGCCACCTTTTGACAGTGATG	mouse

Il1b rev	TCATCTTTTGGGGTCCGTCA	mouse
Il6 for	TAGTCCTTCCTACCCCAATTTCC	mouse
Il6 rev	TTGGTCCTTAGCCACTCCTTC	mouse
Nd5 for	AGCATTCGGAAGCATCTTTG	mouse
Nd5 rev	TTGTGAGGACTGGAATGCTG	mouse
Ndufa for	AGACGCATCTCTGGTGTCAA	mouse
Ndufa rev	GCCAGGAAAATGCTTCCTTA	mouse
Pparg for	ACAAGACTACCCTTTACTGAAATTACCAT	mouse
Pparg rev	TGCGAGTGGTCTTCCATCAC	mouse
Tnfa for	CCCTCACACTCAGATCATCTT	mouse
Tnfa rev	GCTAGGACGTGGGCTACAG	mouse
Ucp1 for	GGATGGTGAACCCGACAACT	mouse
Ucp1 rev	CCTTGGATCTGAAGGCGGAC	mouse
Vegfa for	TCTCTTGGGTGCACTGGACC	mouse
Vegfa rev	GTTACAGCAGCCTGCACAGC	mouse

3.3.4 | RNA-sequencing and analysis

Materials and equipment

- Hiseq 2500 V4 (Illumina)
- High Sensitivity RNA ScreenTape Sample Buffer (Agilent, Cat. No. 5067-5580)
- High Sensitivity RNA ScreenTape Ladder (Agilent, Cat. No. 5067-5581)
- High Sensitivity RNA ScreenTape (Agilent, Cat. No. 5067-5579)
- TapeStation 4200 (Agilent)
- TapeStation Analysis Software A.02.02 (Agilent)
- 3’mRNA library prep kit Quantseq (Lexogen)

Library preparation, RNA integrity analysis and sequencing were performed by Dr. A. Heimbach (Next generation sequencing Core facility, University of Bonn). Bioinformatics analysis was performed by Mr. A. Buness and Mr. S. Sivalingam (Core unit for Bioinformatics Data analysis, University of Bonn). Briefly, sequence reads were trimmed

off their Illumina Universal Adapter sequence using cutadapt (Martin, 2011) and aligned to the mouse genome (mm10) using STAR (Dobin et al., 2013). FeatureCounts (Liao et al., 2014) was used to assign reads to genes, based on the ENSEMBL definition (release GRCm38.94). Statistical analysis was conducted in a R environment v.3.5.2 (R Core Team, 2019) and the help of several R-packages: Bioconductor DESeq2 (M. I. L. and W. H. and S. Anders, 2014; S. Anders et al., 2013), VST transformation (Anders, Simon and Huber, 2010), ggplot2 (Wickham, 2016) and heatmapper (Babicki et al., 2016). Adjusted p-values were calculated according to the Benjamini-Hochberg method.

3.4 | Protein analysis

Materials and equipment

- BioPhotometer D30 (Eppendorf)
- Cell scraper (Labomedic, Cat. No. 2015217)
- Centrifuge 5430R (Eppendorf)
- Complete protease inhibitor cocktail (Roche, Cat. No. 04693116001)
- Phospate buffered saline, PBS (as described at p. 12)
- Sodium deoxycholate (Sigma Aldrich, Cat. No. D6750)
- Sodium fluoride, NaF (Carl Roth, Cat. No. 4530)
- Sodium orthovanadate, Na_3VO_4 (Carl Roth, Cat. No. 0735)
- Syringe filter 0.22 µm (VWR, Cat. No. 514-0061)

3.4.1 | Isolation of proteins

Cells were washed with PBS and lysed in freshly supplemented cold RIPA buffer. Cells were scraped off the wells, transferred to a 1.5 ml reaction tube and centrifuged for 30 min at 4 °C, 13,000 rpm. The clear phase was transferred to a new clean reaction tube and stored at -70 °C or used directly. For tissue samples, a piece of approx. 30 mg was placed in a clean reaction tubes and an appropriate amount of lysis buffer (approx. 100 µl) was added. The tissue was homogenized by using zirconium oxide beads and centrifuged for 20 min at 4 °C and 13,000 rpm. The clear phase was transferred to a new reaction tube and stored at -70 °C or used directly.

Table 7 Radioimmunoprecipitation assay buffer and supplement preparation for protein isolation

RIPA buffer	
Sodium deoxycholate	0.1 %
NaCl	150 mM
NP-40	1 %
SDS	0.1 %
Tris-HCl (pH 7.5)	50 mM
All substances were added to Millipore H_2O and solution was sterile filtered and stored at 4 °C	
Supplement RIPA buffer	
Complete protease inhibitor cocktail	40 µl/ml
NaF	10 mM
Na_3VO_4	1 mM
All substances were added fresh to RIPA buffer prior to use	

3.4.2 | Bradford assay and protein quantification

Table 8 Coomassie solution preparation for protein concentration determination

Coomassie solution	
Coomassie brilliant blue G-250	0.01 %
Ethanol	5 %
Phosphoric acid	8.5 %
All substances were dissolved in H_2O and the solution was stored at 4°C	

To measure protein concentrations a 1:50 dilution was prepared. 2 µl of the sample was diluted in 98 µl of 0.15 M NaCl solution. Next, 1 ml of Coomassie solution was added to each sample and mixed. The absorbance was measured at 595 nm using an Eppendorf BioPhotometer D30. The protein concentration was calculated from serial Bovine serum albumin dilutions.

3.4.3 | Anti-Endothelin-1 enzyme-linked immunosorbent assay

Materials and equipment

- Omnifix 100 Solo 1 ml syringe (B. Braun, Cat. No. 9161708V)
- Sterican 25G needle (B. Braun, Cat. No. 9186158)
- ET-1 ELISA Kit (ThermoFisher, Ca. No. #EIAET1)

Following cervical dislocation, cardiac blood was taken and anticoagulated with 10 ul of 0.5 M sodium EDTA. Plasma was harvested after centrifugation at 2000 rcf for 10 min at 4 °C, snap frozen in liquid nitrogen and stored until analysis at -70 °C. The analysis of plasma ET-1 levels was performed according to the manufacturer's instructions. The extracted plasma protein of 100 µl of plasma was reconstituted in twice the original volume of Assay buffer.

3.5 | Lipolysis assays

Materials and equipment

- 24-well plates (Sarstedt, Cat. No. 83.3921)
- Bovine serum albumin, fatty acids free (Sigma Aldrich, Cat. No. A7030)
- CL316,243 (Tocris, Cat. No.1499)
- Dulbecco's Modified Eagle Medium (DMEM) (Gibco, Cat. No. 21063)
- EnSpire Multimode Plate Reader (Perkin Elmer)
- Free glycerol reagent (Sigma Aldrich, Cat. No. F6428)
- Glycerol standard (Sigma Aldrich, Cat. No. G7793)
- Norepinephrine, NE (Sigma Aldrich, Cat. No. A9512)

3.5.1 | In vitro lipolysis

Lipolysis assay

Differentiated mature BA were washed twice with warm lipolysis medium. 400 µl of premixed compounds in lipolysis medium were applied to each well in a 12-well and incubated for 2 hours at 37 °C, 5 % CO_2. After incubation, 20 to 40 µl of the plate lipolysis

medium supernatant was transferred into a 96-well plate. Free glycerol reagent was added to a total volume of 100 µl. The standard solution was prepared by mixing 5 µl of the glycerol standard solution with equal volume of lipolysis medium used in the sample wells and filled up to 100 µl with Free glycerol reagent. The blank sample was prepared with 20 to 40 µl of the lipolysis medium and filled up to 100 µl with Free glycerol reagent. All samples, standards and controls were measured in duplicates.

Samples were incubated at 37° C for 5 min and absorption was measured at 540 nm and 600 nm as reference wavelength using EnSpire Multimode Plate Reader (Perkin Elmer). The total glycerol release was calculated as indicated by the manufacturer after normalization to the protein concentration for each sample.

Table 9 Preparation of the incubation medium for lipolysis assays

Lipolysis medium	
Fatty acids free BSA	2 % (m/v)
BSA was dissolved in DMEM (Gibco, Cat. No. 21063)	

Protein quantification

Proteins were isolated and quantified as in section 3.4.2.

3.5.2 | Ex vivo lipolysis assay

Fat pads were isolated from mice and stored in ice-cold DMEM. Small pieces of approximately 5 mg of BAT and 10 mg of WATi or WATg were cut and weighted. These tissue pieces were transferred into 400 µl of lipolysis medium, with or without added CL316,243 10 µM and processed further as stated above (see 3.5.1 |). The total glycerol release was calculated using the values obtained for the total glycerol released, normalized to the tissue weight for each sample.

3.6 | Animal models

3.6.1 | Animal experimentation

Wildtype (WT) male C57Bl/6J mice 8 weeks old were purchased from Charles River Laboratories. The Edrna floxed mice were kindly provided by Prof. Dr. J. Backs (University Hospital of Heidelberg). All studies were approved by the Landesamt für Natur, Umwelt und Verbraucherschutz, Nordrhein-Westfalen, Germany, Animal protocol No. 84-02.04.2018.A333 and 81-02.04.2015.A202.

All animals were housed at 23 °C±1 °C at the Haus für experimentelle Therapie, UKB University Hospital Bonn, or at the Department of Pharmacology and Toxicology, UKB University Hospital Bonn, during experiments.

Unless otherwise specified animals were given free access to chow diet and water ad libitum.

3.6.2 | Genotyping of mice

Materials and equipment

- Agarose standard powder (Carl Roth, Cat. No. 9012-36-6)
- Casting platforms (EmbiTech)
- dNTP Mix invitrogen 1 mM (Thermo Fisher, Cat. No. 10534823)
- Electrophoresis chamber (Peqlab)
- Ethidium bromide solution 10 mg/ml (Carl Roth, Cat. No. 2218.1)
- GelDoc XR (Biorad)
- Microwave oven (Panasonic)
- Phire Tissue Direct PCR Master Mix (Thermo Scientific, Cat. No. F-170)
- QuantityOne Software (BioRad)
- Taq Polymerase MP Biomedical kit (Thermo Fisher, Cat. No. 11487020)
- Thermocycler Biometra T-One (Analytik Jena)

To genotype mice, a small biopsy was collected from the ears with an ear puncher or with a scissor from the tail end. DNA was extracted using the Phire tissue direct kit. The small tissue was covered with a Master Mix consisting of 20 µl Dilution Buffer and 0.5 µl DNA Release Additive. The samples were mixed briefly and centrifuged shortly. The

reaction was incubated 2-5 min at RT and subsequently placed in the pre-heated block at 98 °C for 2 min. The samples were frozen at -20 °C if not processed immediately.

Genotyping of Ednra flox allele

Oligonucleotides as listed in Table 10 were diluted into a reaction mix as described in Table 11.

Table 10 Sequence of oligonucleotide utilized to determine the genotype of transgenic Ednra flox animals

Name	**Sequence (5'->3')**
ETAexo1(fwd)	CCT CAG GAA GGA AGT AGC AAG ATT A
RAF (rev):	ACA CAA CCA TGG TGT CGA

Table 11 Preparation of a polymerase chain reaction to selectively amplify the lox-sequence containing DNA-fragment from genomic DNA preparations

Component	**Volume**
10x buffer	2.5 µl
dNTP Mix 1.25 mM	4 µl (final conc. 0.5 µM)
Taq Polymerase	0.25 µl
ETAexo1(fwd)	1.25 µl (final conc. 0.5 µM)
RAF (rev):	1.25 µl (final conc. 0.5 µM)
Sample	1 µl
Nuclease free water	15.75 µl (final volume of 25 µl)

Polymerase chain reaction was performed as shown in Figure 5.

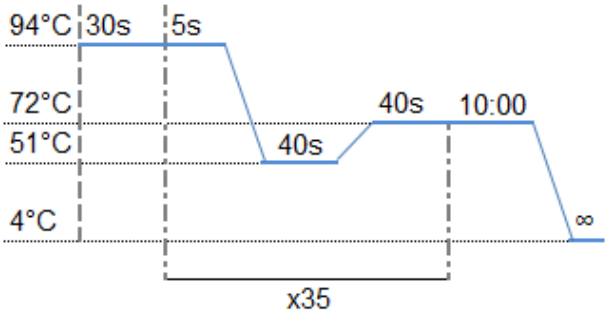

Figure 5 Temperature profile of a polymerase chain reaction program to selectively amplify the lox-sequence containing DNA-fragment

To visualize the PCR products, agarose gel electrophoresis was used. A 2 % gel was prepared by dissolving agarose in TAE buffer in a microwave oven.

Table 12 stock solution preparation for agarose-gel electrophoresis buffer

TAE buffer 50x	
Acetic acid	5.71 %
Na_2-EDTA	50 mM
Tris-HCl	2 M
All substances were dissolved together in deionized water.	

After dissolving the agarose completely, 800 ng/ml of ethidium bromide was added to the agarose solution. The agarose solution was poured into cassettes and left to solidify at RT.

The PCR reaction product was directly added into the 2 % gel. Electrophoresis was performed in TAE buffer at 120 V for 120 min. Separated PCR products were visualized under the UV light excitation at 366 nm using a UV light transilluminator (GelDocXR) in combination with QuantityOne Software. A PCR product at 610 bps corresponds to the WT-allele, while a 650 bps DNA fragment indicates the insertion of a lox sequence.

Genotyping of Adiponectin-Cre allele

Oligonucleotides as listed in Table 13 were diluted into a reaction mix as described in Table 14.

Table 13 Sequence of oligonucleotide utilized to determine the genotype of transgenic Adiponectin-Cre animals

Name	**Sequence (5'->3')**
Oligo 15381	ACG GAC AGA AGC ATT TTC CA
Oligo 18564	GGA TGT GCC ATG TGA GTC TG
oIMR 7388	CTA GGC CAC AGA ATT GAA AGA TCT
oIMR 7339	GTA GGT GGA AAT TCT AGC ATC ATC C

A reaction mix was prepared as follow:

Table 14 Preparation of a polymerase chain reaction to selectively amplify the Cre-transgene from genomic DNA preparations

Component	**Volume**
2X Phire Tissue Direct PCR Master Mix	10 µl
Oligo 15381	1 µl (final conc. 0.5 µM)
Oligo 18564	1 µl (final conc. 0.5 µM)
oIMR 7388	1 µl (final conc. 0.5 µM)
oIMR 7339	1 µl (final conc. 0.5 µM)
Sample	1 µl
Nuclease free Water	5 µl (final volume of 20 µl)

A touch-down PCR protocol (see Figure 6) was used to amplify the cre allele and internal control fragment from genomic DNA preparations.

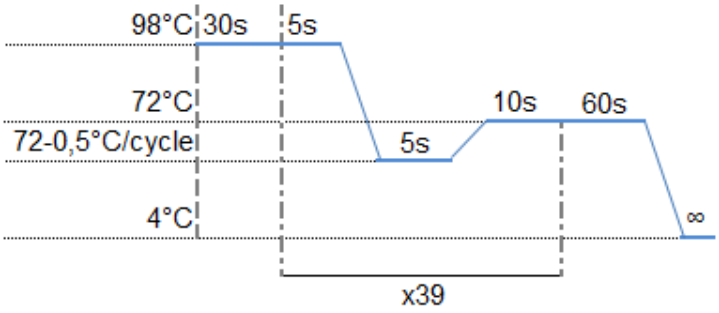

Figure 6 Temperature profile of a touch-down polymerase chain reaction program to selectively amplify the transgenic Cre-allele from genomic DNA preparations

The product sizes were analyzed by gel electrophoresis as described above at 120 V and 45 min. An internal control band is observed at 324 bps and the DNA-fragment at 200 bps corresponds to the adiponectin-Cre allele.

3.7 | In vivo experiments

3.7.1 | Diet induced obesity experiment

Materials and equipment

- Control Diet; 10 kJ% fat (Ssniff Spezialdiäten, Cat. No. D12450)
- High fat diet; 60 kJ% fat (Ssniff Spezialdiäten, Cat. No. D12492)

7 weeks old males were randomly assigned to control (CD, 10 kJ% fat) or HFD, 60 kJ% fat) fed group. The mice were fed ad libitum with CD or HFD for 12 weeks and had free access to water. The body weight was recorded weekly or twice weekly. At the end of the 12 weeks, body composition, glucose tolerance, whole body metabolism and thermogenic BAT capacity test, after acute cold-stimulation were analyzed (see below, sections 3.7.3, 3.7.4, 3.7.5 and 3.7.6)

3.7.2 | Sustained cold-exposure

Materials and equipment

- Phenomaster (TSE Systems)

8 weeks old males were randomly assigned to control or cold-exposure group. The mice were housed in single cages with minimal bedding and free access to food and water on a daily cycle of 12 h light (06:00 to 18:00) and 12 h darkness (18:00 to 06:00). The mice were either kept for 3 days at 16 °C (TVV81-02.04.2015A.202) or 7 days at 18 °C (TVV84-02.04.2018A.333) for cold-acclimatization and subsequently cold-exposed for 7 days at 4 °C. Body composition of mice was measured before cold-acclimatization and prior to sacrifice. Indirect calorimetry measurements were performed on day 5 to 7 of cold-exposure.

3.7.3 | Glucose tolerance test

Materials and equipment

- Accu-Check Nano (Roche)
- Accu-Check Test Strips (Roche)
- Omnifix 100 Solo 1 ml syringe (B. Braun, Cat. No. 9161708V)

– Sterican 27G needle (B. Braun, Cat. No. 4665406)

Animals were fasted for 5 hours with free access to water. The weight of the mice was recorded and the basal fasted levels of glucose measured from the blood collected from a small cut on the tail. The mice were then injected with glucose solution i.p. 8 µl/g body weight and the blood glucose was measured after 15, 30, 60, 90 and 120 min following the same procedure. The mice were let to recover for 24 h in standard housing conditions before to perform any other experiment.

Table 15 Preparation of solutions for intraperitonal injections during a Glucose tolerance test

Glucose solution	
D-Glucose	2.5 g/ml
Glucose was dissolved in sterile NaCl 0.9 % saline solution prior to use	

3.7.4 | Body composition analysis

Materials and equipment

– Minispec Whole Body Composition Analyzer (Bruker)

The whole-body composition (fat mass, lean mass and free water) of mice was measured with TD-NMR in a Bruker Minispec.

3.7.5 | Indirect calorimetry

Materials and equipment

– Phenomaster (TSE Systems)

The mice were housed in single cages with free access to food and water on a daily cycle of 12 h light (06:00 to 18:00) and 12 h darkness (18:00 to 06:00) at the desired temperature (23°C or 4°C) and 45% humidity. Following 24 h of acclimatization, the oxygen and CO_2 consumption, the respiratory exchange rate and locomotor activity were recorded.

3.7.6 | BAT capacity analysis

Materials and equipment

- Phenomaster (TSE Systems)

The mice were placed in pre-cooled cages and exposed to 4 °C cold-environment. The oxygen and CO_2 consumption, the respiratory exchange rate and locomotor activity were recorded for 1 h. Thereafter, the mice had a 24 h regeneration phase until further experiments.

3.7.7 | BQ-123 administration

Materials and equipment

- BQ-123 sodium salt (Alomone, Cat. No. 136655-57-7)
- Omnifix 100 Solo 1 ml syringe (B. Braun, Cat. No. 9161708V)
- Sterican 27G needle (B. Braun, Cat. No. 4665406)

7 weeks old C56Bl6/J male mice were injected intraperitoneally with a dose of 1 mg/kg body weight each day during the course of a HFD/CD regime (see section 3.7.1). Injection volumes were adapted to the cohort's average body weight twice a week. During sustained cold-exposure, 8 weeks old male mice received BQ-123 (see section 3.7.2) at 1 mg/kg body weight for 7 days. BQ-123 powder was resuspended to a final concentration of 0.2 mg/ml in NaCl 0.9% saline and dissolved by warming to 37 °C in a water bath. Aliquots were snap frozen in liquid nitrogen and stored at -70 °C. For subsequent use the next day, aliquots were taken from short term storage at -20 °C to thaw over night at 4°C. All intraperitoneal injections were performed using a 27G needle.

3.8 | Immunohistochemistry

3.8.1 | Tissue preparation

Materials and equipment

- Microtome HM315 (Microm)

Isolated BAT, WATi, WATg and liver pads were fixed in a 4 % solution of para-formaldehyde (PFA) in PBS. After 24 h, samples were dehydrated in increasing concentrations of ethanol: 50 %, 70 %, 95 % and 100 %. Samples were soaked while shaking in each solution 3 times for 20 min each. The tissues were then defatted in xylol 3 times for 10 min each. Afterwards, samples were washed in liquid paraffin in 3 subsequent steps for 1 h at 60 °C and then incubated in the liquid paraffin overnight. Finally, tissues were embedded in paraffin and left to solidify at RT. 5 µm sections of the tissues were cut using a microtome and dried on histological glass slides at 40 °C overnight.

3.8.2 | Hematoxylin/Eosin staining

Materials and equipment

- Eosin Y-solution (Merck, Cat. No. 1.09844)
- Mayer´s hemalum solution (Merck, Cat. No. 1.09249)
- Roti-Histokitt (Carl Roth, Cat. No. 6640)

Tissue sections were defatted for 2 min in xylol. Rehydration was achieved by incubating the slides in decreasing ethanol concentrations: 100 %, 95 %, 90 %, 75 % and 50 %, 2 min each, followed by 2 min in deionized water. Next, slides were incubated for 2 to 4 s in Mayer's hemalum solution and destained under running tap water for 10 min. Eosin Y-solution was activated by addition of 0.5 % (v/v) acetic acid. The staining with eosin was performed by incubating the tissue section in eosin for 2 min and washing for 4 min with distilled water under constant agitation. Tissue was dehydrated by immersing the slides in increasing ethanol concentrations: 75 %, 90 %, 95 % and 100 %, for 2 min each, washed for 2 min in xylol and mounted using Roti-Histokitt.

3.8.3 | Endothelin-1/Endothelin-1 receptor A staining

Materials and equipment

- Alexa Flour 488 Tyramid Super Boost kit (Invitrogen, Cat. No. B40922)
- Anti-rabbit, HRP-conjugated secondary antibody (Cell Signaling, Cat. No. 7074)
- Anti-mouse, HRP-conjugated secondary antibody (Cell Signaling, Cat. No. 7076)
- Monoclonal anti-ET-1 antibody TR.ET.48.5 (Sigma Aldrich, Cat. No. E-166)
- Monoclonal anti-ETA antibody ab117521 (Abcam, Cat. No. ab117521)
- NucRed Live 647 ReadyProbes (Invitrogen, Cat. No. R37106)

Tissue sections were defatted for 3x5 min in xylol. Rehydration was achieved by incubating the slides in decreasing ethanol concentrations: 100 %, 95 %, 90 %, 75 % and 50 %, 2x5 min each, followed by 5 min in PBS. Next, slides were incubated in sodium citrate buffer 20 mM and sodium citrate buffer 10 mM for 5 min at 75-80 °C each. Sections were washed 5 min in destilled water and 10 min in 3 % hydrogen peroxide (v/v) to quench endogenous peroxide activity. Further staining procedure was performed according to the manufacturer's recommendations. The blocking step was 1 h at RT, the primary antibody was diluted (ET-1: TR.ET.48.5 1:250 and ETA: ab117521 1:500) in blocking solution and incubated on the sections overnight at 4°C. The following day, slides were washed 3 times for 5 min with PBST. The incubation in secondary horseradish peroxidase (HRP)-linked antibody (1:200) was 1 h at RT. Anti-rabbit HRP-conjugated antibody was used for ab117521 and anti-mouse HRP-conjugated antibody for TR.ET.48.5. Sections were developed in 30 µl of freshly prepared staining solutions for 6 min, stopped in Stop solution and washed 3x5 min in PBST. Nuclei counterstaining was performed in diluted NucRed 647 solution for 15 min. After 3x5 min final washing steps, sections were mounted in aqueous mounting solution, dried over night at RT and stored under light occlusion until visualization.

3.8.4 | UCP1 staining

Materials and equipment

- Anti-rabbit, HRP-conjugated secondary antibody (Cell Signaling, Cat. No. 7074)
- DAB peroxidase HRP-substrate kit (Vector laboratories, Cat. No. SK-4100)
- Mayer´s hemalaun solution (Merck, Cat. No. 1.09249)
- Normal goat serum (Alpha laboratories, Cat. No. 143-06561)
- UCP1 primary antibody (Sigma Aldrich, Cat. No. sc-6529)
- Roti Histokit (Carl Roth, Cat. No. 6638.2)

Tissue sections were washed 2 times for 2 min in xylol to remove the paraffin. Rehydration was achieved by incubating the slides in decreasing ethanol concentrations: 100 %, 95 %, 90 %, 75 % and 50 %, 2 times for 2 min, followed by 2 times in PBS for 5 min. Slides were next incubated in 20 mM sodium citrate (pH 6.0) for 5 min, followed by another 5 min incubation with 10 mM sodium citrate (pH 6.0) at 75-80 °C. Next, peroxidase activity was quenched by incubation in 3 % hydrogen peroxide (v/v) for 10 min and washed in water for 5 min. In order to reduce unspecific antibody binding, blocking was performed in PBST 2.5 % normal goat serum (v/v) for 1 h at RT. Incubation with UCP1 antibody (1:500 in 2.5 % normal goat serum (v/v) in PBST) was performed overnight at 4 °C. The following day, slides were washed 3 times for 5 min with PBST. Incubation with the secondary antibody (1:200 in PBST) was performed for 1 h at RT. Slides were washed 3 times for 5 min in PBST. Sections were developed for 30 s to 90 s in 3,3'-Diaminobenzidine substrate according to manufacturer’s instruction. Sections were mounted in Roti Histokit solution and dried overnight at RT.

3.8.5 | Oil Red O staining

Materials and equipment

– Oil Red O (Sigma Aldrich, Cat. No. O0625)

Mature BA were washed 2 times with PBS at RT and fixed for 10 min in 4 % PFA solution at RT. The PFA was removed and the cells were further washed for 2 times with PBS, then incubated for 1 to 4 hours at RT in cold Oil Red O working solution. After staining, the plate was carefully washed with distilled water and scans of cell-culture plates were acquired using an office-scanner device.

Table 16 Solutions utilized for Oil Red O staining

Oil Red O stock solution	
Oil Red O	0.5 g
Isopropanol	100 ml
Oil Red O stock solution was stirred overnight and stored at RT	
Oil Red O working solution	
Oil Red O stock solution	60 % (v/v)
Oil Red O stock solution was diluted in water and filtered two times with filter papers prior to use	

3.9 | Statistical analysis

Data are represented as mean ± standard error of the mean (s.e.m). "n" represents individual experiments with cells seeded independently or derived from different mice for the in vitro experiments, or different individual mice for the ex vivo and in vivo experiments.

For datasets n≥8, D'Agostino-Pearson omnibus normality test was performed to assure normal distribution of the data. Statistical analyses of normally distributed data was performed using one-way or two-way analysis of variance (ANOVA) with a Tukey post-hoc test (multiple comparisons) or multiple two-tailed student's t-tests (pairwise comparison). For non-normal datasets Kruskal-Wallis test with a Dunn's post-hoc test (multiple comparisons) or multiple Mann-Whitney tests (pairwise comparison) were performed. All calculations and analysis were performed using GraphPad Prism software Version 6.01 for Windows.

4 | Results

4.1 | ET-1 expression in murine BAT

Two separate approaches were undertaken to estimate the localization of ET-1 and ETA in the BAT.

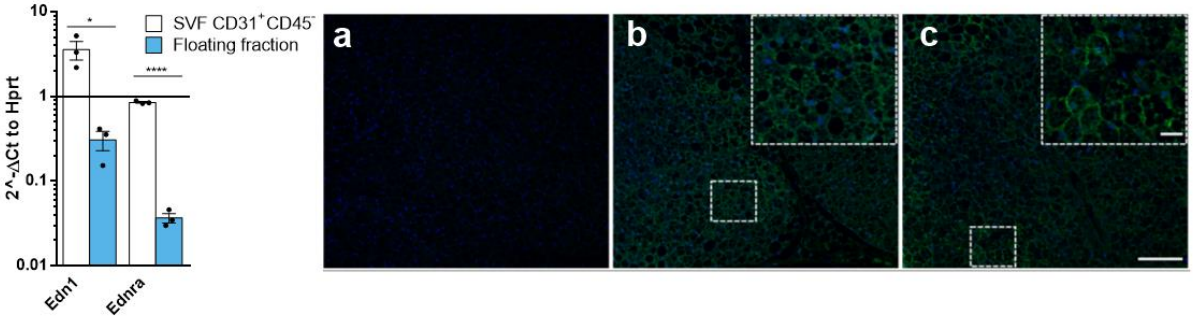

Figure 7 Cellular localization of ET-1 and ETA in the adipose tissue

left: RT-qPCR analysis of digested and fractionized BAT by gravity separation and further magnetic cell sorting of 19-week old male C57Bl6 mice. **right**: Immunohistochemical analysis of Ednra floxed mice after 12-week control diet regime. Counterstain of cell nuclei with NucRed 647 and is displayed in blue. Detection of targets was achieved by HRP mediated coupling of tyramine-derivatized AlexaFluor 488 to molecular targets using the tyramide signal amplification method. Molecular targets are highlighted in green **a)** green: anti-rabbit secondary antibody red: anti-mouse sec antibody control **b)** ET-1 TR.ET.48.5 1:250 **c)** ETA ab117521 1:500. ±s.e.m. n=3, * $p \leq 0.05$ unpaired student's t-test SVF: stromal vascular fraction. HRP: horseradish peroxidase. White scale bar corresponds to 100 µm. 5x Magnified images highlight a 100x100 µm area. The magnified images' scale bar corresponds to 20 µm

In the first approach the tissue was enzymatically digested, separated by the cells' buoyancy, purified by magnetic bead sorting and analyzed by RT-qPCR. This tissue digestion and crude fractionation of BAT yielded the stromal vascular fraction (SVF), which is the cell fraction with the lowest buoyancy. This fraction was further sorted for ECs, analyzed for ET-1 and ETA transcript expression and compared to the adipocyte-rich floating fraction (see Figure 7). In isolated fractions of BAT, more ET-1 transcript was determined in the EC-fraction (11.6±2.6 fold) than in the adipocyte-enriched fraction. Similarly, ETA mRNA was expressed higher in the isolated EC-fraction (23.0± 0.5 fold).

In a second approach the tissue was left intact and stained for immunoreactive antigens of ET-1 and ETA. This immunohistochemical analysis was performed on murine BAT of 20 weeks old animals and fixated in PFA for 16 h (see Figure 7a-c). Please note, that 7a is a

control to assess background fluorescence generated by unspecific binding of secondary antibodies used in this experiment series and therefore appears dark. The molecular targets' subcellular localization in the BAT is predominantly cytoplasmatic for ET-1 (see Figure 7b) and plasma membrane-bound for ETA (see Figure 7c). Lipid droplets in BA cells are devoid of ET-1 immunoreactivity, whereas the cytoplasma exhibits immunoreactivity. In case of ETA, membranes and intracellular vesicles were labelled immunohistochemically.

4.2 | Regulation of ET-1 transcript levels by cAMP in adipocytes and their precursors in vitro

It was shown that norepinephrine (NE) inhibits secretion of ET-1 from BA in vitro. NE is a substance liberated by sympathic nerve endings in BAT and elevates the intracellular concentrations of the second messenger cAMP. Here, the effect is visible on transcript level in vitro. ET-1 transcripts are quantified by RT-qPCR in different cell-types after treatment with NE, which induces cAMP-elevation or 8-Bromoadenosine 3',5'-cyclic monophosphate (8Br-cAMP), which is analogous to endogenous cAMP.

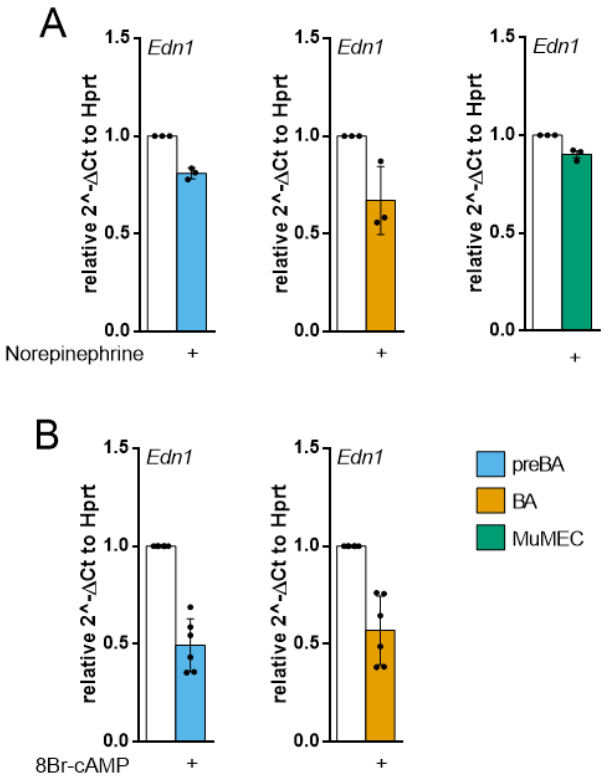

Figure 8 Regulation of ET-1 transcript levels upon norepinephrine and 8Br-cAMP stimulation in vitro

RT-qPCR analysis of different cell-types with (**A**) Norepinephrine 1 µM or (**B**) 8Br-cAMP 200 µM. preBA (**blue**), BA (**orange**) and MuMEC (**green**) were stimulated with indicated compounds for 8 ±s.e.m. n=3-6.

Treatment with NE for 8 h produced a reduction of ET-1 mRNA in mature BA (32.9± 10.0 %), preBA (19.1±1.7 %) and in a murine microvascular endothelial cell line: MuMEC (9.8± 1.7 %), shown in Figure 8A. Similarly, the treatment with the cell-permeable

and phosphodiesterase stable cAMP analogue 8Br-cAMP induced a reduction in ET-1 mRNA levels in preBA (50.6± 5.5 %) and BA (43.1± 7.1 %), as seen in Figure 8B.

Stimulation of mature BA with cAMP-analogues that target different cAMP-signaling pathways produced distinct responses (Figure 9A). 6-MB-cAMP is a selective agonist of PKA, while 8Cpt-2OMe-cAMP specifically targets exchange factor directly activated by cAMP 1 (Epac). Use of 6-MB-cAMP and 8Cpt-2OMe-cAMP yielded a reduction of 88.3± 1.7 % and 42.2± 17.9 % ET-1 mRNA expression, respectively. Next, stimulation via 8Br-cAMP with simultaneous pharmacological antagonism of PKA was conducted. The utilized antagonists have different binding sites at the PKA. The respective treatment of preBA with 8Br-cAMP and H89 or Rp-cAMPs was not significantly different from 8Br-cAMP treatment alone (Figure 9B).

To test for the contribution of Epac to cAMP-mediated ET-1 mRNA downregulation, preBA lacking Epac were utilized. These preBA were kindly provided by Dr. L. Reverte-Salisa and isolated as described in section 3.2.1 from Epac1-KO animals (B6;129S/J-Rapgef3^{tm1Geno}). WT-preBA and Epac-KO preBA were exposed to 8Br-cAMP. A similar reduction of ET-1 mRNA was achieved in WT (51.6± 1.4 %) and Epac-KO preBA cells (50.5± 19.5 %).

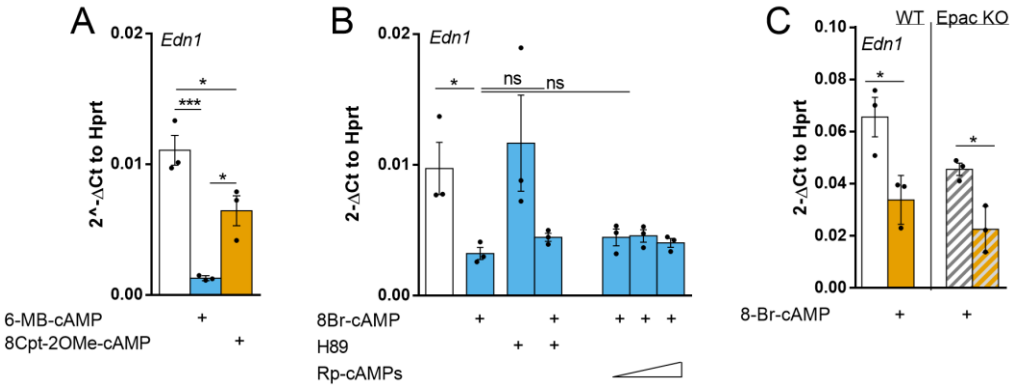

Figure 9 Signaling through Protein kinase A and Exchange factor directly activated by cAMP

Mature BA treated with 6MBcAMP 200 µM (PKA selective agonist) or 8Cpt2OMe-cAMP 200 µM (Epac selective agonist). (**A**) Activation with 8Br-cAMP 200 µM and inhibition using H89 10 µM (Inhibitor of catalytic PKA subunit) and Rp-cAMPs 50-200 µM (Inhibitor of regulatory PKA subunit) in preBA (**B**) 8Br-cAMP stimulation in preBA isolated from B6/129S2/J genetic background and their corresponding Epac-KO littermates (**C**) PKA-related experiments (**blue**) Epac-related experiments (**orange**). ±s.e.m. n=3, * p≤0.05 unpaired student's t-test

Interestingly, Epac KO preBA exhibit a basal ET-1 mRNA expression lacking one third, as compared to their WT-littermates (Figure 9C).

Next, PKA- and Epac-independent mechanism were investigated. First the hypothesis of an auto-regulatory loop which down-regulates ET-1 mRNA was investigated. PreBA were treated with ET-1 1-21 peptide and selective ET-1 receptor antagonists. ET-1 significantly induced ET-1 mRNA levels by 25.8± 8.3 %. Treatment with BQ-123 or BQ-788 did not change basal transcription and failed to suppress upregulation of ET-1 mRNA by ET-1 peptide (Figure 10A).

My second approach focused on calcium-channels, which are targets of intracellular cAMP. Therefore, BABTA AM, which is an intracellular calcium scavenger was used. Combined treatment of preBA with BAPTA AM and 8Br-cAMP produced results which were not significantly different from 8Br-cAMP alone (Figure 10B).

ET-1 transcription is regulated by changes in histone modifications, which can be triggered by cAMP and is described for e.g. uncoupling protein 1 (Ucp1) in preBA. Trichostatin A (TSA) is an inhibitor of histone deacetylases (HDACs) and thus a molecular tool to study transcriptional responses to histone modification. TSA suppressed ET-1 mRNA transcription in a dose-dependent manner (TSA 500 nM 53.8± 10.5 %), but did not reverse the effect induced by 8Br-cAMP (Figure 10C).

ET-1 mRNA is subject to post-transcriptional regulation and degradation. Actinomycin D (ActD) is an inhibitor of RNA-polymerases. Thus, transcription is stopped after addition of ActD and observed changes must be non-transcriptional. Comparing ET-1 mRNA-decay induced by ActD with concomitant treatment of 8Br-cAMP did not show significant

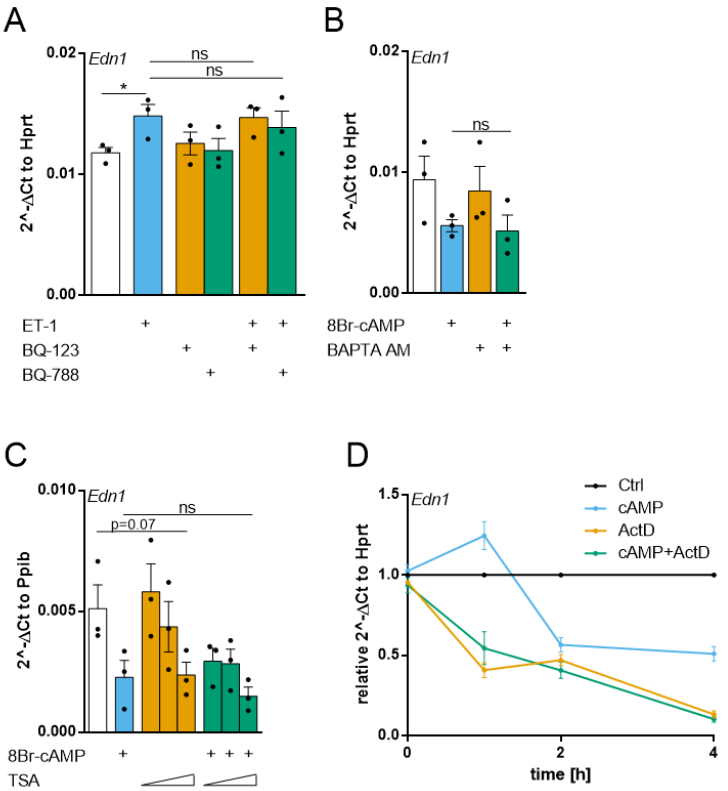

Figure 10 Other pathways and factors independent of PKA and Epac, which are involved in regulating ET-1 transcript abundance

Experiments in preBA: Autocrine regulation by ET-1 10 nM. BQ-123 (ETA antagonist) and BQ-788 200 nM (ETB antagonist) (**A**) Regulation by cAMP activated Calcium channels: 8-Br-cAMP 200 µM BAPTA AM 10 µM (**B**) Regulation via Histone modification: 8-Br-cAMP 200 µM, Trichostatin A 5, 50 and 500 nM (**C**) Posttranscriptional regulation by cAMP: 8-Br-cAMP 200 µM, Actinomycin D 5µg/ml (**D**) Controls are displayed in **white** or black **lines**. Pharmacological treatments are indicated by different colors. ±s.e.m. n=3, * p≤0.05 unpaired student's t-test

differences. Interestingly, 8Br-cAMP control treatment induced a peak (24.6± 15.0 %) of ET-1 mRNA expression after 1 h (Figure 10D).

Lastly, I tested the hypothesis, whether or not cAMP induces nitric oxide (NO) production, which could exert effects on ET-1 mRNA regulation.

PreBA were treated with DETA-NONOate, which is a donor of NO. It produced a dose-dependent downregulation of ET-1 mRNA (Figure 11A). Next, NG-Nitro-L-arginine methyl ester (L-NAME), an inhibitor of nitric oxide synthases (NOS) was employed to suppress NO production. Combined treatment of 8Br-cAMP stimulation and L-NAME retained 20.0± 3.9 % more ET-1 mRNA, than 8Br-cAMP alone. This corresponds to 12 % of basal ET-1 mRNA levels (Figure 11B).

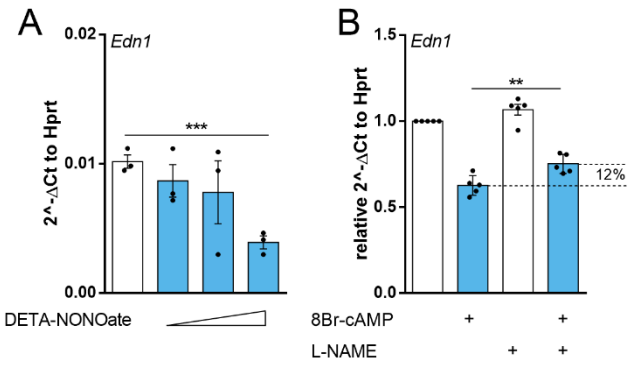

Figure 11 Effect of nitric oxide-donators and nitric oxide synthase-inhibition on ET-1 mRNA expression in preBA

preBA treatment with rising concentrations of DETA NONOate 10, 30 and 100 µM (**A**) Inhibition of nitric oxide synthase by LNAME 10 µM and stimulation by 8Br-cAMP 200 µM 8 h (**B**) Controls are shown in **white**. Treatment conditions are displayed in **blue**. n=3-5 ** p≤0.01, *** p≤0.001 unpaired student's t-test

4.3 | RNA sequencing of AT-MEC

This chapter focuses on adipose tissue derived microvascular ECs (AT-MEC) and their regulation by cold-exposure stimulus in vivo.

WAT derived from cold-exposed 6-8 week old male WT C57Bl6J animals underwent a process called browning. Tissue weight after this process was increased for BAT and reduced for WAT (Figure 12A). First, the SVF was further purified for CD31-expression by magnetic activated cell sorting (MACS). This elution fraction was subsequently further purified to acquire live cell fractions, which express common EC surface markers ($CD31^+$, $CD102^+$, $CD144^+$ and $CD146^+$) by fluorescence-activated cell sorting (FACS). Elution fractions of BAT-derived anti-CD31-MACS contained 1.8± 0.1-fold more cells with EC-surface markers and negativity for $CD45^-$ and $DAPI^-$ signal, as compared to WAT-MACS eluates (Figure 12B). The overall AT-MEC yield per tissue weight showed significant differences in BAT and WATi. AT-MEC yield of cold-exposed animals was significantly reduced in BAT by 42.9± 13.7% and 1.7± 0.2 fold increased in WATi as compared to animals kept at 23 °C (Figure 12C). Principal component analysis yielded 3 distinct clusters (highlighted in Figure 12D), which correspond to the samples' fat depot-origin: WATi and WATg-derived AT-MEC cluster overlap and separate from the BAT-derived AT-MEC cluster. WATg-derived AT-MEC distance further from BAT-derived AT-MEC than WATi-derived AT-MEC on principal component axis 1 (Figure 12D).

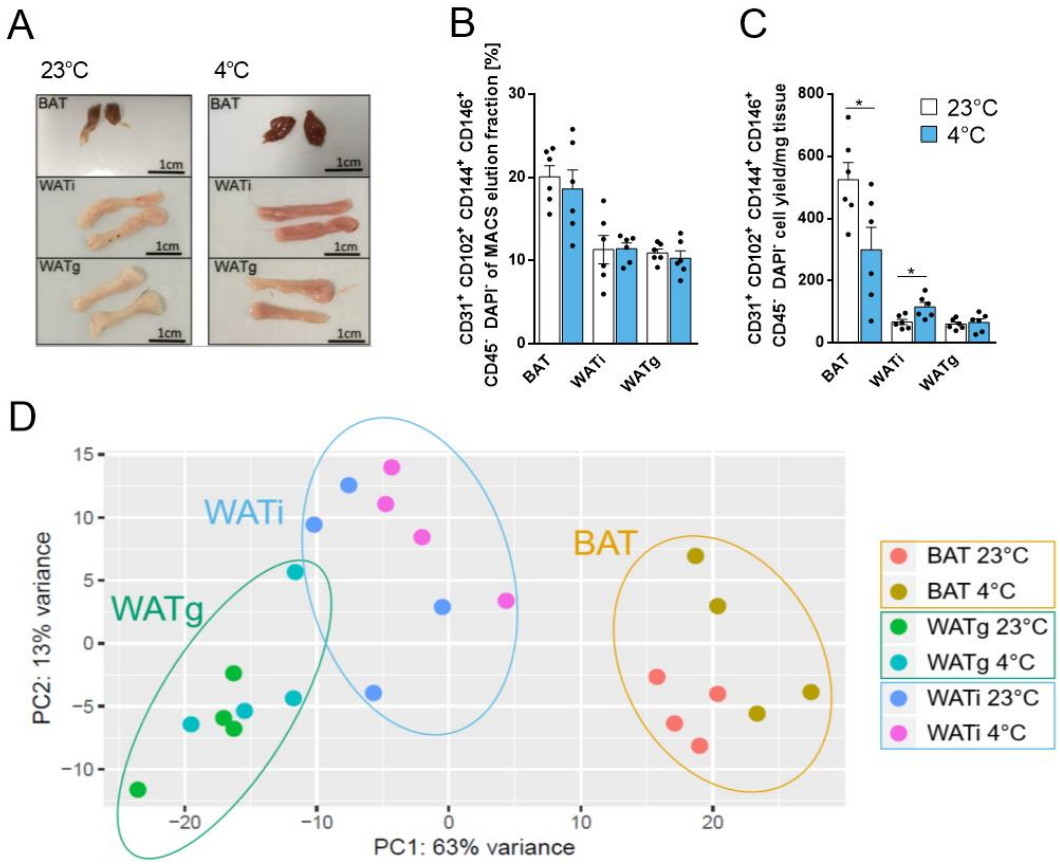

Figure 12 AT-MEC isolation and homogeneity of RNA-sequencing results

Extracted fat tissues from male animals housed at 23 °C for 2 weeks (**23 °C** and displayed further in **white**) and animals acclimatized 7 days to 18 °C and cold-exposed at 4°C for 7 days (**4 °C** and displayed in **blue)** (**A**). Fraction of cells positively selected by fluorescence-activated cell sorting ($CD31^+$, $CD102^+$, $CD144^+$, $CD146^+$, $CD45^-$, $DAPI^-$) of anti-CD31 magnetic-activated cell sorting eluate (**B**). Cell yield normalized to extracted adipose tissue weight (**C**). Principal component analysis of AT-MEC sequencing (**D**). ±s.e.m, n=4-6 * $p \leq 0.05$, unpaired student's t-test

Mapped reads of genes involved in the endothelin system were extracted from the dataset, normalized by row to its average expression level and sorted by tissue-origin, treatment and replicate number. Genes in the endothelin system include receptors (Ednra and Ednrb), ligands (Edn1-3) and processing enzymes (Furin and Ece1-2). For some genes, one or less normalized reads were mapped. These are the Edn2, Edn3 and Ece2 loci. A distinct pattern was observed for Edn1, as it was upregulated in all 4 replicates in BAT-derived and cold-exposed AT-MECs (Figure 13).

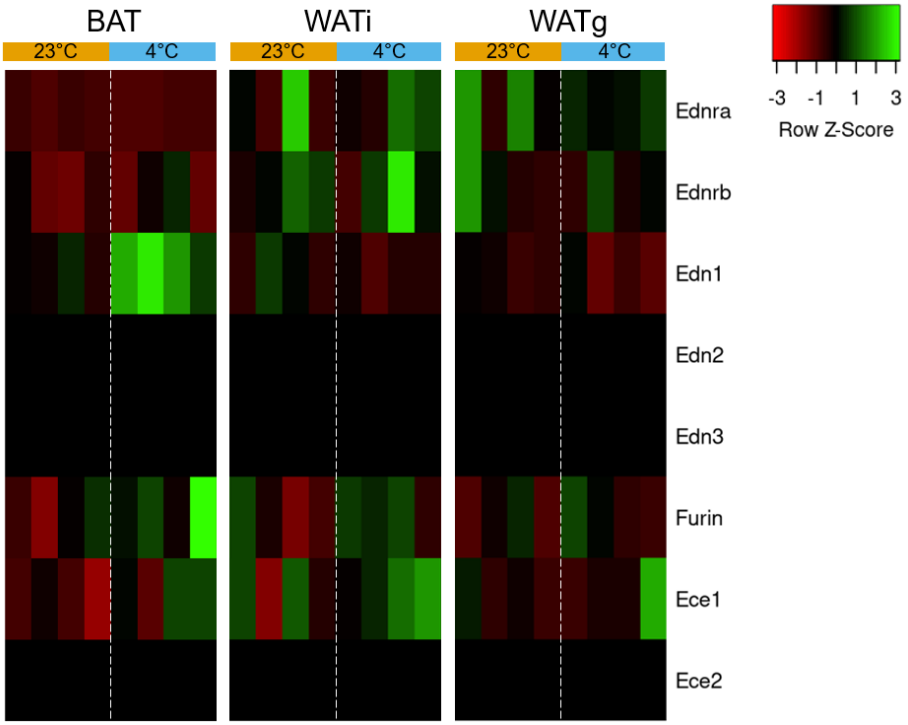

Figure 13 Regulation of the endothelin system mRNA in adipose tissue derived endothelial cells upon sustained cold exposure

Relative gene expression is depicted in green and red. Representing either a below average (red) or above average (green) gene expression. Please note that Edn2, Edn3 and Ece1 had less than one mapped normalized read per sample and are therefore considered as absent in AT-MEC and appear black. *Vertical*: Paired replicates 23 °C (control treatment) and 4 °C (sustained cold-treatment) in different adipose tissues. *Horizontal*: Genes involved in the endothelin system: receptors, ligands and processing enzymes; n=4. BAT: brown adipose tissue, WATi: inguinal white adipose tissue, WATg: gonadal white adipose tissue.

To verify that the observed effect in vivo is present in short-term cold-exposure as well, tissue analysis of short-term cold-exposed animals was conducted. Whole BAT lysate of animals, which were cold exposed for 1 hour, was analyzed for ET-1 mRNA levels. ET-1 mRNA levels were significantly elevated by 2.0± 0.2 fold as compared to control treatment (Figure 14).

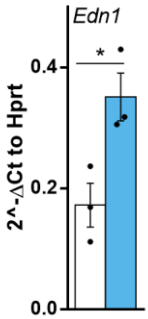

Figure 14 Short term regulation of ET-1 mRNA in vivo

Whole BAT lysate RT-qPCR analysis of acutely cold-exposed animals for 1 h at 4 °C(**blue**) and animals kept at 23 °C (**white**). ±s.e.m, n=3 * p≤0.05, unpaired student's t-test

4.4 | Metabolic characterization after pharmacological inhibition of ET1-Receptor A in vivo

4.4.1 | Pharmacological inhibition of ET1-Receptor A in a model of diet-induced obesity

To investigate the effect of ETA-inhibition during the onset of obesity, BQ-123 was administered, which is a highly selective and competitive antagonist of the ETA. Starting at the age of 8 weeks, C57Bl6/J mice received daily injections of BQ-123 1 mg/kg body weight. The corresponding control group received equivoluminal injections of the corresponding solvent, which was saline.

There was no apparent difference in body weight-gain of the BQ-123 and vehicle-treated animal groups subjected to 12 week of standardized CD experiment (Figure 15A). Body composition, food intake and glucose tolerance were unchanged upon the treatment with BQ-123 (Figure 15B-F). Resting energy expenditure, as measured by the amount of oxygen consumed within 24 h, was equal between treated and control-group animals. Analysis of co-variance (ANCOVA) of body weight and oxygen consumption did not yield differences in basal respiration between treated and untreated animals (Figure 15G-I). Although oxygen consumption was equal between BQ-123 and vehicle-treated animals, BQ-123-treated animals exhibited significantly (2.2± 0.4 fold) higher spontaneous locomotor activity than the control (Figure 15J-K). Comparison of maximal respiratory capacity, measured during a 1 h cold exposure between groups, showed no significant difference (Figure 15L-M). Albeit not significant, BQ-123-treated animals moved 21.1± 5.8 % less in acute cold-stimulation (Figure 15N-O). Ex vivo lipolysis analysis revealed no differences in maximal lipolytic response as provoked by β3-Adrenoreceptor agonist CL316,243 (Figure 15P). Plasma ET-1 levels remained unchanged upon BQ-123-treatment (Figure 15Q).

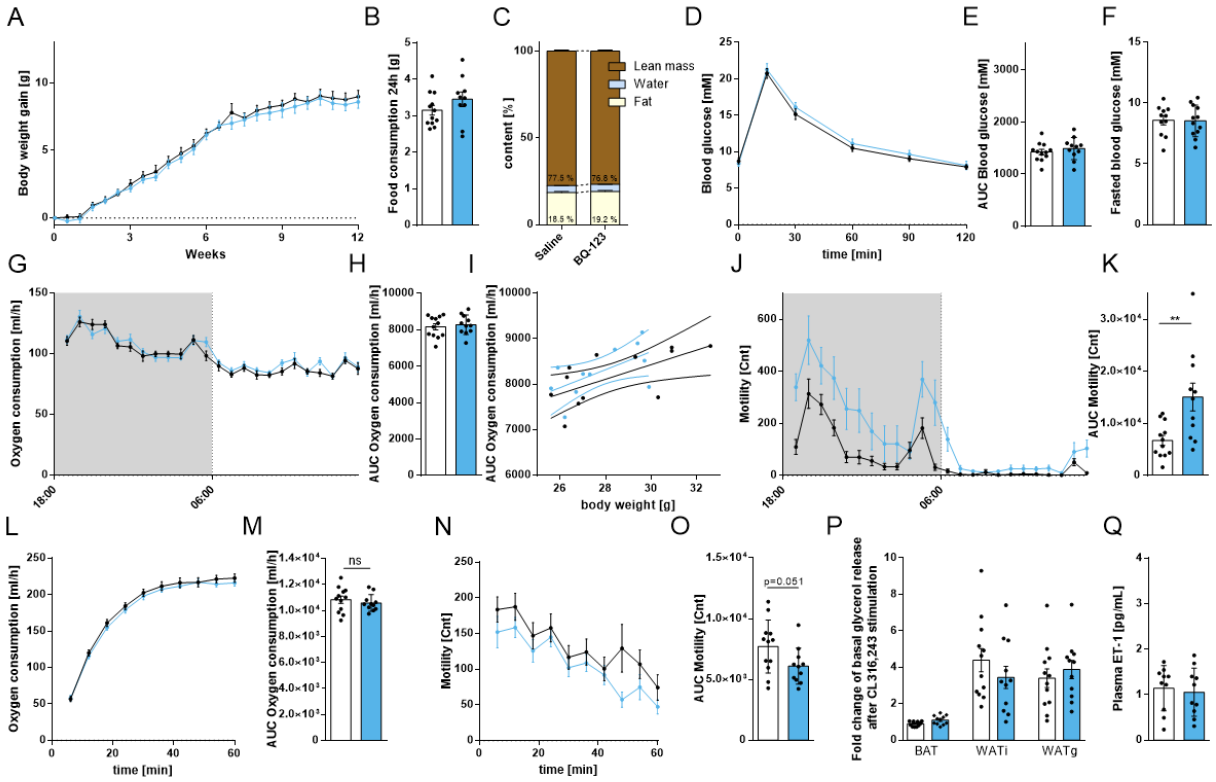

Figure 15 Physiological parameters and indirect calorimetric measurements after pharmacological inhibition of ETA using BQ-123 1 mg/kg body weight in a control diet experiment

Black/White: C57Bl6J WT animals treated with saline (0.9 % sodium chloride 5 µl/g body weight i.p.). **Blue**: C57Bl6J WT animals treated with BQ-123 (1 mg/kg i.p. body weight). Body weight gain (**A**) during the 12-week experiment. Food consumption (**B**) during 24 h indirect calorimetric measurements and body composition measured by NMR prior to the animals' sacrifice (**C**). Glucose tolerance test performed using 2 mg glucose/g fasted body weight in experiment-week 11 (**D**), its area under the curve analysis (**E**) and t=0 after a 5 h fasting interval (**F**). 24 h oxygen consumption measurement in a metabolic cage system (**G**), its area under the curve analysis (**H**) and ANCOVA with body weight (**I**). Locomotor activity during 24 h indirect calorimetric measurements (**J**) and its area under the curve analysis (**K**). Maximal respiratory capacity as induced by 1 h cold exposure challenge at 4 °C and measured in metabolic cage system (**L**), its quantification (**M**), corresponding animal's locomotor activity (**N**) and its quantification (**O**). Maximal l ±s.e.m. n=11-12 * $p \leq 0.05$ unpaired student's t-test/Mann-Whitney-test; CL:CL 316,243, i.p.: intraperitoneal, NMR: nuclear magnetic resonance.

Monitoring BQ-123-treated and control-group animals for 12 weeks during a HFD regime revealed differences. Animals having received BQ-123 gained less weight within the first

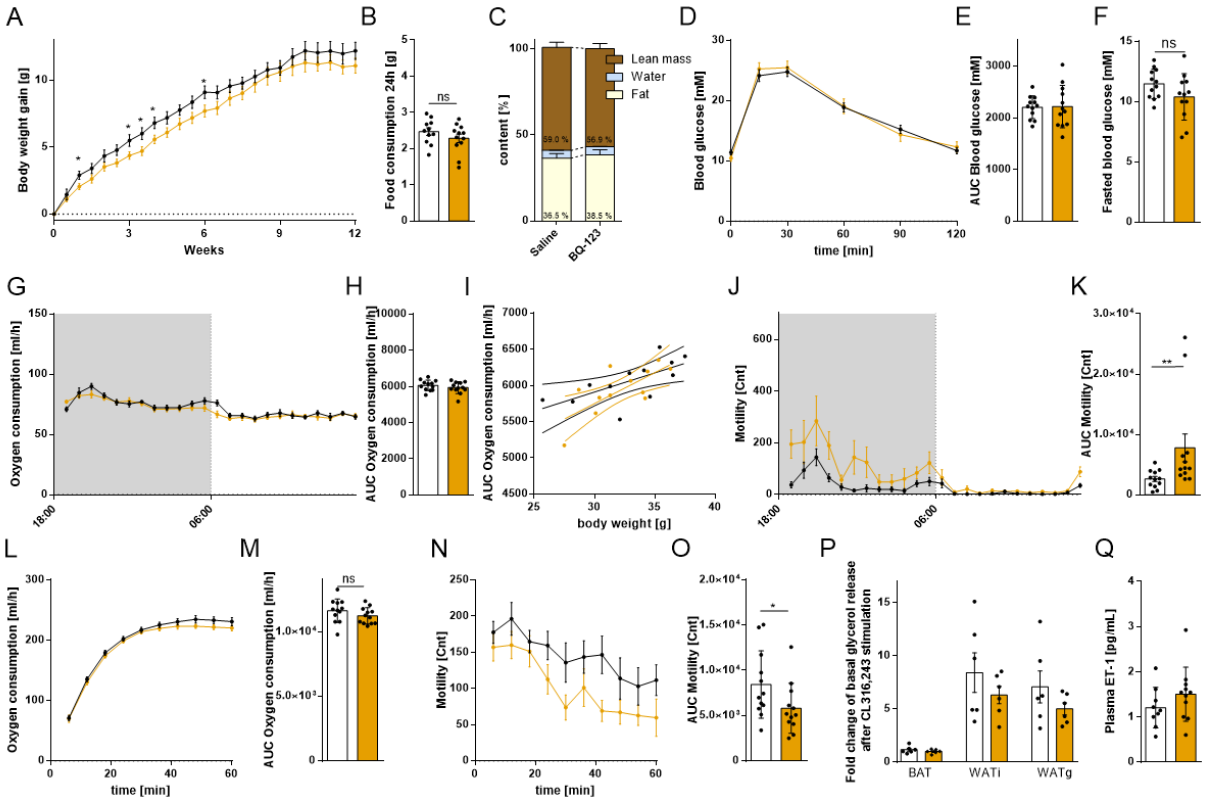

Figure 16 Physiological parameters and indirect calorimetric measurements after pharmacological inhibition of ETA using BQ-123 1mg/kg body weight in animals with diet-induced obesity

Black/White: C57Bl6J WT animals treated with saline (0.9 % sodium chloride 5 µl/g body weight i.p). and HFD. **Orange**: C57Bl6J WT animals treated with BQ-123 (1 mg/kg i.p. body weight) and HFD. Body weight gain (**A**) during the 12-week experiment. Food consumption (**B**) during 24 h indirect calorimetric measurements and body composition measured by NMR prior to the animals' sacrifice (**C**). Glucose tolerance test performed using 2 mg glucose/g fasted body weight in experiment-week 11 (**D**), its area under the curve analysis (**E**) and t=0 after a 5 h fasting interval (**F**). 24 h oxygen consumption measurement in a metabolic cage system (**G**), its area under the curve analysis (**H**) and ANCOVA with body weight (**I**). Locomotor activity during 24 h indirect calorimetric measurements (**J**) and its area under the curve analysis (K). Maximal respiratory capacity as induced by 1 h cold exposure challenge at 4 °C and measured in metabolic cage system (**L**), its quantification (**M**), corresponding animal's locomotor activity (**N**) and its quantification (**O**). Maximal l ±s.e.m. n=6-12, * p≤0.05 unpaired student's t-test/Mann-Whitney-test; CL: CL 316,243, i.p.: intraperitoneal, HFD: high fat diet NMR: nuclear magnetic resonance

half of the experiment, but reached similar levels by the end of the 12-week experiment (Figure 16A). BQ-123-treated animals exhibited equal feeding behavior. However, the mice consisted of 2 % more total fat mass and 2 % less total lean mass (Figure 16B-C). Glucose

tolerance test results were similar in animals, independent of whether or not BQ-123 was received. Although not significant, BQ-123-treated animals had lower fasted blood glucose levels (Figure 16D-F). Indirect calorimetric data parallels observations made in the CD group (see Figure 15). Resting energy expenditure was unchanged, although BQ-123-treated animals moved significantly (3.0± 0.9 fold) more and cold-induced maximal respiration is similar, while BQ-123-treated animals moved significantly (31.3± 9.5 %) less (Figure 16G-O). Average levels of maximal lipolysis response were not significantly reduced upon administration of BQ-123 (Figure 16P). Plasma ET-1 levels are slightly elevated (Figure 16Q).

The weight of the extracted ATs was measured and is expressed relatively to the animal's total body weight. There was no difference between animals treated with BQ-123 and saline. Analysis of whole-tissue mRNA content by RT-qPCR showed a 2.6± 0.2 fold increase in levels of ET-1 mRNA (Edn1) in BAT, heightened levels (1.12± 0.04 fold) of adipocyte protein 2 mRNA (Ap2 of which the gene name is Fabp4) in WATi and 30.0± 5.8 % lowered vascular endothelial growth factor A mRNA (Vegfa) levels in BAT of BQ-123-treated animals (Figure 17 A-C).

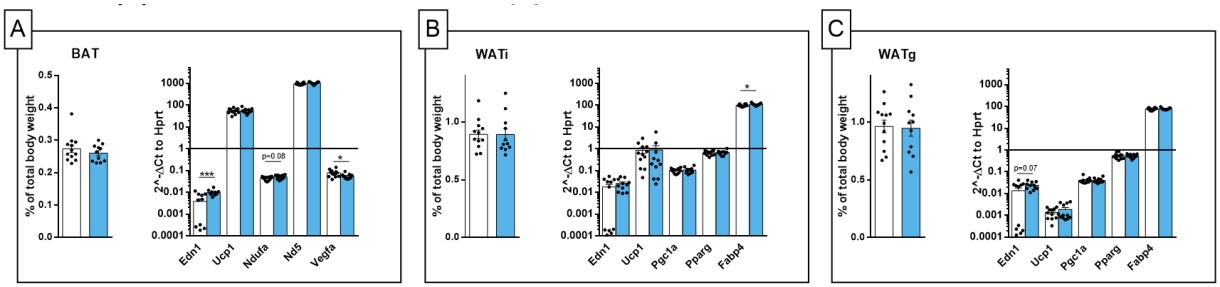

Figure 17 Adipose tissue analysis after pharmacological inhibition of ETA using BQ-123 1 mg/kg body weight in a control diet experiment

White: C57Bl6J WT animals treated with saline (0.9 % sodium chloride 5 µl/g body weight i.p.). **Blue**: C57Bl6J WT animals treated with BQ-123 (1 mg/kg i.p. body weight). Analysis of brown adipose tissue (**A**) inguinal white adipose tissue (**B**) and gonadal white adipose tissue (**C**). Tissue weight is normalized to whole body weight. RT-qPCR analysis of thermogenic and adipogenic marker genes are quantified relative to Hprt. Edn1: Endothelin-1; Ucp1: Uncoupling protein 1; Ndufa: NADH-dehydrogenase; Nd5: NADH-ubiquinone oxireductase; Vegfa: Vascular endothelial growth factor A; Pgc1a: Pparγ-coactivator 1-α; Pparg: Peroxisome proliferator-activated receptor gamma; Fabp4: Fatty acid binding protein 4 (adipocyte protein 2). ±s.e.m. n=12, * p≤0.05 unpaired student's t-test/Mann-Whitney-test, , i.p.: intraperitoneal

Further histological analysis showed no substantial differences in the adipose tissues' composition between animals, which received BQ-123 or saline (Figure 18A-C)

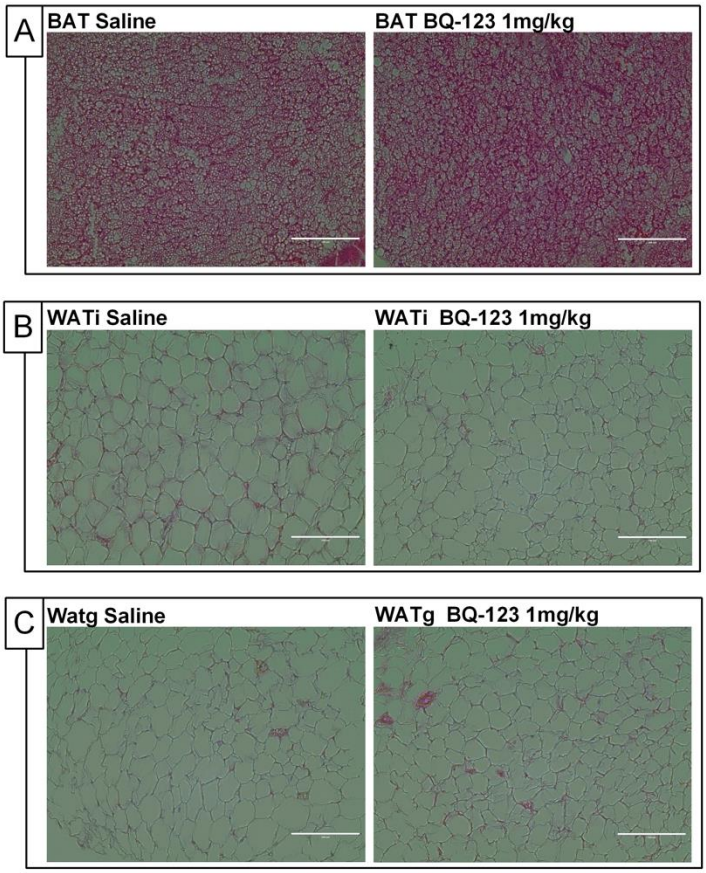

Figure 18 Histological analysis of adipose tissues after pharmacological inhibition of ETA using BQ-123 1 mg/kg body weight in a control diet experiment.

Histological analysis of brown adipose tissue (**A**) inguinal white adipose tissue (**B**) and gonadal white adipose tissue (**C**). Panel of images depict representative images of H&E stained tissue preparation at 40 x magnification. White bar corresponds to 100 µm, n=3.

In the HFD groups, neither tissue weight nor tissue morphology (Figure 20) nor transcript content were changed significantly upon the treatment with BQ-123 (Figure 19).

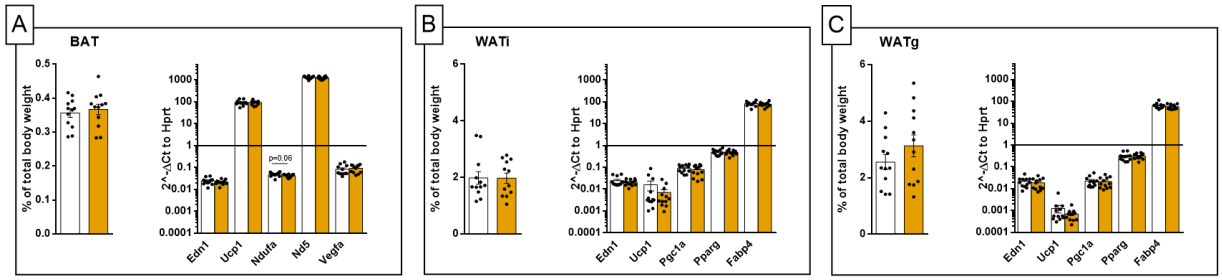

Figure 19 Adipose tissue analysis after pharmacological inhibition of ETA using BQ-123 1 mg/kg body weight in animals with diet-induced obesity

White: C57Bl6J WT animals treated with saline (0.9 % sodium chloride 5 µl/g body weight i.p.) and HFD **Orange**: C57Bl6J WT animals treated with BQ-123 (1 mg/kg i.p. body weight) and HFD. Analysis of brown adipose tissue (**A**) inguinal white adipose tissue (**B**) and gonadal white adipose tissue (**C**). Tissue weight is normalized to whole body weight. RT-qPCR analysis of thermogenic and adipogenic marker genes are quantified relative to Hprt. Edn1:Endothelin-1; Ucp1: Uncoupling protein 1; Ndufa: NADH-dehydrogenase; Nd5: NADH-ubiquinone oxireductase; Vegfa: Vascular endothelial growth factor A; Pgc1a: Pparγ-coactivator 1-α; Pparg: Peroxisome proliferator-activated receptor gamma; Fabp4: Fatty acid binding protein 4 (adipocyte protein 2) ±s.e.m. n=12, * p≤0.05 unpaired student's t-test/Mann-Whitney-test, HFD: High fat diet.

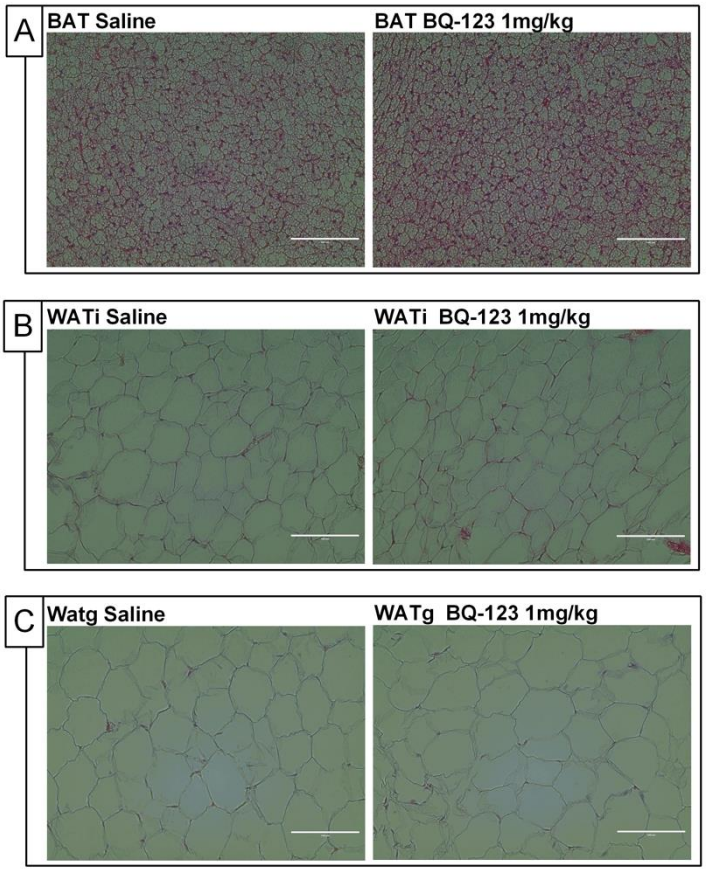

Figure 20 Histological analysis of adipose tissues after pharmacological inhibition of ETA using BQ-123 1 mg/kg body weight in animals with diet-induced obesity

Histological analysis of brown adipose tissue (**A**) inguinal white adipose tissue (**B**) and gonadal white adipose tissue (**C**). Panel of images depict representative images of H&E stained tissue preparation at 40 x magnification. White bar corresponds to 100 µm.

4.4.2 | Pharmacological inhibition of ET1-Receptor A during cold-exposure

Starting at the age of 8 weeks, C57Bl6 animals were acclimatized to the cold environment for 3 days at 16 °C and further cold-exposed to 4 °C for 7 days. To investigate the effect of pharmacological ETA-inhibition during sustained cold-exposure, animals either received 1 mg BQ-123/kg body weight or the equivalent volume of saline once per day during the 4 °C experiment cold-exposure phase.

Over the course of the 10-day control experiment at 23 °C, the animals' body weight remained on similar levels and was not significantly different at the start and end of the experiment. No significant differences were observed between BQ-123-treated and saline

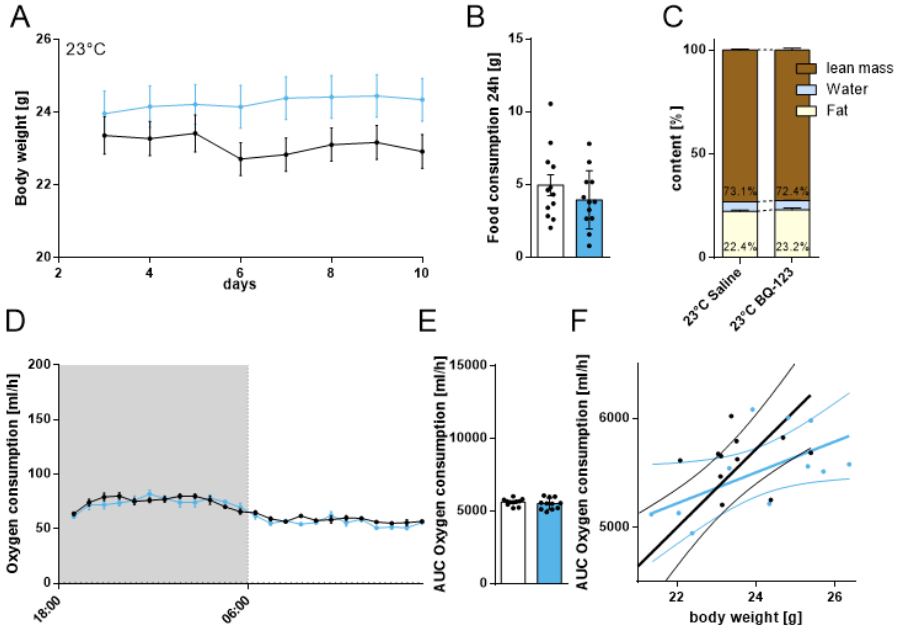

Figure 21 Physiological parameters and indirect calorimetric measurements after pharmacological inhibition of ETA using BQ-123 1mg/kg body weight for one week at 23 °C

Black/White: C57Bl6J WT animals treated with saline (0.9 % sodium chloride 5 µl/g body weight i.p). **Blue**: C57Bl6J WT animals treated with BQ-123 (1 mg/kg i.p. body weight). All animals received 7 daily treatments from day 3 to day 9. Body weight (**A**) during the 10-days experiment. Food consumption (**B**) during 24 h indirect calorimetric measurements and body composition measured by NMR prior to the animals' sacrifice (**C**). 24 h oxygen consumption measurement in a metabolic cage system at 23 °C (**D**), its area under the curve analysis (**E**) and ANCOVA with body weight (**F**). ±s.e.m. n=12, * p≤0.05 unpaired student's t-test/Mann-Whitney-test; i.p.: intraperitoneal, NMR: nuclear magnetic resonance

treated animals. Food consumption, energy expenditure and body composition were about equal (see Figure 21A-E). Correlation of body weight with oxygen consumption showed that slopes differed with p=0.0504 as shown in Figure 21F.

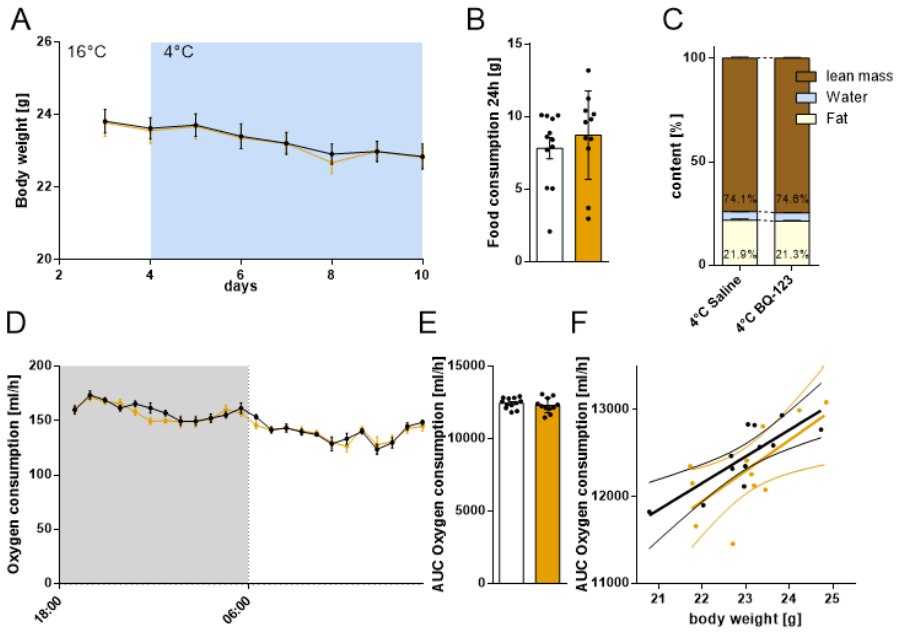

Figure 22 Physiological parameters and indirect calorimetric measurements after pharmacological inhibition of ETA using BQ-123 1mg/kg body weight during one week of cold exposure

Black/White: C57Bl6J WT animals treated with saline (0.9 % sodium chloride 5 µl/g body weight i.p.) and **Orange**: C57Bl6J WT animals treated with BQ-123 (1 mg/kg i.p. body weight) during the experiment of cold exposure. All animals received 7 daily treatments from day 3 to day 9. Body weight (**A**) during the 10-days experiment. Food consumption (**B**) during 24 h indirect calorimetric measurements and body composition measured by NMR prior to the animals' sacrifice (**C**). 24 h oxygen consumption measurement in a metabolic cage system at 23 °C (**D**), its area under the curve analysis (**E**) and ANCOVA with body weight (**F**). ±s.e.m. n=12, * p≤0.05 unpaired student's t-test/Mann-Whitney-test; i.p.: intraperitoneal, NMR: nuclear magnetic resonance

After 16 °C for 3 days of cold acclimatization and 7 days at 4 °C animals consumed similar amounts of food and exhibited the similar body weight and body composition (Figure 22A-C). Oxygen consumption measurements and respective ANCOVA did not uncover significant differences between treatment groups (Figure 22D-F).

Albeit not significant, slight differences in mRNA content were apparent for Edn1 (p=0.085), Pgc1a (p=0.089), Pparg (p=0.056), Fabp4 (p=0.063) in WATi and Ucp1 (p=0.054) in BAT. Tissue weight appeared unchanged upon treatment (Figure 23).

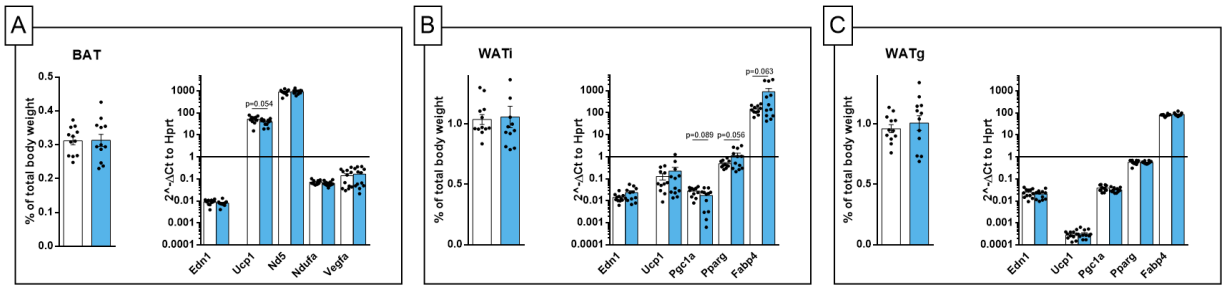

Figure 23 Adipose tissue analysis after pharmacological inhibition of ETA using BQ-123 1 mg/kg body weight for one week at 23 °C

White: C57Bl6J WT animals treated with saline (0.9 % sodium chloride 5 µl/g body weight i.p.). **Blue**: C57Bl6J WT animals treated with BQ-123 (1 mg/kg i.p. body weight). Analysis of brown adipose tissue (**A**) inguinal white adipose tissue (**B**) and gonadal white adipose tissue (**C**). Tissue weight is normalized to whole body weight. RT-qPCR analysis of thermogenic and adipogenic marker genes are quantified relative to Hprt. Edn1: Endothelin-1; Ucp1: Uncoupling protein 1; Ndufa: NADH-dehydrogenase; Nd5: NADH-ubiquinone oxireductase; Vegfa: Vascular endothelial growth factor A; Pgc1a: Pparγ-coactivator 1-α; Pparg: Peroxisome proliferator-activated receptor gamma; Fabp4: Fatty acid binding protein 4 (adipocyte protein 2) ±s.e.m. n=12, * $p \leq 0.05$ unpaired student's t-test/Mann-Whitney-test.

Adipose tissue morphology remained unchanged upon BQ-123 treatment as revealed by histological analysis (see Figure 24).

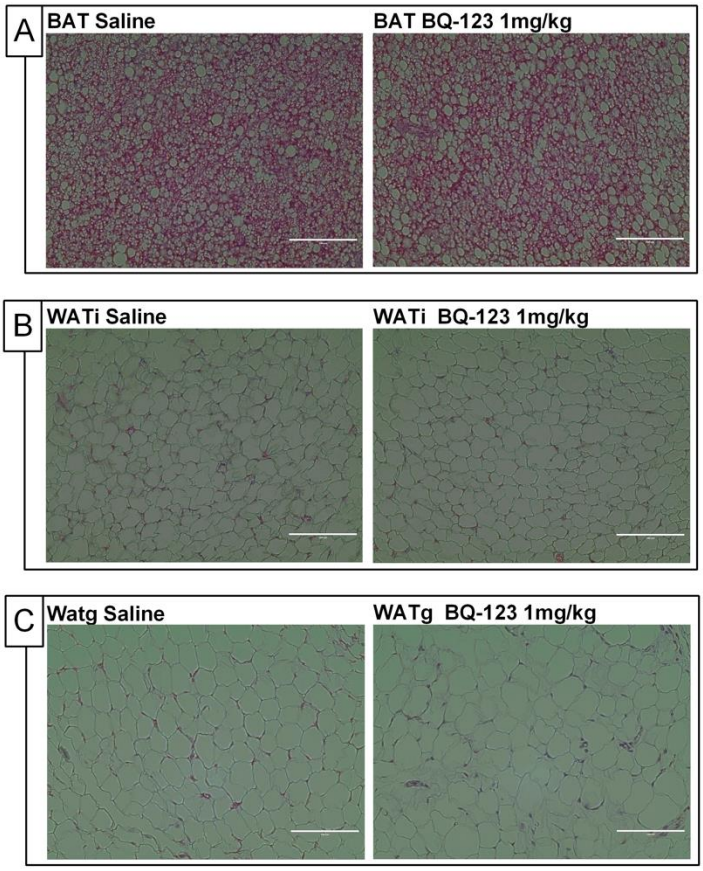

Figure 24 Histological analysis of adipose tissues after pharmacological inhibition of ETA using BQ-123 1 mg/kg body weight for one week at 23 °C

Histological analysis of brown adipose tissue (**A**) inguinal white adipose tissue (**B**) and gonadal white adipose tissue (**C**). Panel of images depict representative images of H&E stained tissue preparation at 40 x magnification. White bar corresponds to 100 µm, n=3.

Normalized tissue weight was not different between BQ-123 and control treatment (Figure 25A-C). Combined cold and BQ-123 treatment produced a highly significant 1.15± 0.04 fold increase of Ucp1 mRNA in BAT over control treatment (Figure 25A).

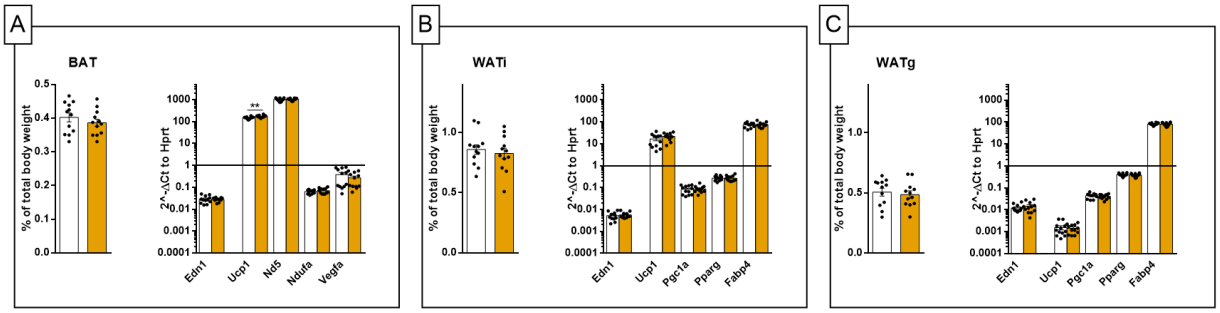

Figure 25 Adipose tissue analysis after pharmacological inhibition of ETA using 1 mg BQ-123/kg body weight in the treatment regime of sustained cold exposure for one week

White: C57Bl6J WT animals treated with saline (0.9 % sodium chloride 5 µl/g body weight i.p.). **Orange**: C57Bl6J WT animals treated with BQ-123 (1 mg/kg i.p. body weight). Analysis of brown adipose tissue (**A**) inguinal white adipose tissue (**B**) and gonadal white adipose tissue (**C**). Tissue weight is normalized to whole body weight. RT-qPCR analysis of thermogenic and adipogenic marker genes are quantified relative to Hprt. Edn1: Endothelin-1; Ucp1: Uncoupling protein 1; Ndufa: NADH-dehydrogenase; Nd5: NADH-ubiquinone oxireductase; Vegfa: Vascular endothelial growth factor A; Pgc1a: Pparγ-coactivator 1-α; Pparg: Peroxisome proliferator-activated receptor gamma; Fabp4: Fatty acid binding protein 4 (adipocyte protein 2) ±s.e.m. n=12, * p≤0.05 unpaired student's t-test/Mann-Whitney-test.

AT morphology remained unchanged upon BQ-123, assessed by Hematoxylin/Eosine-staining and immunohistological analysis of samples (Figure 26) derived from the corresponding other paired AT pad indicated elevated Ucp1 expression in BAT (Figure 26A lower panel).

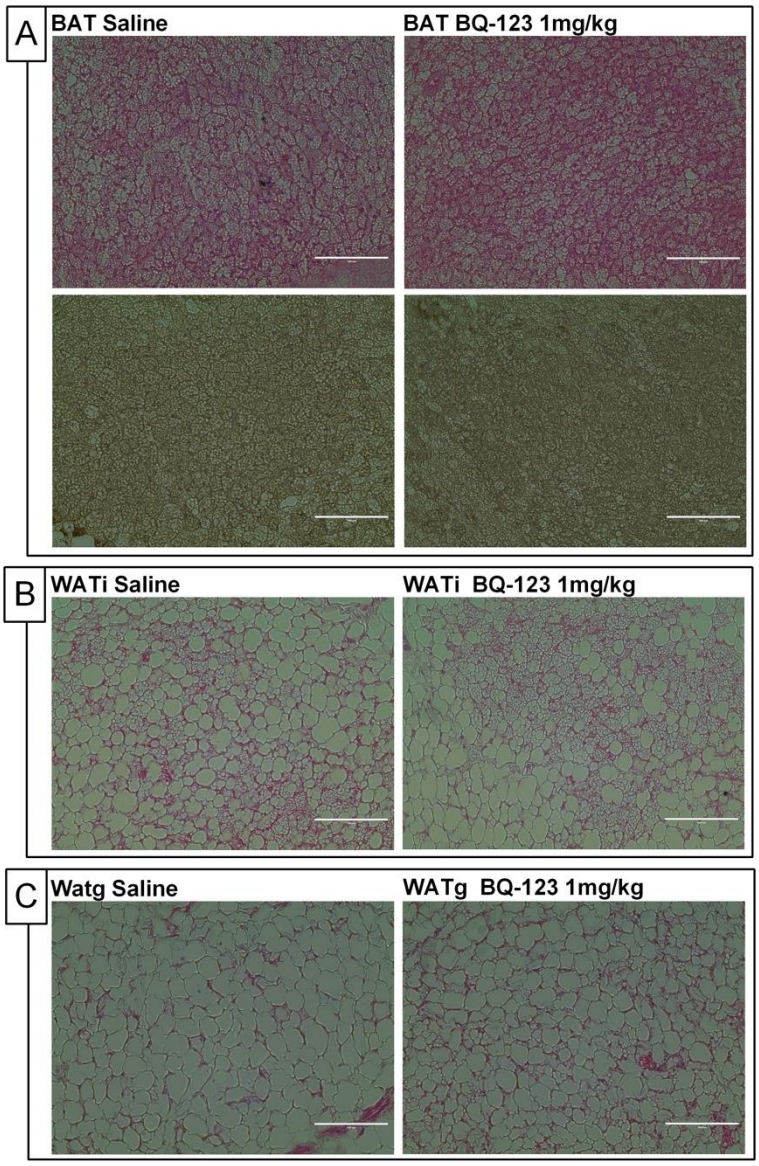

Figure 26 Histological adipose tissue analysis after pharmacological inhibition of ETA using 1 mg BQ-123/kg body weight in the treatment regime of sustained cold exposure for one week

Histological analysis of brown adipose tissue (**A**) inguinal white adipose tissue (**B**) and gonadal white adipose tissue (**C**). Upper Panel of images depict representative images of H&E stained tissue preparation at 40 x magnification. The lower panel of images display representative micrographs of immunohistochemical staining against UCP1. White bar corresponds to 100 µm, n=3.

4.5 | Metabolic characterization after genetic depletion of ET1-Receptor A in vivo

4.5.1 | Exposure of Ednra AT-KO animals to diet-induced obesity

Starting at the age of 8 weeks, animals received either HFD or CD for 12 weeks. The test groups were composed of animals with an adipocyte-specific depletion of ETA (Ednra AT-KO) and their respective ETA flox littermates.

Over the course of the 12-week control diet experiment, body weight gain in Ednra AT-KO animals and control group was similar (Figure 27A). Food intake, body composition, blood glucose levels and glucose tolerance testing produced no significant differences between tested groups (Figure 27A-F). No significant differences became apparent in indirect calorimetric measurements to quantify resting energy expenditure (Figure 27G-I) or maximal respiratory response (Figure 27J-K).

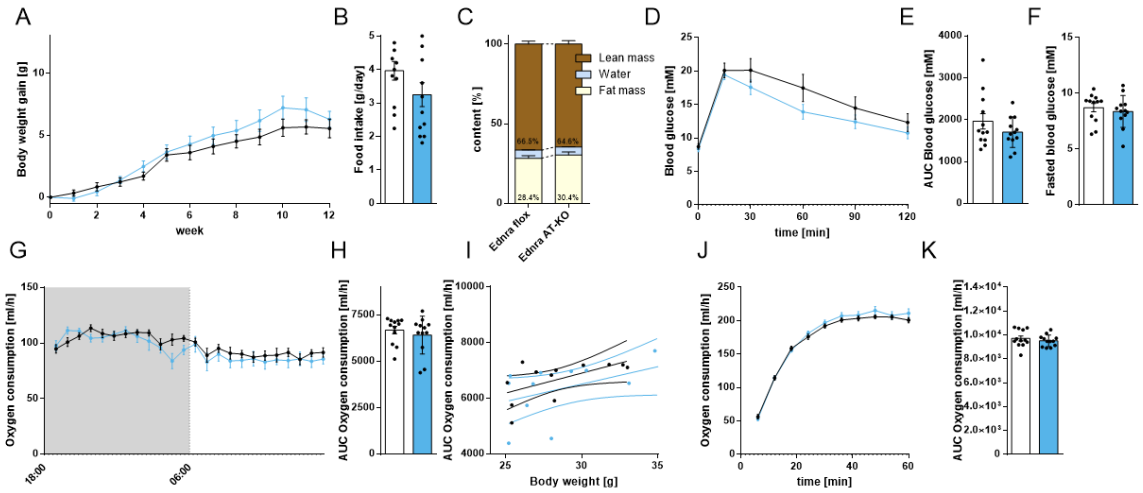

Figure 27 Physiological parameters and indirect calorimetric measurements of Ednra floxed and Ednra AT-KO animals after 12-week control diet experiment

Ednra floxed (**black**) and Ednra AT-KO (**blue**) animals having received control diet chow ad libido. Body weight gain (**A**) during the 12-week experiment. Food consumption (**B**) during 24 h indirect calorimetric measurements and body composition measured by NMR prior to the animals' sacrifice (**C**). Glucose tolerance test performed using 2 mg glucose/g fasted body weight in experiment-week 12 (**D**), its area under the curve analysis (**E**) and t=0 after a 5 h fasting interval (**F**). 24 h oxygen consumption measurement in a metabolic cage system (**G**), its area under the curve analysis (**H**) and ANCOVA with body weight (**I**). Maximal respiratory capacity as induced by 1 h cold exposure challenge at 4 °C and measured in metabolic cage system (**J**) and its quantification (**K**). ±s.e.m. n=12, * $p \leq 0.05$ unpaired student's t-test/Mann-Whitney-test; CL:CL 316,243, i.p.: intraperitoneal, NMR: nuclear magnetic resonance

Ednra-AT KO animals and their respective floxed littermates, which received HFD for 12 weeks showed transient differences in weight gain. Ednra AT-KO animals gained more weight, which was significant at experimental week 7 (Figure 28A). The average food intake was 1.23± 0.09 fold higher in the Ednra AT-KO group (Figure 28B). The experiment groups exhibited similar body composition (Figure 28C). Similarly, no significant difference was revealed by glucose tolerance testing. The mean response, as quantified by area under curve analysis, and mean fasting blood glucose levels were slightly lower in Ednra AT-KO animals (Figure 28C-F). Resting energy expenditure was similar between treatment groups (Figure 28G-H), but ANCOVA revealed a significant difference between slopes (Figure 28I). The maximal respiratory response, provoked by cold-exposure, revealed no significant differences between analyzed groups (Figure 28J-K).

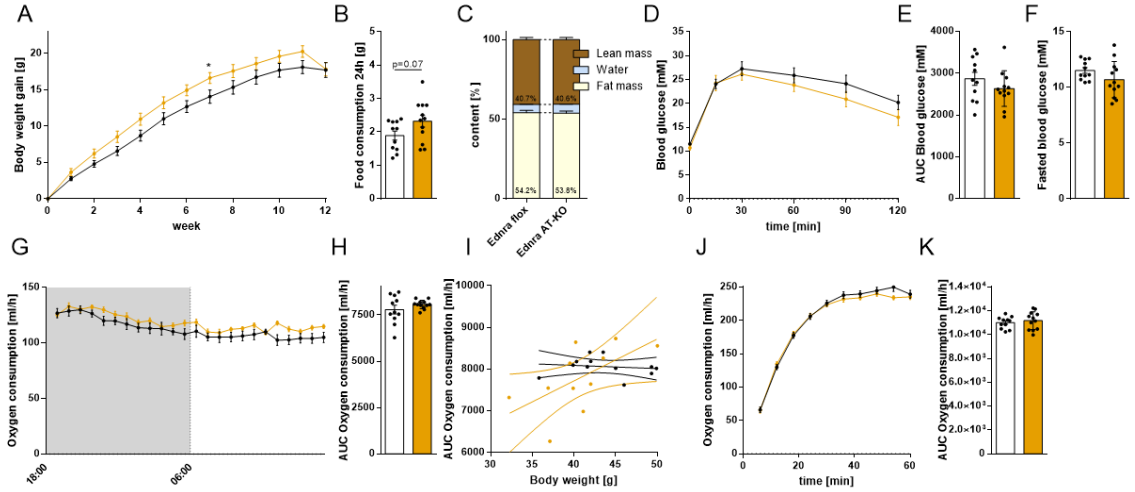

Figure 28 Physiological parameters and indirect calorimetric measurements of Ednra floxed and Ednra AT-KO animals after 12 weeks in a diet regime to induce obesity

Ednra floxed (**black**) and Ednra AT-KO (**orange**) animals having received high fat diet ad libido. Body weight gain (**A**) during the 12-week experiment. Food consumption (**B**) during 24 h indirect calorimetric measurements and body composition measured by NMR prior to the animals' sacrifice (**C**). Glucose tolerance test performed using 2 mg glucose/g fasted body weight in experiment-week 12 (**D**), its area under the curve analysis (**E**) and t=0 after a 5 h fasting interval (**F**). 24 h oxygen consumption measurement in a metabolic cage system (**G**), its area under the curve analysis (**H**) and ANCOVA with body weight (**I**). Maximal respiratory capacity as induced by 1 h cold exposure challenge at 4 °C and measured in metabolic cage system (J) and its quantification (K). ±s.e.m. n=11-12, * p≤0.05 unpaired student's t-test/Mann-Whitney-test; CL:CL 316,243, i.p.: intraperitoneal, NMR: nuclear magnetic resonance

Ednra AT-KO animals and Ednra floxed animals had similar AT weight, ex vivo basal lipolysis rates (Figure 29A-C upper panel) and AT morphology (Figure 30) after having received control diet for 12 weeks. RT-qPCR analysis revealed differences in mRNA expression of genes in the endothelin system, as well as adipogenic and inflammatory marker genes. Confirming the introduced genetic modification, Ednra AT-KO exhibited significantly less ETA transcript than their respective littermates in all adipose tissues analyzed. Tissue specific KO of Edrna under control of the adiponectin-cre promoter produced a highly significant reduction of 38.6± 7.0 % in BAT, 84.3± 2.0 % in WATi and 62.6± 5.1 % in WATg. In Addition, Endothelin receptor B mRNA (Ednrb) was reduced in BAT (42.9±5.7 %) and in WATi (36.8±10.3 %) of Ednra AT-KO animals (Figure 29A-B lower panel). In BAT of Ednra AT-KO animals mitochondrial marker genes Nd5 and Ndufa

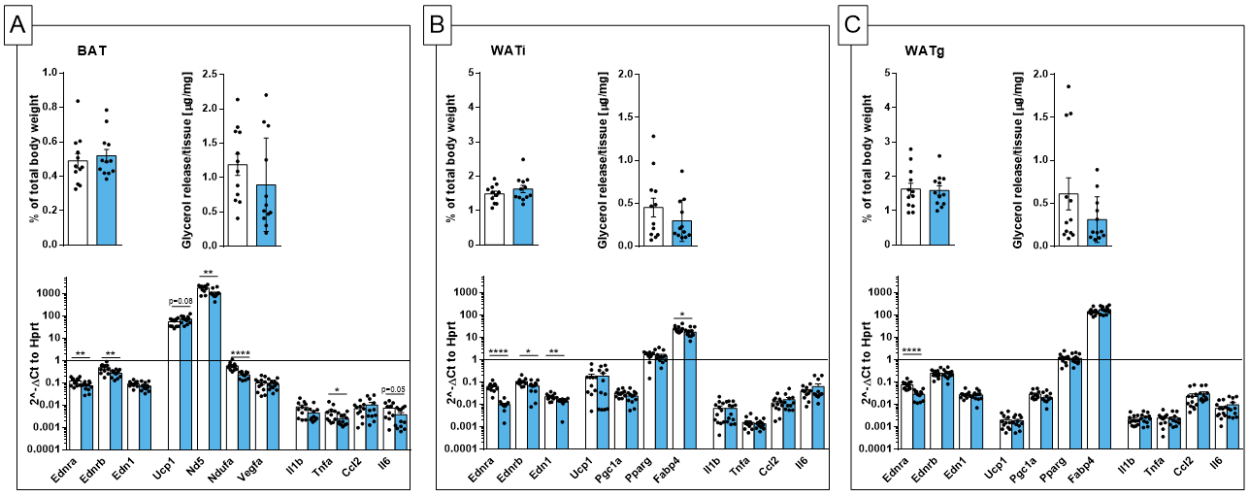

Figure 29 Adipose tissue analysis of Ednra floxed and Ednra AT-KO animals after a 12-week control diet experiment

Ednra floxed (**white**) and Ednra AT-KO (**blue**) animals having received control diet chow ad libidum. Analysis of brown adipose tissue (A) inguinal white adipose tissue (B) and gonadal white adipose tissue (C). Tissue weight is normalized to whole body weight. Glycerol release was assessed by ex vivo lipolysis immediately after the animals' sacrifice. RT-qPCR analysis of genes in the endothelin system, thermogenic, adipogenic and proinflammatory marker genes are quantified relative to Hprt. Ednra: Endothelin-1 receptor A; Ednrb: Endothelin-1 receptor B; Edn1: Endothelin-1; Ucp1: Uncoupling protein 1; Ndufa: NADH-dehydrogenase; Nd5: NADH-ubiquinone oxireductase; Vegfa: Vascular endothelial growth factor A; Il1b: Interleukin-1β; Tnfa: Tumor necrosis factor α; Ccl2: Chemokine ligand 2 (Monocyte chemoattractant protein 1); Il6:Interleukin 6; Pgc1a: Pparγ-coactivator 1-α; Pparg: Peroxisome proliferator-activated receptor gamma; Fabp4: Fatty acid binding protein 4 (adipocyte protein 2). ±s.e.m. n=12, * p≤0.05 unpaired student's t-test/Mann-Whitney-test

were highly significantly reduced (Nd5 41.0± 7.2 % and Ndufa 60.4± 3.6 %). Simultaneously, a tendency (p=0.08) towards elevated Ucp1 mRNA levels (1.33± 0.14 fold) was observed. Significantly reduced transcript levels of pro-inflammatory cytokine mRNA of tumor necrosis factor α (Tnfa reduced by 49.7± 8.2 %) and just below significance reduced (p=0.0503) interleukin 6 (Il6 reduced by 48.7± 12.9 %) were detected (Figure 29A). In WATi of Ednra AT-KO animals Ap2 mRNA was reduced by 27.4± 8.9 % and in addition, ET-1 mRNA levels were lowered by 35.5± 6.1 % (Figure 29B lower panel).

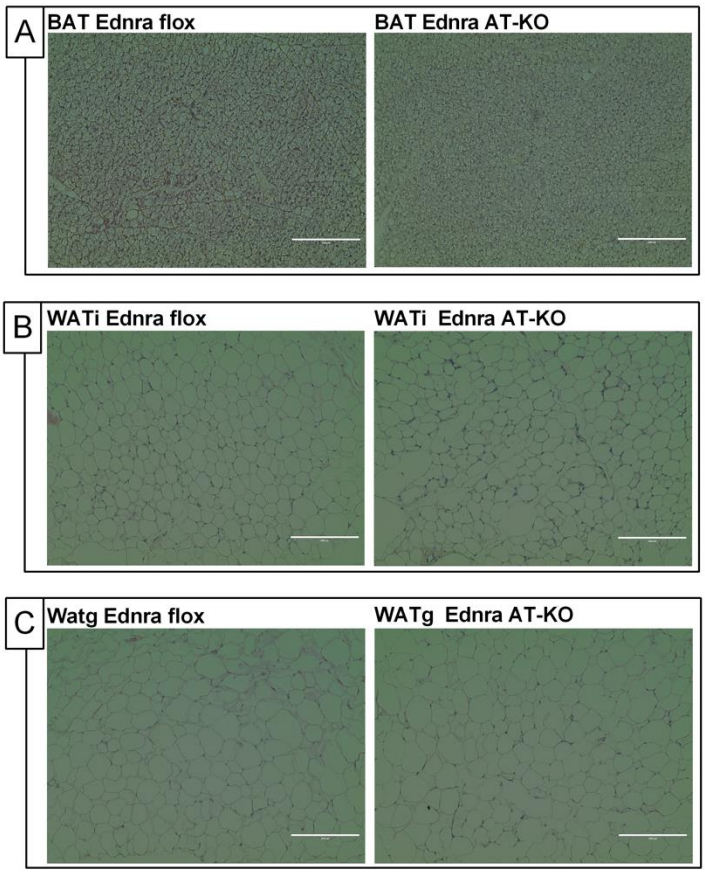

Figure 30 Histological analysis of adipose tissue of Ednra floxed and Ednra AT-KO animals after a 12-week control diet experiment

Analysis of brown adipose tissue (A) inguinal white adipose tissue (B) and gonadal white adipose tissue (C) Panel of images depict representative images of H&E stained tissue preparation at 20 x magnification. White bar corresponds to 200 µm. n=3

Ednra floxed and Ednra AT-KO animals, having received a HFD regime for the duration of 12 weeks, exhibited no apparent differences in AT weight, basal lipolysis rates or morphological changes (Figure 31) when probed for by H&E staining (Figure 32A-C). Ednra mRNA was highly significantly reduced in WAT-depots (by 94.4± 1.6 % in WATi and by 52.1± 4.1 % in WATg). No significant reduction of Ednra mRNA in BAT of Ednra AT-KO was observed. Additionally, a highly significant reduction by 76.8± 6.9 % of Ednrb mRNA was accompanied in WATi.

A 4.1± 1.2 fold increased monocyte chemotactic protein 1 transcript levels (Ccl2), was detected in BAT of Ednra AT-KO animals (Figure 31A). A trend towards increased Ucp1 and Pparγ mRNA levels and a significant increase of Ap2 mRNA levels (2.6±0.5 fold) was apparent in WATi. Representative images of anti-UCP1 staining of WATi depict more UCP1 positive areas than in Ednra floxed controls (Figure 32B).

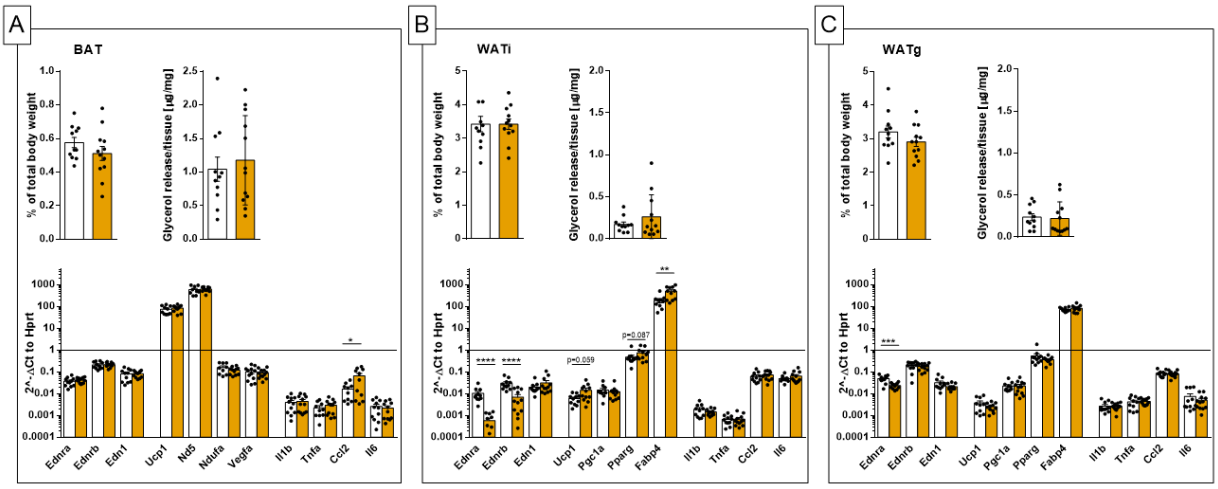

Figure 31 Adipose tissue analysis of Ednra floxed and Ednra AT-KO animals after a 12-week high fat diet

Ednra floxed (**white**) and Ednra AT-KO (**orange**) animals having received high fat diet chow ad libidum. Analysis of brown adipose tissue (**A**) inguinal white adipose tissue (**B**) and gonadal white adipose tissue (**C**). Tissue weight is normalized to whole body weight. Glycerol release was assessed by ex vivo lipolysis immediately after the animal's sacrifice. RT-qPCR analysis of genes in the endothelin system, thermogenic, adipogenic and proinflammatory marker genes are quantified relative to Hprt. Ednra: Endothelin-1 receptor A; Ednrb: Endothelin-1 receptor B; Edn1:Endothelin-1; Ucp1: Uncoupling protein 1; Ndufa: NADH-dehydrogenase; Nd5: NADH-ubiquinone oxireductase; Vegfa: Vascular endothelial growth factor A; Il1b: Interleukin-1β; Tnfa: Tumor necrosis factor α; Ccl2: Chemokine ligand 2 (Monocyte chemoattractant protein 1); Il6:Interleukin 6; Pgc1a: Pparγ-coactivator 1-α; Pparg: Peroxisome proliferator-activated receptor gamma; Fabp4: Fatty acid binding protein 4 (adipocyte protein 2). ±s.e.m. n=12, * p≤0.05 unpaired student's t-test/Mann-Whitney-test

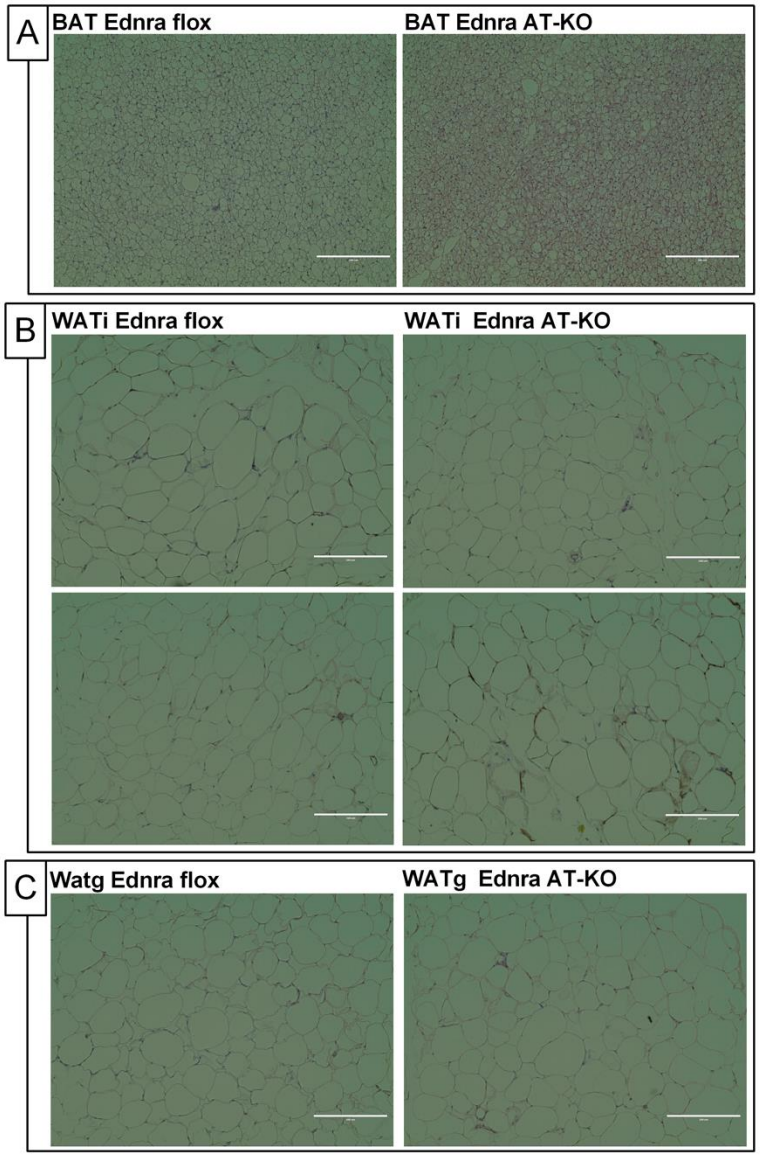

Figure 32 Histological analysis of adipose tissue of Ednra floxed and Ednra AT-KO animals after a 12-week high fat diet

Histological analysis of brown adipose tissue (**A**) inguinal white adipose tissue (**B**) and gonadal white adipose tissue (**C**). Panel of images depict representative images of H&E stained tissue preparation at 20 x magnification. The lower panel of images display representative micrographs of immunohistochemical staining against UCP1. White bar corresponds to 200 µm. n=3.

4.5.2 | Chronic cold-exposure of Ednra AT-KO animals

To investigate the role of ET-1 via ETA during sustained cold exposure, Ednra AT-KO animals and their respective Ednra floxed littermates were exposed to 16 °C for 3 days and 4 °C for 7 days.

Littermates used in this experiment show a tendency towards reduced body weight in the Ednra AT-KO group (Figure 33A). Ednra AT-KO animals exhibited higher food-intake, but conversely had less fat and increased lean mass as compared to their Ednra floxed littermates (Figure 33B-C). Indirect calorimetric measurements indicated a lower oxygen consumption by animals in the Ednra KO group (Figure 33D-F).

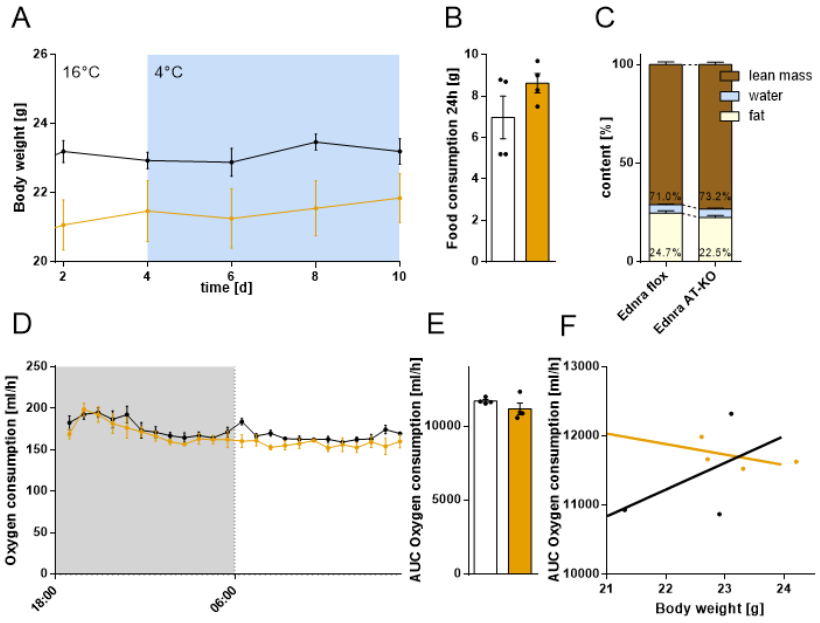

Figure 33 Physiological parameters and indirect calorimetric measurements of Ednra AT-KO animals and their corresponding Ednra flox littermates during and after sustained cold exposure for one week

Black: Ednra floxed and **Orange**: Ednra AT-KO animals during sustained cold exposure. Body weight (A) during the 10-days experiment. Food consumption (B) during 24 h indirect calorimetric measurements and body composition measured by NMR prior to the animals' sacrifice (C). 24 h oxygen consumption measurement in a metabolic cage system at 23 °C (D), its area under the curve analysis (E) and ANCOVA with body weight (F). ±s.e.m. n=4, * p≤0.05 unpaired student's t-test/Mann-Whitney-test NMR: nuclear magnet resonance

After sustained cold-exposure for 7 days at 4 °C, no significant difference in tissue weight was measured. However, a tendency towards increased mass of BAT and reduced mass of WAT could be observed. Ednra mRNA was reduced in WATi of Ednra AT-KO animals (by 73.8± 3.1 %) and WATg (by 72.8± 2.8 %). The reduction of Ednra mRNA in BAT was not significant (Figure 34A-C).

The average of Ucp1 transcript is higher in BAT of Ednra AT-KO and significantly lower in its WATi (by 45.9± 3.6 %). This was not trivially detected by means of immune-histochemical staining (Figure 35B lower panel). The overall Ucp1 expression in WATi after cold-exposure was high in both groups (Figure 34B and Figure 35B).

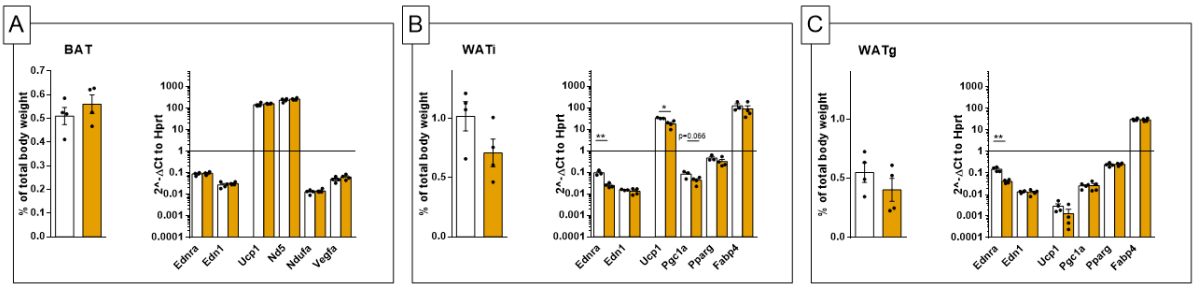

Figure 34 Adipose tissue analysis of Ednra AT-KO animals and their corresponding Ednra floxed littermates after sustained cold exposure for one week

Black: Ednra floxed and **Orange**: Ednra AT-KO after sustained cold exposure. Analysis of brown adipose tissue (**A**) inguinal white adipose tissue (**B**) and gonadal white adipose tissue (**C**). Tissue weight is normalized to whole body weight. RT-qPCR analysis of genes in the endothelin system, thermogenic, adipogenic marker genes are quantified relative to Hprt. Ednra: Endothelin-1 receptor A; Edn1: Endothelin-1; Ucp1: Uncoupling protein 1; Ndufa: NADH-dehydrogenase; Nd5: NADH-ubiquinone oxireductase; Vegfa: Vascular endothelial growth factor A; Pgc1a: Pparγ-coactivator 1-α; Pparg: Peroxisome proliferator-activated receptor gamma; Fabp4: Fatty acid binding protein 4 (adipocyte protein 2). ±s.e.m. n=4, * p≤0.05 unpaired student's t-test/Mann-Whitney-test.

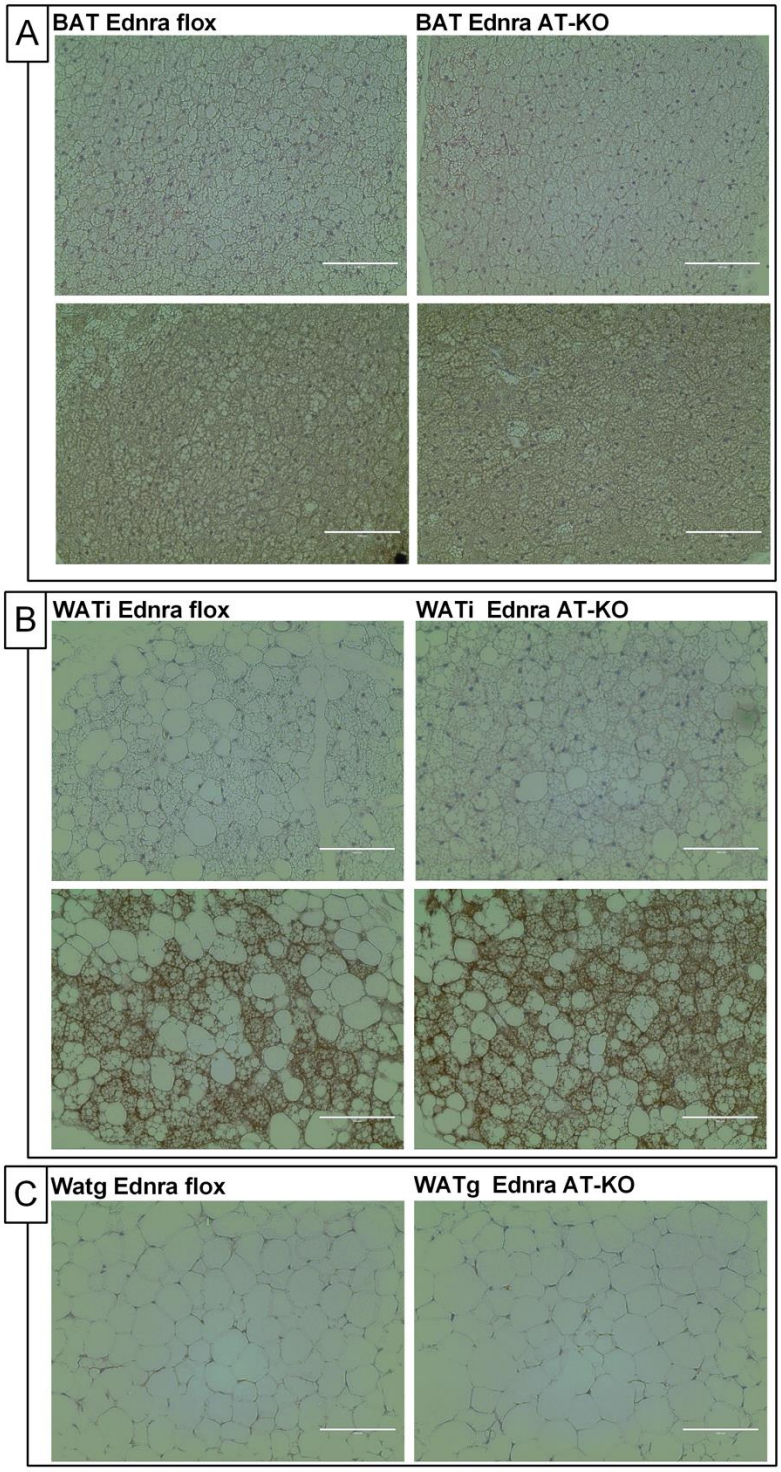

Figure 35 Histological analysis of adipose tissue of Ednra AT-KO animals and their corresponding Ednra floxed littermates after sustained cold exposure for one week

Panel of images depict representative images of H&E stained tissue preparation at 20 x magnification. The lower panel of images display representative micrographs of immunohistochemical staining against UCP1. White bar corresponds to 200 µm.

5 | Discussion

5.1 | The source of Endothelin-1 in BAT

To address the source of ET-1 in BAT, two experimental approaches were chosen: fractionation and immunohistochemical analysis. In the fractionation experiment, adipocytes separated naturally by centrifugation after digestion, due to the higher buoyancy of the cells because of their lipid-content. Cells with low buoyancy formed a pellet at the bottom of the reaction container and were further purified for EC surface marker expression by affinity purification.

These fractionation experiments indicate higher intracellular levels of ET-1 and ETA mRNA in isolated ECs as compared to the lipid-rich, adipocyte-containing fraction in BAT. This finding is in accordance with the current literature, in which ECs are being described as the main producer of ET-1 (as reviewed by Davenport et al., 2016). However, emerging evidence indicates that other cell types like epithelial cells (van de Water et al., 2006), monocytes (Ehrenreich et al., 1993) or astrocytes (as reviewed by Hostenbach et al., 2016) can produce ET-1 during pathophysiological conditions and pathogenesis of infectious diseases (as reviewed by Freeman et al., 2014; and reviewed by Kowalczyk et al., 2015). In addition, BA are able to produce ET-1 in a potentially autocrine manner (Klepac et al., 2016).

Alternatively in the immunohistochemical approach, antigens were detected on thin section of fixed BAT using antibodies. In accordance, I observed ET-1 immunoreactivity and transcript expression, in both EC and BA. Although ET-1 transcripts were significantly higher in isolated fractions of EC, the corresponding immunohistochemistry implies BA to be a source of ET-1 as well. Moreover, the cell volume and number of adipocytes in the AT is expected to be higher than those of ECs. For this reason I hypothesize that both EC and BA contribute to ET-1 in BAT.

5.2 | cAMP reducing ET-1 mRNA is partially mediated through nitric oxide

This subchapter focuses on adipocytes and their regulation by cAMP, which is a second messenger liberated in rodent AT upon cold-exposure (Habara, 1989). During cold-exposure NE is released from sympathetic nerve endings, which in turn induces cAMP in adipocytes via G_S-coupled adrenergic receptors. Recently published results indicate a negative regulation and reduced secretion of ET-1 by NE in BA and preBA in vitro (Klepac et al., 2016).

Intracellularly released cAMP can produce many different cellular responses. The activation of both classical cAMP-receptors: PKA and Epac are well studied pathways (as reviewed by Cheng et al., 2008). Selective agonists, which are directed against PKA or Epac produced a distinct response in BA at equimolar concentration. Selective activation of PKA by 6-MB-cAMP was more effective at diminishing ET-1 transcript levels than selective activation of Epac. By contrast, neither pharmacological inhibition of catalytic and regulatory subunit of PKA nor genetic depletion of Epac did rescue the effect induced by 8Br-cAMP. I could show that ET-1 mRNA reduction via cAMP is both dependent on PKA and Epac. Experiments using antagonists to inhibit cAMP receptors PKA and Epac indicate either that (1) cAMP receptors compensate for each other's function to mediate cAMP signaling or (2) parallel signaling through other independent signaling pathways is important.

Beyond its classical signaling pathways, cAMP can activate transcription of Edn1 or influence the abundance of ET-1 directly. Intracellular cAMP and calcium ions are known to stimulate exocytosis of Weibel-Palate bodies, which are carriers for multiple secretory factors, including ET-1 (as reviewed by Schillemans et al., 2019). Moreover, secreted ET-1 is known to regulate its own transcription via ETB and protein kinase C signaling in cell cultures of porcine aortic ECs (Farhat et al., 2008). Therefore, the influence of extracellular ET-1 on its own transcription was studied. ET-1 significantly modulates ET-1 mRNA levels in preBA. Opposed to the effect described by (Farhat et al., 2008) in EC, I observed an increase of ET-1 mRNA levels by extracellular ET-1.

Additionally, I tested, whether or not the observed reduction of ET-1 mRNA is mediated through cAMP-activated calcium-channels. For this, an intracellular Ca^{2+} scavenger

compound was utilized to chelate released calcium-ions. As a result, the ET-1 mRNA reduction triggered by cAMP could not be blocked by chelating of intracellular calcium. This indicates, that release of calcium ions is not an essential step of cAMP mediated ET-1 mRNA downregulation.

Transcriptional control of thermogenic genes are known to be regulated by class I and II HDACs in BA within hours (Li et al., 2016; Rajan et al., 2018). It could be possible, that cAMP triggers activation of the HDAC-system and thus suppress ET-1 mRNA levels. Using a HDAC inhibitor at different concentrations, histone modification via HDACs was suppressed. It became apparent that ET-1 transcription was sensitive to HDAC-inhibition, which is in accordance to previous findings in bone-marrow derived macrophages (Shakespear et al., 2013). The effect produced by cAMP was not reversed upon addition of HDAC-inhibitor TSA. From this, I conclude that the effect of ET-1 mRNA reduction is not primarily dependent of HDAC-activity.

Besides the transcriptional control, post-transcriptional regulation is a well described mechanism for ET-1 mRNA, which is summarized in section 1.3. Several effector proteins, which target the untranslating region within mRNA for degradation, belonging to the HuR and TTPs protein family, are activated by cAMP (Klöss et al., 2004; Rataj et al., 2016). I hypothesized that cAMP mediated ET-1 mRNA downregulation is triggered by accelerated mRNA decay due to post-transcriptional mechanisms. To suppress transcription, Act D was utilized, which is a potent inhibitor of RNA-polymerases. After addition of Act D, the resulting ET-1 mRNA decay was compared to the decay in presence of cAMP over 4 hours. I could not observe modulations of RNA-decay induced by cAMP within 4 h. Therefore I conclude, that the observed mechanism of ET-1 mRNA reduction via cAMP is not induced post-transcriptionally.

NE is known to induce a dose- and time-dependent production of NO in BA of rats (Nisoli et al., 1997). NO is a functional antagonist of ET-1 and is known to directly reduce ET-1 mRNA upon exposure in EC (Kelly et al., 2004). Furthermore, cAMP can induce NO-production via PKA and Epac in human EC (García-Morales et al., 2014). I hypothesize a cAMP-induced release of NO (**A**), which caused a reduction of ET-1 mRNA (**B**). In line with my hypothesis, DETA NONO induced a dose-dependent reduction of ET-1 mRNA (**B**). The pharmacological antagonist L-NAME inhibits NOS, which are the enzymes producing NO. Simultaneous treatment of 8Br-cAMP and L-NAME produced a less pronounced reduction of ET-1 mRNA as compared to 8Br-cAMP alone. This indicates that 8Br-cAMP activates NOS in the utilized preBA cell-system (**A**) and that the released NO is partially responsible for ET-1 mRNA reduction and accounts for 12 % of basal ET-1 mRNA levels. In conclusion, cAMP-induced downregulation of ET-1 mRNA is dependent on NO production to an extend of 12 % in preBA (Figure 36).

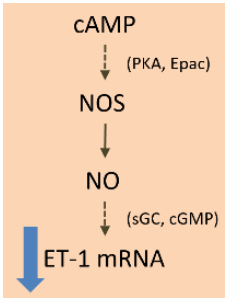

Figure 36 Proposed mechanism of partial ET-1 mRNA downregulation by cAMP in preBA

cAMP: cyclic adenosine monophosphate, NOS: nitric oxide synthase, NO: nitric oxide, PKA: protein kinase A, Epac: Exchange factor directly activated by cAMP 1, sGC: soluble gunylatcyclase, cGMP: cyclic guanosine monophosphate

5.3 | ET-1 mRNA is differentially regulated in brown adipose tissue derived microvascular endothelial cells during cold-exposure

Tissue digestion and MACS of fat tissues yielded elution fractions of cells with a similar set of surface marker expression. These populations of cells were found after control- as well as cold-exposure treatment of animals using FACS data analysis. But it became apparent that the content of these cell populations varied by the type of digested tissue. Thus, the isolation-process was primarily dependent on tissue type, rather than treatment. The overall yield per tissue weight of AT-MEC was higher in BAT than in WAT. This is in accordance with findings by Frazier et al., 2018, who showed that younger male mice have about 50 % more EC-like cells in SVF of BAT as compared to WAT. Interestingly, yield increased in WATi and decreased in BAT after cold-exposure, which points towards tissue remodeling upon sustained cold-stimulus. Principal component analysis shows primarily clustering by tissue-type. WATi and WATg cluster together, while BAT forms its own distinct entity. One could hypothesize that the microenvironment of AT-MEC within the WATi and WATg are more alike to each other than to the BAT. Based on this assumption, I would attribute the observed transcriptomic differences to the microenvironment (as reviewed by Aird, 2007; Minami et al., 2019), which might be the dominant factor governing AT-MEC heterogeneity.

Opposed to results obtained in vitro by stimulation by intracellular cAMP-elevation (see Figure 9), acute and sustained cold-exposure (see Figure 13 and Figure 14) produced an upregulation of ET-1 mRNA in BAT/BA/EC in vivo. Therefore the in vitro-models might lack aspects, which are crucial for the regulation in vivo. Transient hypoxia and subsequent transcriptional regulation by Hif-1a is a mechanism present in vivo and absent in vitro, which was recently described to induce ET-1 mRNA in hypoxic adipocyte cell culture (Rivera-Gonzalez et al., 2020). Similar effects of heightened ET-1 mRNA levels were observed after intermittent hypoxia and in WA tissue culture (Briançon-Marjollet et al., 2016).

5.4 | Antagonism of Endothelin-1 Receptor A induces transient weight loss and enhanced UCP1 expression after cold-exposure

Since its characterization by Yanagisawa et al., 1988 as an endothelium-derived vasoconstrictive factor, ET-1 has been studied in the context of cardiovascular and inflammatory disease. More recently the focus shifted towards adipocyte differentiation: ET-1 is known to inhibit adipogenesis of preWA (Lien et al., 2016) and preBA via ETA (Klepac et al., 2016) in vitro. My hypothesis is based on the inhibitory effect ET-1 on adipocyte differentiation and its reversal by inhibition of the respective receptor (ETA) in vitro. Furthermore, inhibition of ETA with BQ-123 enhanced differentiation of BA as measured by UCP1 expression in differentiated adipocytes. I therefore expected to observe elevated brown adipogenic marker expression, increased differentiation and recruitment of BA, increased whole energy expenditure and thus protection from DIO and accompanied co-morbidity in vivo.

To inhibit the molecular interaction of ET-1 and ETA, the well-established ETA-inhibitor BQ-123 was chosen. It is a cyclic penta-peptide with reversible competitive antagonist behavior and it has a high selectivity profile of ETA over ETB (Ihara et al., 1995; Vigne et al., 1993). BQ-123 was repeatedly utilized in animal studies to successfully induce acute (Warner et al., 1994) and/or chronic (Polak et al., 2018) ETA-antagonism by e.g. repeated intraperitoneal injections for up to 4 weeks (Alrashdi et al., 2018). BQ-123 is a “gold standard”, commonly used to reference ETA-treatment efficacy of new antagonists (Haque et al., 2013), tested in ascending doses in humans (Spratt et al., 2001) and often used to investigate ET-1 mediated vasoconstrictive tone in human forearm studies (Cameron et al., 2020).

Table 17 Summary of significant effects achieved by pharmacological intervention. Changes are depicted by arrows relative to control treatment

Endothelin-1 Receptor A antagonism: BQ123 1 mg/kg			
Treatment	Tissue	RT-qPCR	Metabolic characterization
Control diet +/- BQ-123	BAT WATi WATg	Edn1↑ Vegfa↓ Fabp4↑	Motility 23°C↑
High fat diet +/- BQ-123	BAT WATi WATg		Transient weight loss Motility 23°C↑ Motility acute 4°C↓
23 °C Control treatment +/- BQ-123	BAT WATi WATg		
4 °C Cold-exposure treatment +/- BQ-123	BAT WATi WATg	Ucp1↑	

Deviant from my original hypothesis, only transient weight loss was observed during the HFD feeding experiment week 3-7. Conflictingly, neither elevation of BA marker genes, nor increased energy expenditure was observed. The final resulting body weight, fat mass and glucose sensitivity remained unchanged upon BQ-123 treatment. Based on this data, I conclude that ETA-receptor antagonism-treatment using BQ-123 does not prevent the DIO-phenotype by using HFD. BQ-123 treatment altered spontaneous locomotor activity at RT and in response to acute cold exposure.

I tested the hypothesis, whether or not BQ-123-treatment can enhance BA-differentiation during sustained cold-exposure. Sustained cold-exposure is a treatment which induces remodeling of BAT. More specifically, preBA-proliferation and subsequent differentiation to BA during cold-exposure is induced in BAT during cold-acclimatization (Bukowiecki et al., 1986).

I hypothesize enhanced BA differentiation, as assessed by BA-marker expression and increased whole body energy expenditure due to an increased BA-number. Indeed, Ucp1 mRNA content of BAT was slightly (1.15± 0.04 fold), but highly significantly, increased upon BQ-123 treatment. Furthermore, immunohistochemical analysis parallels the findings on mRNA level. Whole body energy expenditure was not impacted by treatment with BQ-123. On this basis my initial hypothesis has merit. I could show increased BA-marker mRNA expression, although, there was no measurable difference in whole body energy expenditure.

Energy expenditure was measured during 4 °C cold-exposure experiment, which provoked a very high rate of respiration and energy expenditure. Since the BA-marker elevation produced by ETA-antagonism is quantitatively little, one may measure resting energy expenditure after reacclimatizing the animals back to 23 °C. According to my hypothesis, BQ-123 treated animals should retain more Ucp1 after reacclimatizing to 23 °C. This could prove that the small difference in Ucp1 transcript translates to a relevant difference in basal oxygen consumption. This might not have been apparent at peak respiratory conditions at 4 °C before.

5.5 | Adipocyte-specific deletion of Endothelin-1 Receptor A does not protect from diet-induced obesity

Similarly to the pharmacological approach, I based my hypothesis on previous findings in vitro. I expected to achieve beneficial effects by genetically ablating ETA and thus inhibit the action of ET-1. More specifically, I expected to observe enhanced BA-marker expression, increased differentiation and recruitment of BA, increased whole energy expenditure and thus protection from DIO and accompanied co-morbidity in a mouse model with a targeted deletion of Ednra.

To target ETA, Ednra-floxed animals (generated by Kedzierski et al., 2003) were crossed with a mouse line, which expressed the cre recombinase under the control of the adiponectin promoter. Detectable adiponectin protein expression is indirect proof of its promotor activity and Cre-recombinase expression. The moment at which adiponectin surfaces, marks the time point at which cells express the cre recombinase. The recombinase excises coding regions of the Ednra gene, which are flanked by its recognition sequences. As a result, only functionally inactive ETA should be produced in adiponectin-expressing cells of Ednra-AT KO animals. In mice, adiponectin expression was detected during terminal differentiation of adipocytes in vitro (day 0 of primary preBA culture isolated from 2-3 week old pups) and embryogenesis of BAT in vivo (E16.5) (Fujimoto et al., 2005). It was suggested by Shao et al 2016 that the time point of adiponectin expression in differentiation events of adipocytes is dependent on the animals' developmental stage. The adiponectin promoter is active earlier in fetal adipocyte differentiation than in adult animals. This was shown by comparison of the

inducible versus constitutive active adiponectin-cre-promoter-driven expression of a transcription factor, essential for terminal differentiation of adipocytes (Shao et al., 2016). The adiponectin cre mouse lines were utilized in various studies to both study effects in differentiating and in mature adipocytes (Z. V Wang et al., 2010 and reviewed by Q. A. Wang et al., 2014).

Table 18 Summary of significant effects achieved by cre-mediated genetic ablation of Endothelin receptor A under control of the adiponectin promoter. Changes are depicted by arrows relative to control treatment

Endothelin-1 Receptor A genetic depletion			
Treatment	Tissue	RT-qPCR	Metabolic characterization
Control diet +/- Adipo-Cre	BAT WATi WATg	Ednra↓ Ednrb↓ Nd5↓ Ndufa↓ Tnfa↓ Il6↓ Ednra↓ Ednrb↓ Fabp4↓ Edn1↑ Ednra↓	
High fat diet +/- Adipo-Cre	BAT WATi WATg	Ccl2↑ Ednra↓ Ednrb↓ Fabp4↑ Ednra↓	Transient weight gain
4 °C Cold-exposure treatment +/- Adipo-Cre	BAT WATi WATg	- Ednra↓Ucp1↓ Ednra↓	

In my experiment, mRNA of ETA was successfully ablated and thus reduced expression of intact ETA mRNA in RT-qPCR analysis of whole tissue lysates of adipose tissues. For example the 19-week old Ednra AT-KO animals utilized in the CD study exhibited significantly less intact ETA-transcript as compared to ETA-floxed littermates (38.6± 7.0 % in BAT, 84.3± 2.0 % in WATi and 62.6± 5.1 % in WATg). An exception was the BAT-analysis in the HFD group. This might be attributed to differential turn-over rates in AT-depots induced by high-fat feeding (reviewed by Kahn et al., 2019) or lower adiponectin promoter activity in preBA and BA. As BAT is highly vascularized compared to WAT, this hypothesis is hard to prove or disprove. ECs strongly express ETA and the high EC-content could therefore partly mask the genetic ablation in BA.

Ednra-depletion was accompanied by Ednrb downregulation in CD-BAT, WATi and HFD-WATi (Table 18). So far, no co-regulatory effect of ETA and ETB has been described in the literature. This effect is potentially causatively linked and ETA-signaling may partially sustain ETB-transcription in the adipose tissue in vivo.

In BAT, mitochondrial markers are significantly reduced upon ETA-ablation, while Ucp1 has a tendency to be increased. Mitochondrial and thermogenic gene expression have been shown to be induced together through Pgc1a in BA-differentiation (reviewed by Pellegrinelli et al., 2014). In this specific case, the thermogenic gene Ucp1 tends to be increased while the mitochondrial genes like Nd5 and Ndufa are reduced. ET-1 is known to control mitochondrial gene expression in retinal ganglia cells (Chaphalkar et al., 2020), mt-eNOS translocation in pulmonary arterial ECs (Sun et al., 2014) and induce mitochondrial fission (C. Chen et al., 2017). By ablating ETA in adipocytes, any postulated physiological ET-1 signaling to mitochondria would have been ablated as well. As a result, mitochondrial function could have been altered in adipocytes with high mitochondrial content, like BA. Further studies on mitochondrial morphology and gene expression of Ednra AT-KO are needed in order to verify this hypothesis.

ET-1 is known to induce lipolysis via ETA in WAT. Genetic ablation of ETA might have reduced basal lipolysis and this could explain slightly increased adiposity of Ednra AT-KO in my CD study (2 % at 19 weeks) and previous studies, reporting basally increased adiposity in animals (4.1 % 24 weeks) with an adipocyte-specific knock-out (KO) of the ETA (Rivera-Gonzalez & Speed, 2020). Following this line of argumentation, increased weight gain during the HFD study could be explained by ET-1 effects.

I observed reduced interleukin-6 mRNA in BAT of Ednra AT-KO animals. ET-1 is known to strongly induce il6-transcription and secretion in 3T3L1 (white adipocyte) tissue culture, which could be reversed by the ETA-antagonist BQ-123 (Chai et al., 2009). I hypothesize the existence of a similar mechanism in BA and thus attribute il6-reduction to a lack of ETA signaling in vivo.

Tnfa and Il6 are typical factors derived from AT macrophages in crown-like structures (Strissel et al., 2007). Downregulation in Ednra in control diet animals might simply represent a reduced number of crown-like structures and tissue inflammation. In WATi, Ap2-transcript levels are reduced upon KO of Ednra, which is similar to the tendency observed in the BQ-123-treated animals in the control diet regime (see Figure 17).

Although not significant, metabolic characterization indicates increased food-intake, ameliorated glucose metabolism and increased oxygen consumption of Ednra AT-KO

animals (Figure 28). In contrast to the situation of animals having received CD, BAT of Ednra AT-KO showed increased Mcp-1 mRNA (Ccl2) levels after HFD. Mcp-1 upregulation indicates infiltration of classically activated macrophages. RT-qPCR analysis of WATi showed a highly significant increase of Ap2 and increase of Ucp1 and Pparγ transcript levels just below significance ($p=0.059$ and 0.087). This trend towards AT-browning was consistently reflected by increased UCP1-immunoreactivity in tissue sections of WATi from Ednra AT-KO animals (Figure 31). None of these effects were apparent in WATi of BQ-123-treated animals (see Figure 19).

In Ednra AT-KO animals, who were exposed to sustained cold environment, a trend towards increased Ucp1-levels in BAT and reduced Ucp1 mRNA levels in WATi became apparent in my experiments. Clearly, further experiments are warranted to reach a higher level of confidence since only 4 animals per group were analyzed so far. Nevertheless, this trend observed in BAT of Ednra AT-KO animals after sustained cold-exposure parallels the observation made in the animal model of pharmacological antagonism.

6 | Summary

Overall, I found cyclic adenosine monophosphate (cAMP)-mediated downregulation of endothelin-1 (ET-1) mRNA to have a different selectivity for exchange factor directly activated by cAMP 1 (Epac) and the protein kinase A (PKA)-signaling in brown adipocytes in vitro. Equimolar concentrations of selective agonists of Epac and PKA induced distinct effects. Involvement of Epac-signaling was confirmed by cAMP-treatment in an Epac-KO cell line. Furthermore, part of the induced effect by cAMP is antagonizable via L-NAME and therefore indicates the involvement of nitric oxide in the process. In addition to the in vitro-effect, ET-1 is positively regulated by chronic cold-exposure in endothelial cells in BAT in vivo. Moreover, short-term cold-exposure induces ET-1 mRNA as quantified by whole tissue real time quantitative polymerase chain reaction analysis. Antagonism of ET-1 signaling at the respective level of the Endothelin-1 receptor A (ETA) enhanced differentiation of brown adipocytes in vitro, which was quantified by increased brown adipocyte-marker expression. Based on the previous in vitro data, in vivo studies were conducted in order to put the therapeutic strategy of ETA-antagonism to the test. In the conducted studies two approaches were taken to realize whether or not beneficial effects arise from ETA-antagonism: First, ETA was antagonized pharmacologically with BQ-123. Secondly, ETA was genetically deleted in the adipose tissue using the cre-lox system. Both approaches were tested in a setting of diet-induced obesity and chronic cold-exposure. In the settings of diet-induced obesity, neither pharmacological inhibition nor genetic ablation proved to be clearly beneficial. The pharmacological antagonism upon BQ-123-treatment induced a minor but significant upregulation of the functional marker Ucp1 in brown adipose tissue after chronic cold-exposure. In course of these studies, genetic ablation of ETA was successfully introduced in a transgenic mouse model. The resulting unexpected changes to basal mitochondrial marker expression might indicate a novel link of ET-1 signaling and mitochondria in the brown adipose tissue.

7 | References

Adiarto, S., Emoto, N., Iwasa, N., & Yokoyama, M. (2007). Obesity-induced upregulation of myocardial endothelin-1 expression is mediated by leptin. *Biochemical and Biophysical Research Communications*, *353*(3), 623–627. https://doi.org/10.1016/j.bbrc.2006.12.066

Aird, W. C. (2007a). Phenotypic heterogeneity of the endothelium: I. Structure, function, and mechanisms. *Circulation Research*, *100*(2), 158–173. https://doi.org/10.1161/01.RES.0000255691.76142.4a

Aird, W. C. (2007b). Phenotypic heterogeneity of the endothelium: II. Representative vascular beds. *Circulation Research*, *100*(2), 174–190. https://doi.org/10.1161/01.RES.0000255690.03436.ae

Alrashdi, S. F., Deliyanti, D., & Wilkinson-Berka, J. L. (2018). Intravitreal administration of endothelin type A receptor or endothelin type B receptor antagonists attenuates hypertensive and diabetic retinopathy in rats. *Experimental Eye Research*, *176*, 1–9. https://doi.org/https://doi.org/10.1016/j.exer.2018.06.025

Anders, Simon and Huber, W. (2010). Differential expression analysis for sequence count data. *Nature Precedings*. https://doi.org/10.1038/npre.2010.4282.2

Anders, M. I. L. and W. H. and S. (2014). Moderated estimation of fold change and dispersion for RNA-seq data with DESeq2. *Genome Biology*, *15*(12), 550. https://doi.org/10.1186/s13059-014-0550-8

Anders, S., McCarthy, D. J., Chen, Y., Okoniewski, M., Smyth, G. K., Huber, W., & Robinson, M. D. (2013). Count-based differential expression analysis of RNA sequencing data using R and Bioconductor. *Nature Protocols*, *8*(9), 1765–1786. https://doi.org/10.1038/nprot.2013.099

Babicki, S., Arndt, D., Marcu, A., Liang, Y., Grant, J. R., Maciejewski, A., & Wishart, D. S. (2016). Heatmapper: web-enabled heat mapping for all. *Nucleic Acids Research*, *44*(W1), W147–W153. https://doi.org/10.1093/nar/gkw419

Barton, M., & Sorokin, A. (2015). Endothelin and the glomerulus in chronic kidney disease. *Seminars in Nephrology*, *35*(2), 156–167. https://doi.org/10.1016/j.semnephrol.2015.02.005

Biswas, S., Feng, B., Thomas, A., Chen, S., Aref-Eshghi, E., Sadikovic, B., & Chakrabarti, S. (2018). Endothelin-1 regulation is entangled in a complex web of epigenetic mechanisms in diabetes. *Physiological Research*. https://doi.org/10.33549/physiolres.933836

Briançon-Marjollet, A., Monneret, D., Henri, M., Hazane-Puch, F., Pepin, J. L., Faure, P., & Godin-Ribuot, D. (2016). Endothelin regulates intermittent hypoxia-induced lipolytic remodelling of adipose tissue and phosphorylation of hormone-sensitive

lipase. *Journal of Physiology*, *594*(6), 1727–1740. https://doi.org/10.1113/JP271321

Bukowiecki, L. J., Geloen, A., & Collet, A. J. (1986). Proliferation and differentiation of brown adipocytes from interstitial cells during cold acclimation. *American Journal of Physiology-Cell Physiology*, *250*(6), C880–C887. https://doi.org/10.1152/ajpcell.1986.250.6.C880

Cahill, P. A., & Redmond, E. M. (2016). Vascular endothelium – Gatekeeper of vessel health. *Atherosclerosis*, *248*, 97–109. https://doi.org/10.1016/j.atherosclerosis.2016.03.007

Cameron, A. C., Welsh, P., Neves, K. B., Newby, D. E., Touyz, R. M., & Lang, N. N. (2020). Acute vascular effects of vascular endothelial growth factor inhibition in the forearm arterial circulation. *Journal of Hypertension*, *38*(2), 257–265. https://doi.org/10.1097/HJH.0000000000002230

Carratù, P., Ventura, V. A., Maniscalco, M., Dragonieri, S., Berardi, S., Ria, R., Quaranta, V. N., Vacca, A., Devito, F., Ciccone, M. M., Phillips, B. A., & Resta, O. (2016). Echocardiographic findings and plasma endothelin-1 levels in obese patients with and without obstructive sleep apnea. *Sleep and Breathing*, *20*(2), 613–619. https://doi.org/10.1007/s11325-015-1260-5

Chai, S. P., Chang, Y. N., & Fong, J. C. (2009). Endothelin-1 stimulates interleukin-6 secretion from 3T3-L1 adipocytes. *Biochimica et Biophysica Acta - General Subjects*, *1790*(3), 213–218. https://doi.org/10.1016/j.bbagen.2008.12.002

Chaphalkar, R. M., Stankowska, D. L., He, S., Kodati, B., Phillips, N., Prah, J., Yang, S., & Krishnamoorthy, R. R. (2020). Endothelin-1 Mediated Decrease in Mitochondrial Gene Expression and Bioenergetics Contribute to Neurodegeneration of Retinal Ganglion Cells. *Scientific Reports*, *10*(1), 3571. https://doi.org/10.1038/s41598-020-60558-6

Chen, C., Gao, J.-L., Liu, M.-Y., Li, S.-L., Xuan, X.-C., Zhang, X.-Z., Zhang, X.-Y., Wei, Y.-Y., Zhen, C.-L., Jin, J., Shen, X., & Dong, D.-L. (2017). Mitochondrial Fission Inhibitors Suppress Endothelin-1-Induced Artery Constriction. *Cellular Physiology and Biochemistry*, *42*(5), 1802–1811. https://doi.org/10.1159/000479536

Chen, G.-F., & Sun, Z. (2006). Effects of chronic cold exposure on the endothelin system. *Journal of Applied Physiology*, *100*(5), 1719–1726. https://doi.org/10.1152/japplphysiol.01407.2005

Cheng, X., Ji, Z., Tsalkova, T., & Mei, F. (2008). Epac and PKA: a tale of two intracellular cAMP receptors. *Acta Biochimica et Biophysica Sinica*, *40*(7), 651–662. https://doi.org/10.1111/j.1745-7270.2008.00438.x

Chester, A. H., & Yacoub, M. H. (2014). The role of endothelin-1 in pulmonary arterial hypertension. *Global Cardiology Science & Practice*, *2014*(2), 62–78. https://doi.org/10.5339/gcsp.2014.29

Chien, Y., Lai, Y.-H., Kwok, C. F., & Ho, L.-T. (2011). Endothelin-1 Suppresses Long-Chain Fatty Acid Uptake and Glucose Uptake Via Distinct Mechanisms in 3T3-L1 Adipocytes. *Obesity*, *19*(1), 6–12. https://doi.org/10.1038/oby.2010.124

Chomczynski, P., & Sacchi, N. (2006). The single-step method of RNA isolation by acid guanidinium thiocyanate-phenol-chloroform extraction: Twenty-something years on. *Nature Protocols*, *1*(2), 581–585. https://doi.org/10.1038/nprot.2006.83

Davenport, A. P., Hyndman, K. A., Dhaun, N., Southan, C., Kohan, D. E., Pollock, J. S., Pollock, D. M., Webb, D. J., & Maguire, J. J. (2016). Endothelin. *Pharmacological Reviews*, *68*(2), 357 LP – 418. https://doi.org/10.1124/pr.115.011833

Dobin, A., Davis, C. A., Schlesinger, F., Drenkow, J., Zaleski, C., Jha, S., Batut, P., Chaisson, M., & Gingeras, T. R. (2013). STAR: ultrafast universal RNA-seq aligner. *Bioinformatics*, *29*(1), 15–21. https://doi.org/10.1093/bioinformatics/bts635

Douma, L. G., Solocinski, K., Masten, S. H., Barral, D. H., Barilovits, S. J., Jeffers, L. A., Alder, K. D., Patel, R., Wingo, C. S., Brown, K. D., Cain, B. D., & Gumz, M. L. (2020). EDN1-AS, A Novel Long Non-coding RNA Regulating Endothelin-1 in Human Proximal Tubule Cells . In *Frontiers in Physiology* (Vol. 11, p. 209). https://www.frontiersin.org/article/10.3389/fphys.2020.00209

Ehrenreich, H., Rieckmann, P., Sinowatz, F., Weih, K. A., Arthur, L. O., Goebel, F. D., Burd, P. R., Coligan, J. E., & Clouse, K. A. (1993). Potent stimulation of monocytic endothelin-1 production by HIV-1 glycoprotein 120. *The Journal of Immunology*, *150*(10), 4601 LP – 4609. http://www.jimmunol.org/content/150/10/4601.abstract

Ergul, A. (2011). Endothelin-1 and diabetic complications: focus on the vasculature. *Pharmacological Research*, *63*(6), 477–482. https://doi.org/10.1016/j.phrs.2011.01.012

Fareed, M. U., Hans, G. H., Atanda Jr, A., Strichartz, G. R., & Davar, G. (2000). Pharmacological characterization of acute pain behavior produced by application of endothelin-1 to rat sciatic nerve. *The Journal of Pain*, *1*(1), 46–53. https://doi.org/10.1016/S1526-5900(00)90087-7

Farhat, N., Matouk, C. C., Mamarbachi, A. M., Marsden, P. A., Allen, B. G., & Thorin, E. (2008). Activation of ETB receptors regulates the abundance of ET-1 mRNA in vascular endothelial cells. *British Journal of Pharmacology*, *153*(7), 1420–1431. https://doi.org/10.1038/bjp.2008.25

Farrah, T. E., Anand, A., Gallacher, P. J., Kimmitt, R., Carter, E., Dear, J. W., Mills, N. L., Webb, D. J., & Dhaun, N. (2019). Endothelin Receptor Antagonism Improves Lipid Profiles and Lowers PCSK9 (Proprotein Convertase Subtilisin/Kexin Type 9) in Patients With Chronic Kidney Disease. *Hypertension (Dallas, Tex. : 1979)*, *74*(2), 323–330. https://doi.org/10.1161/HYPERTENSIONAHA.119.12919

Ferri, C., Bellini, C., Desideri, G., Di Francesco, L., Baldoncini, R., Santucci, A., & De

Mattia, G. (1995). Plasma Endothelin-1 Levels in Obese Hypertensive and Normotensive Men. *Diabetes*, *44*(4), 431 LP – 436. https://doi.org/10.2337/diab.44.4.431

Frazier, T., Lee, S., Bowles, A., Semon, J., Bunnell, B., Wu, X., & Gimble, J. (2018). Gender and age-related cell compositional differences in C57BL/6 murine adipose tissue stromal vascular fraction. *Adipocyte*, *7*(3), 183–189. https://doi.org/10.1080/21623945.2018.1460009

Freeman, B. D., Machado, F. S., Tanowitz, H. B., & Desruisseaux, M. S. (2014). Endothelin-1 and its role in the pathogenesis of infectious diseases. *Life Sciences*, *118*(2), 110–119. https://doi.org/10.1016/j.lfs.2014.04.021

Fujimoto, N., Matsuo, N., Sumiyoshi, H., Yamaguchi, K., Saikawa, T., Yoshimatsu, H., & Yoshioka, H. (2005). Adiponectin is expressed in the brown adipose tissue and surrounding immature tissues in mouse embryos. *Biochimica et Biophysica Acta (BBA) - Gene Structure and Expression*, *1731*(1), 1–12. /https://doi.org/10.1016/j.bbaexp.2005.06.013

García-Morales, V., Cuíñas, A., Elíes, J., & Campos-Toimil, M. (2014). PKA and Epac activation mediates cAMP-induced vasorelaxation by increasing endothelial NO production. *Vascular Pharmacology*, *60*(3), 95–101. https://doi.org/10.1016/j.vph.2014.01.004

Gogg, S., Nerstedt, A., Boren, J., & Smith, U. (2019). Human adipose tissue microvascular endothelial cells secrete PPARγ ligands and regulate adipose tissue lipid uptake. *JCI Insight*, *4*(5). https://doi.org/10.1172/jci.insight.125914

Gokin, A. P., Fareed, M. U., Pan, H.-L., Hans, G., Strichartz, G. R., & Davar, G. (2001). Local Injection of Endothelin-1 Produces Pain-Like Behavior and Excitation of Nociceptors in Rats. *The Journal of Neuroscience*, *21*(14), 5358 LP – 5366. https://doi.org/10.1523/JNEUROSCI.21-14-05358.2001

Habara, Y. (1989). Effects of cold exposure on cyclic AMP concentration in plasma, liver, and brown and white adipose tissues in cold-acclimated rats. *International Journal of Biometeorology*, *33*(2), 95–100. https://doi.org/10.1007/BF01686285

Haque, S., Dashwood, M. R., Heetun, M., Shiwen, X., Farooqui, N., Ramesh, B., Welch, H., Savage, F. J., Ogunbiyi, O., Abraham, D. J., & Loizidou, M. (2013). Efficacy of the Specific Endothelin A Receptor Antagonist Zibotentan (ZD4054) in Colorectal Cancer: A Preclinical Study. *Molecular Cancer Therapeutics*, *12*(8), 1556 LP – 1567. https://doi.org/10.1158/1535-7163.MCT-12-0975

Hickey, K. A., Rubanyi, G., Paul, R. J., & Highsmith, R. F. (1985). Characterization of a coronary vasoconstrictor produced by cultured endothelial cells. *American Journal of Physiology-Cell Physiology*, *248*(5), C550–C556. https://doi.org/10.1152/ajpcell.1985.248.5.C550

Hocking, S. L., Wu, L. E., Guilhaus, M., Chisholm, D. J., & James, D. E. B. T.-D. (2010). *Intrinsic depot-specific differences in the secretome of adipose tissue, preadipocytes, and adipose tissue--derived microvascular endothelial cells*. *59*(12), 3008+. https://doi.org/10.2337/db10-0483

Hostenbach, S., D'haeseleer, M., Kooijman, R., & De Keyser, J. (2016). The pathophysiological role of astrocytic endothelin-1. *Progress in Neurobiology*, *144*, 88–102. https://doi.org/10.1016/j.pneurobio.2016.04.009

Ibrahim, A., & Arany, Z. (2017). Does Endothelium Buffer Fat? *Circulation Research*, *120*(8), 1219–1221. https://doi.org/10.1161/CIRCRESAHA.117.310865

Ihara, M., Yamanaka, R., Ohwaki, K., Ozaki, S., Fukami, T., Ishikawa, K., Towers, P., & Yano, M. (1995). [3H]BQ-123, a highly specific and reversible radioligand for the endothelin ETA receptor subtype. *European Journal of Pharmacology*, *274*(1), 1–6. https://doi.org/10.1016/0014-2999(94)00670-3

Inoue, A., Yanagisawa, M., Takuwa, Y., Mitsui, Y., Kobayashi, M., & Masaki, T. (1989). The human preproendothelin-1 gene. Complete nucleotide sequence and regulation of expression. *Journal of Biological Chemistry*, *264*(25), 14954–14959.

Jacobs, M. E., Wingo, C. S., & Cain, B. D. (2013). An emerging role for microRNA in the regulation of endothelin-1. *Frontiers in Physiology*, *4*, 22. https://doi.org/10.3389/fphys.2013.00022

Juan, C.-C., Chang, C.-L., Lai, Y.-H., & Ho, L.-T. (2005). Endothelin-1 induces lipolysis in 3T3-L1 adipocytes. *American Journal of Physiology-Endocrinology and Metabolism*, *288*(6), E1146–E1152. https://doi.org/10.1152/ajpendo.00481.2004

Jurrissen, T. J., Grunewald, Z. I., Woodford, M. L., Winn, N. C., Ball, J. R., Smith, T. N., Wheeler, A. A., Rawlings, A. L., Staveley-O'Carroll, K. F., Ji, Y., Fay, W. P., Paradis, P., Schiffrin, E. L., Vieira-Potter, V. J., Fadel, P. J., Martinez-Lemus, L. A., & Padilla, J. (2019). Overproduction of endothelin-1 impairs glucose tolerance but does not promote visceral adipose tissue inflammation or limit metabolic adaptations to exercise. *American Journal of Physiology-Endocrinology and Metabolism*, *317*(3), E548–E558. https://doi.org/10.1152/ajpendo.00178.2019

Kahn, C. R., Wang, G., & Lee, K. Y. (2019). Altered adipose tissue and adipocyte function in the pathogenesis of metabolic syndrome. *The Journal of Clinical Investigation*, *129*(10), 3990–4000. https://doi.org/10.1172/JCI129187

Karkoulias, K, D Lykouras, F Sampsonas, P Drakatos, S Canova, G Tsoukalas, K. S. (2010). The role of Endothelin-1 in obstructive sleep apnea syndrome and pulmonary arterial hypertension: pathogenesis and Endothelin-1 antagonists. *Curr Med Chem*, *17*(11). https://doi.org/ 10.2174/092986710790820624

Kedzierski, R. M., Grayburn, P. A., Kisanuki, Y. Y., Williams, C. S., Hammer, R. E., Richardson, J. A., Schneider, M. D., & Yanagisawa, M. (2003). Cardiomyocyte-

specific endothelin A receptor knockout mice have normal cardiac function and an unaltered hypertrophic response to angiotensin II and isoproterenol. *Molecular and Cellular Biology*, *23*(22), 8226–8232. https://doi.org/10.1128/mcb.23.22.8226-8232.2003

Kelly, L. K., Wedgwood, S., Steinhorn, R. H., & Black, S. M. (2004). Nitric oxide decreases endothelin-1 secretion through the activation of soluble guanylate cyclase. *American Journal of Physiology-Lung Cellular and Molecular Physiology*, *286*(5), L984–L991. https://doi.org/10.1152/ajplung.00224.2003

Klepac, K., Kilić, A., Gnad, T., Brown, L. M., Herrmann, B., Wilderman, A., Balkow, A., Glöde, A., Simon, K., Lidell, M. E., Betz, M. J., Enerbäck, S., Wess, J., Freichel, M., Blüher, M., König, G., Kostenis, E., Insel, P. A., & Pfeifer, A. (2016). The G q signalling pathway inhibits brown and beige adipose tissue. *Nature Communications*, *7*. https://doi.org/10.1038/ncomms10895

Klöss, S., Srivastava, R., & Mülsch, A. (2004). Down-Regulation of Soluble Guanylyl Cyclase Expression by Cyclic AMP Is Mediated by mRNA-Stabilizing Protein HuR. *Molecular Pharmacology*, *65*(6), 1440 LP – 1451. https://doi.org/10.1124/mol.65.6.1440

Kohan, D. E., & Barton, M. (2014). Endothelin and endothelin antagonists in chronic kidney disease. *Kidney International*, *86*(5), 896–904. https://doi.org/10.1038/ki.2014.143

Kopetz, E. S., Nelson, J. B., & Carducci, M. A. (2002). Endothelin-1 as a Target for Therapeutic Intervention in Prostate Cancer. *Investigational New Drugs*, *20*(2), 173–182. https://doi.org/10.1023/A:1015630513908

Kowalczyk, A., Kleniewska, P., Kolodziejczyk, M., Skibska, B., & Goraca, A. (2015). The role of endothelin-1 and endothelin receptor antagonists in inflammatory response and sepsis. *Archivum Immunologiae et Therapiae Experimentalis*, *63*(1), 41–52. https://doi.org/10.1007/s00005-014-0310-1

Kuryłowicz, A., & Puzianowska-Kuźnicka, M. (2020). Induction of Adipose Tissue Browning as a Strategy to Combat Obesity. In *International Journal of Molecular Sciences* (Vol. 21, Issue 17). https://doi.org/10.3390/ijms21176241

Lee, P., Swarbrick, M. M., & Ho, K. K. Y. (2013). Brown Adipose Tissue in Adult Humans: A Metabolic Renaissance. *Endocrine Reviews*, *34*(3), 413–438. https://doi.org/10.1210/er.2012-1081

Li, F., Wu, R., Cui, X., Zha, L., Yu, L., Shi, H., & Xue, B. (2016). Histone Deacetylase 1 (HDAC1) Negatively Regulates Thermogenic Program in Brown Adipocytes via Coordinated Regulation of Histone H3 Lysine 27 (H3K27) Deacetylation and Methylation. *The Journal of Biological Chemistry*, *291*(9), 4523–4536. https://doi.org/10.1074/jbc.M115.677930

Liao, Y., Smyth, G. K., & Shi, W. (2014). featureCounts: an efficient general purpose program for assigning sequence reads to genomic features. *Bioinformatics*, *30*(7), 923–930. https://doi.org/10.1093/bioinformatics/btt656

Lidell, M. E., Betz, M. J., & Enerbäck, S. (2014). Brown adipose tissue and its therapeutic potential. *Journal of Internal Medicine*, *276*(4), 364–377. https://doi.org/10.1111/joim.12255

Lien, C. C., Jiang, J. L., Jian, D. Y., Kwok, C. F., Ho, L. T., & Juan, C. C. (2016). Chronic endothelin-1 infusion causes adipocyte hyperplasia in rats. *Obesity*, *24*(3), 643–653. https://doi.org/10.1002/oby.21394

Lim, S., Honek, J., Xue, Y., Seki, T., Cao, Z., Andersson, P., Yang, X., Hosaka, K., & Cao, Y. (2012). Cold-induced activation of brown adipose tissue and adipose angiogenesis in mice. *Nature Protocols*, *7*(3), 606–615. https://doi.org/10.1038/nprot.2012.013

Livak, K. J., & Schmittgen, T. D. (2001). Analysis of relative gene expression data using real-time quantitative PCR and the 2-ΔΔCT method. *Methods*, *25*(4), 402–408. https://doi.org/10.1006/meth.2001.1262

Malek, A., Greene, A., & Izumo, S. (1993). Regulation of endothelin 1 gene by fluid shear stress is transcriptionally mediated and independent protein kinase C and cAMP. *Proceedings of the National Academy of Sciences of the United States of America*, *90*, 5999–6003. https://doi.org/10.1073/pnas.90.13.5999

Martin, M. (2011). Cutadapt removes adapter sequences from high-throughput sequencing reads. *EMBnet.Journal*, *17*(1), 10–12. http://dx.doi.org/10.14806/ej.17.1.200

Minami, T., Muramatsu, M., & Kume, T. (2019). Organ/Tissue-Specific Vascular Endothelial Cell Heterogeneity in Health and Disease. *Biological and Pharmaceutical Bulletin*, *42*(10), 1609–1619. https://doi.org/10.1248/bpb.b19-00531

Mrzilkova, J., Michenka, P., Seremeta, M., Kremen, J., Dudak, J., Zemlicka, J., Musil, V., Minnich, B., & Zach, P. (2020). Morphology of the Vasculature and Blood Supply of the Brown Adipose Tissue Examined in an Animal Model by Micro-CT. *BioMed Research International*, *2020*, 7502578. https://doi.org/10.1155/2020/7502578

Nisoli, E., Tonello, C., Briscini, L., & Carruba, M. O. (1997). Inducible Nitric Oxide Synthase in Rat Brown Adipocytes: Implications for Blood Flow to Brown Adipose Tissue*. *Endocrinology*, *138*(2), 676–682. https://doi.org/10.1210/endo.138.2.4956

Pellegrinelli, V., Rouault, C., Veyrie, N., Clément, K., & Lacasa, D. (2014). Endothelial cells from visceral adipose tissue disrupt adipocyte functions in a three-dimensional setting: Partial rescue by angiopoietin-1. *Diabetes*, *63*(2), 535–549. https://doi.org/10.2337/db13-0537

Pfeifer, A., & Hoffmann, L. S. (2015). Brown, Beige, and White: The New Color Code of Fat and Its Pharmacological Implications. *Annual Review of Pharmacology and Toxicology*, *55*(1), 207–227. https://doi.org/10.1146/annurev-pharmtox-010814-

124346

Polak, J., Punjabi, N. M., & Shimoda, L. A. (2018). Blockade of Endothelin-1 Receptor Type B Ameliorates Glucose Intolerance and Insulin Resistance in a Mouse Model of Obstructive Sleep Apnea. *Frontiers in Endocrinology*, *9*, 280. https://doi.org/10.3389/fendo.2018.00280

R Core Team. (2019). *A language and environment for statistical computing. R*. Foundation for Statistical Computing. https://www.r-project.org/.

Rajan, A., Shi, H., & Xue, B. (2018). Class I and II Histone Deacetylase Inhibitors Differentially Regulate Thermogenic Gene Expression in Brown Adipocytes. *Scientific Reports*, *8*(1), 13072. https://doi.org/10.1038/s41598-018-31560-w

Rataj, F., Planel, S., Desroches-Castan, A., Le Douce, J., Lamribet, K., Denis, J., Feige, J. J., & Cherradi, N. (2016). The cAMP pathway regulates mRNA decay through phosphorylation of the RNA-binding protein TIS11b/BRF1. *Molecular Biology of the Cell*, *27*(24), 3841–3854. https://doi.org/10.1091/mbc.E16-06-0379

Reimunde, F. M., Castañares, C., Redondo-Horcajo, M., Lamas, S., & Rodríguez-Pascual, F. (2005). Endothelin-1 expression is strongly repressed by AU-rich elements in the 3́-untranslated region of the gene. *Biochemical Journal*, *387*(3), 763–772. https://doi.org/10.1042/BJ20041687

Richards, J., Welch, A. K., Barilovits, S. J., All, S., Cheng, K.-Y., Wingo, C. S., Cain, B. D., & Gumz, M. L. (2014). Tissue-specific and time-dependent regulation of the endothelin axis by the circadian clock protein Per1. *Life Sciences*, *118*(2), 255–262. https://doi.org/10.1016/j.lfs.2014.03.028

Rivera-Gonzalez, O., & Speed, J. S. (2020). SUN-592 Adipocyte Specific Endothelin a Receptor Knockout Increases Adiposity in Mice. *Journal of the Endocrine Society*, *4*(Suppl 1), SUN-592. https://doi.org/10.1210/jendso/bvaa046.1897

Rivera-Gonzalez, O., Stapel, J., & Speed, J. S. (2020). Hypoxia increases endothelin-1 production via Hif1α in adipocytes. *The FASEB Journal*, *34*(S1), 1. https://doi.org/10.1096/fasebj.2020.34.s1.05432

Rodriguez-Pascual, F., Redondo-Horcajo, M., Magan-Marchal, N., Lagares, D., Martinez-Ruiz, A., Kleinert, H., & Lamas, S. (2008). Glyceraldehyde-3-Phosphate Dehydrogenase Regulates Endothelin-1 Expression by a Novel, Redox-Sensitive Mechanism Involving mRNA Stability. *Molecular and Cellular Biology*, *28*(23), 7139–7155. https://doi.org/10.1128/mcb.01145-08

Rutkowski, J. M., Davis, K. E., & Scherer, P. E. (2009). Mechanisms of obesity and related pathologies: The macro- and microcirculation of adipose tissue. *FEBS Journal*, *276*(20), 5738–5746. https://doi.org/10.1111/j.1742-4658.2009.07303.x

Scalia, R. (2013). The microcirculation in adipose tissue inflammation. *Reviews in Endocrine & Metabolic Disorders*, *14*(1), 69–76. https://doi.org/10.1007/s11154-013-

9236-x

Schillemans, M., Karampini, E., Kat, M., & Bierings, R. (2019). Exocytosis of Weibel–Palade bodies: how to unpack a vascular emergency kit. *Journal of Thrombosis and Haemostasis*, *17*(1), 6–18. https://doi.org/10.1111/jth.14322

Shakespear, M. R., Hohenhaus, D. M., Kelly, G. M., Kamal, N. A., Gupta, P., Labzin, L. I., Schroder, K., Garceau, V., Barbero, S., Iyer, A., Hume, D. A., Reid, R. C., Irvine, K. M., Fairlie, D. P., & Sweet, M. J. (2013). Histone deacetylase 7 promotes Toll-like receptor 4-dependent proinflammatory gene expression in macrophages. *The Journal of Biological Chemistry*, *288*(35), 25362–25374. https://doi.org/10.1074/jbc.M113.496281

Shao, M., Hepler, C., Vishvanath, L., MacPherson, K. A., Busbuso, N. C., & Gupta, R. K. (2016). Fetal development of subcutaneous white adipose tissue is dependent on Zfp423. *Molecular Metabolism*, *6*(1), 111–124. https://doi.org/10.1016/j.molmet.2016.11.009

Spratt, J. C. S., Goddard, J., Patel, N., Strachan, F. E., Rankin, A. J., & Webb, D. J. (2001). Systemic ETA receptor antagonism with BQ-123 blocks ET-1 induced forearm vasoconstriction and decreases peripheral vascular resistance in healthy men. *British Journal of Pharmacology*, *134*(3), 648–654. https://doi.org/10.1038/sj.bjp.0704304

Stewart, D. J., Cernacek, P., Mohamed, F., Blais, D., Cianflone, K., & Monge, J. C. (1994). Role of cyclic nucleotides in the regulation of endothelin-1 production by human endothelial cells. *American Journal of Physiology-Heart and Circulatory Physiology*, *266*(3), H944–H951. https://doi.org/10.1152/ajpheart.1994.266.3.H944

Stow, L. R., Jacobs, M. E., Wingo, C. S., & Cain, B. D. (2011). Endothelin-1 gene regulation. *The FASEB Journal*, *25*(1), 16–28. https://doi.org/10.1096/fj.10-161612

Strissel, K. J., Stancheva, Z., Miyoshi, H., Perfield, J. W., DeFuria, J., Jick, Z., Greenberg, A. S., & Obin, M. S. (2007). Adipocyte Death, Adipose Tissue Remodeling, and Obesity Complications. *Diabetes*, *56*(12), 2910 LP – 2918. https://doi.org/10.2337/db07-0767

Sun, X., Kumar, S., Sharma, S., Aggarwal, S., Lu, Q., Gross, C., Rafikova, O., Lee, S. G., Dasarathy, S., Hou, Y., Meadows, M. L., Han, W., Su, Y., Fineman, J. R., & Black, S. M. (2014). Endothelin-1 induces a glycolytic switch in pulmonary arterial endothelial cells via the mitochondrial translocation of endothelial nitric oxide synthase. *American Journal of Respiratory Cell and Molecular Biology*, *50*(6), 1084–1095. https://doi.org/10.1165/rcmb.2013-0187OC

Trayhurn, P. (2018). Brown Adipose Tissue—A Therapeutic Target in Obesity? . In *Frontiers in Physiology* (Vol. 9, p. 1672). https://www.frontiersin.org/article/10.3389/fphys.2018.01672

van de Water, F. M., Russel, F. G. M., & Masereeuw, R. (2006). Regulation and expression

of endothelin-1 (ET-1) and ET-receptors in rat epithelial cells of renal and intestinal origin. *Pharmacological Research*, *54*(6), 429–435. https://doi.org/10.1016/j.phrs.2006.08.006

Vigne, P., Breittmayer, J. P., & Frelin, C. (1993). Competitive and non competitive interactions of BQ-123 with endothelin ETA receptors. *European Journal of Pharmacology*, *245*(3), 229–232. https://doi.org/10.1016/0922-4106(93)90101-e

Virtanen, K. A., Lidell, M. E., Orava, J., Heglind, M., Westergren, R., Niemi, T., Taittonen, M., Laine, J., Savisto, N.-J., Enerbäck, S., & Nuutila, P. (2009). Functional Brown Adipose Tissue in Healthy Adults. *New England Journal of Medicine*, *360*(15), 1518–1525. https://doi.org/10.1056/NEJMoa0808949

Wang, Q. A., Scherer, P. E., & Gupta, R. K. (2014). Improved methodologies for the study of adipose biology: insights gained and opportunities ahead. *Journal of Lipid Research*, *55*(4), 605–624. https://doi.org/10.1194/jlr.R046441

Wang, Z. V, Deng, Y., Wang, Q. A., Sun, K., & Scherer, P. E. (2010). Identification and characterization of a promoter cassette conferring adipocyte-specific gene expression. *Endocrinology*, *151*(6), 2933–2939. https://doi.org/10.1210/en.2010-0136

Warner, T. D., Allcock, G. H., & Vane, J. R. (1994). Reversal of established responses to endothelin-1 in vivo and in vitro by the endothelin receptor antagonists, BQ-123 and PD 145065. *British Journal of Pharmacology*, *112*(1), 207–213. https://doi.org/10.1111/j.1476-5381.1994.tb13053.x

Wickham, H. (2016). *ggplot2: Elegant Graphics for Data Analysis*. Springer-Verlag. https://ggplot2.tidyverse.org

Wilkes, J. J., Hevener, A., & Olefsky, J. (2003). Chronic Endothelin-1 Treatment Leads to Insulin Resistance In Vivo. *Diabetes*, *52*(8), 1904 LP – 1909. https://doi.org/10.2337/diabetes.52.8.1904

Yanagisawa, M., Kurihara, H., Kimura, S., Tomobe, Y., Kobayashi, M., Mitsui, Y., Yazaki, Y., Goto, K., & Masaki, T. (1988). A novel potent vasoconstrictor peptide produced by vascular endothelial cells. *Nature*, *332*(6163), 411–415. https://doi.org/10.1038/332411a0

Zhang, X., Sessa, W. C., & Fernández-Hernando, C. (2018). Endothelial Transcytosis of Lipoproteins in Atherosclerosis . In *Frontiers in Cardiovascular Medicine* (Vol. 5, p. 130). https://www.frontiersin.org/article/10.3389/fcvm.2018.00130

8 | List of Tables

9 | List of Figures

10 | Appendix

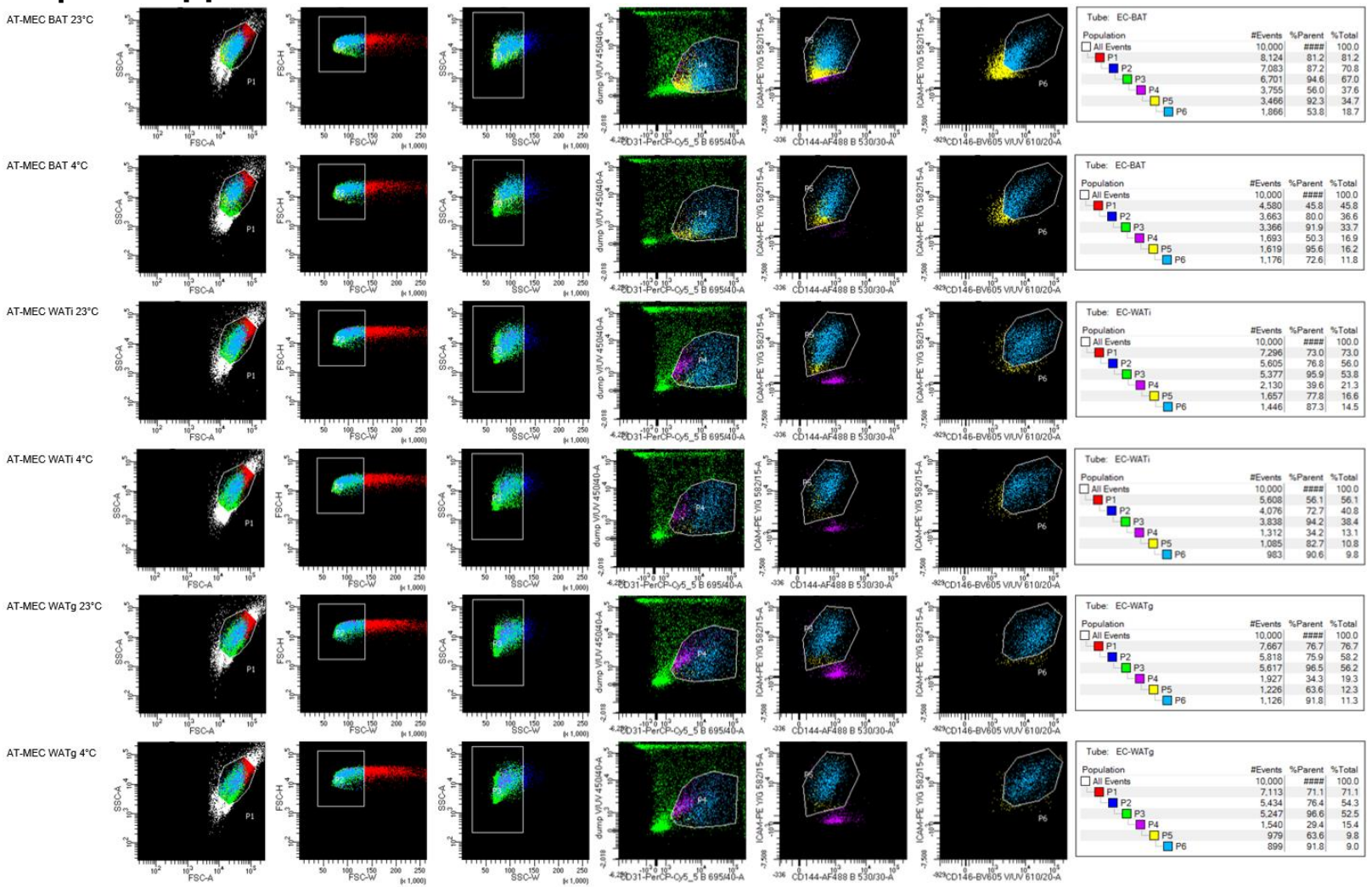

Figure 37 Representative FACS data, showing the utilized gating strategy to further purify CD31⁺ MACS-elution fractions from different adipose tissues. Relevant gates are displayed in order from left to right and quantified on the right. Samples are ordered by adipose tissue type and treatment vertically.

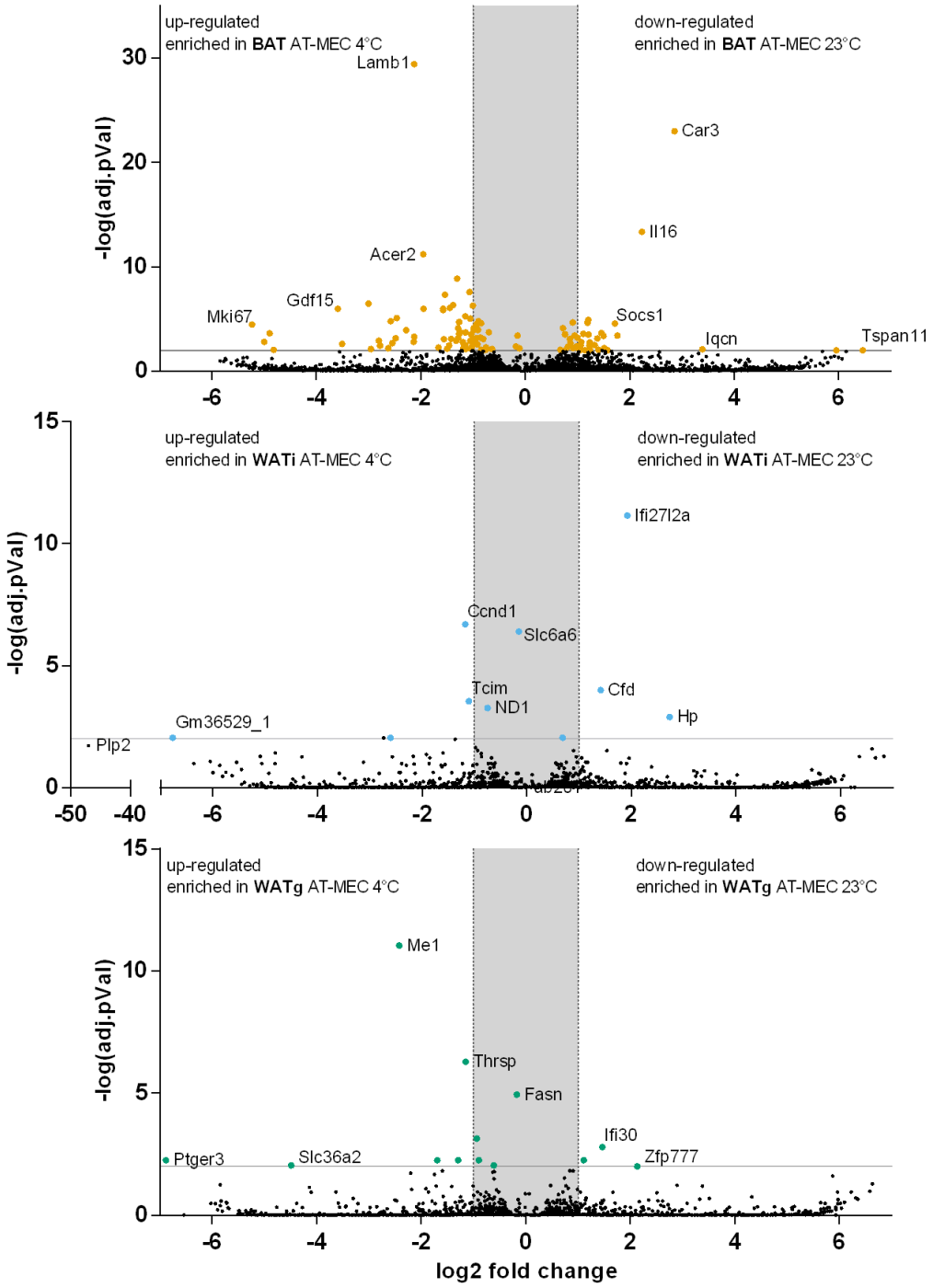

Figure 38 Vulcano plots displaying AT-MEC RNA-sequencing results of BAT (top) WATi (mid) and WATg (lower panel).

Level of significance (p=0.05) is indicated by the horizontal line. Differentially regulated genes are represented by colored dots. Area of less than 2-fold change is bordered by vertical dashed grey lines and highlighted in grey.

Table 19 Differentially regulated genes of AT-MEC in BAT upon chronic cold exposure

Gene Symbol	logFC	adj.P.Val	baseMean
Lamb1	-2.1280589	3.84E-30	1344.132022
Car3	2.85534673	1.02E-23	505.8467379
Il16	2.23387751	4.41E-14	192.8085257
Acer2	-1.9536262	6.04E-12	616.3129591
Lipa	-1.3088816	1.29E-09	535.5471965
Lrrc8c	-1.0720887	2.48E-08	1476.838614
Fmo2	-1.5379873	4.62E-08	419.0846355
Ankrd37	-3.0016155	3.20E-07	162.8951365
Clec14a	-1.3869084	4.67E-07	624.7217815
Anxa3	-1.0077909	5.14E-07	1918.926456
Smad7	-1.4464502	7.95E-07	489.0092178
Gdf15	-3.5915075	1.03E-06	52.00572698
Smad6	-1.5746102	1.03E-06	553.281496
Fads3	-1.9514876	1.03E-06	233.7302027
Meox1	-1.576539	1.36E-06	475.7607086
Cxcl12	-1.1486885	5.41E-06	7795.663808
Nid2	-2.4653511	7.70E-06	80.78896275
Anxa2	-1.0572668	8.63E-06	2353.535188
Aqp1	1.20346177	1.14E-05	18711.34654
Ccnd1	-2.5799085	1.54E-05	1851.740202
Tbx3	-0.8957824	1.54E-05	1955.162551
Fam117b	-1.2684373	1.80E-05	340.0400201
Thra	0.90663894	2.09E-05	1483.988556
Egr1	1.188136	2.21E-05	3155.669226
Id1	-0.8497973	2.42E-05	5633.783148
Socs1	1.71536184	2.54E-05	198.9564346
Mki67	-5.231116	3.33E-05	24.84867287
Egln1	-0.9407104	3.47E-05	1074.026393
Myadm	-0.9842057	7.10E-05	1219.936346
Afdn	0.72112016	7.14E-05	6591.510561
Depp1	-1.2873568	7.45E-05	5834.69072
Slc6a6	-0.909465	0.000108543	3488.03761
Nostrin	-2.2826275	0.000116095	107.6546861
Ctla2a	-0.984086	0.000116095	2003.772671
Tcim	-1.24886	0.000177391	2815.091763
Sparc	-0.7010313	0.000177391	25632.38139
Nedd9	-1.1467789	0.000195346	940.9954799
Fosb	1.45804127	0.000219199	484.0147753
Brip1	-4.8976588	0.000229009	22.91571161
Hey1	-1.2695804	0.000251456	774.4570319
Fbxl18	1.10975833	0.000256404	317.6502542
Brd2	0.75759362	0.00028152	3262.525407
Bok	1.20946338	0.000296208	193.3394664
Sgk1	-1.0359803	0.000296208	2882.33612
Ldha	-1.5099455	0.000368137	516.7798708
Igfbp4	1.76416071	0.00037763	324.6545697
Sap18	0.9441949	0.000381707	483.8799556
Mafb	1.49760887	0.00039229	163.4889005
Dusp8	-2.1276124	0.000468147	154.8030469
Ddah2	-0.8577471	0.000611102	916.9722828
Ccdc85a	0.99649246	0.000611323	1018.438607
Cables1	-2.4844992	0.00064886	46.76947989
Alas2	-1.2891569	0.00064886	636.7773008
Thbd	-0.9410709	0.000657627	2884.116724
Cd247	1.37892046	0.000689535	137.7391913
Srsf5	0.85274241	0.000770002	2752.266483
Dlc1	-0.8078589	0.000804341	3593.970391
Phactr4	-1.4218258	0.000804341	371.3642843
Ak1	-1.5609864	0.000844815	136.9961616
Setx	-1.0533145	0.001150511	414.8976873
Rbp7	-1.0301292	0.001152427	1983.498164
Olfr1396	-1.324542	0.001197271	185.1489395
Mycn	-2.8031841	0.00120831	29.15431166
Amotl2	-0.9829732	0.00127774	647.5735387
Cdk1	-4.9994248	0.001440622	21.05051017
Osgin1	-2.1379972	0.001460699	55.23344371
Cxcl9	1.07261866	0.001566074	1163.82686
Il2rg	-1.1950695	0.001691128	583.6755459
Parm1	1.23128939	0.001691128	137.4239709
Iigp1	0.86160312	0.001948982	2032.188348
Pxdc1	-2.5504885	0.001948982	86.20789108
Cyp1a1	-3.5052884	0.00238708	159.1828323
Heg1	-0.9194772	0.002586696	2498.530205
Slbp	1.32707637	0.003017369	232.6887723
Fam198b	-1.1476083	0.003045167	904.6967021
Nus1	-1.4595082	0.003256366	220.5196212
Sncg	1.06267727	0.00336714	348.8479283
Syvn1	-2.7826405	0.003473998	48.96526652
Ecm2	1.22580849	0.003551968	153.1068192
Slit3	-1.7928063	0.004125178	73.83057812
Apoe	0.97943891	0.004125178	2450.423171
Zfas1	0.81798435	0.004198128	767.6555939
Edn1	-1.0211835	0.004201866	896.5417235
Igtp	1.00632734	0.004329691	555.2805422
Prelp	0.97056765	0.004861795	307.4682702
Ctps	-1.6617524	0.005247791	86.53472819

Adgre5	-0.7557696	0.005247791	1310.406224
Ssh2	0.97372995	0.005247791	3200.946829
Pdzd2	0.99013747	0.005490023	948.4477037
Aplnr	0.91275822	0.005701499	979.9874072
Gramd1b	1.50786441	0.005824971	101.1424916
Magix	-1.1907725	0.005865448	153.0291354
Phlda3	-1.1542297	0.005983326	173.9962774
Lrrc8b	-2.6225821	0.006154274	38.15392189
P4ha1	-1.4972166	0.006404561	226.405689
Mxi1	-1.0489915	0.006407793	223.1399763
Chchd10	1.01748175	0.006407793	543.9074845
Actn4	-0.6383447	0.007292814	3726.016847
Plpp6	-1.1421618	0.007292814	237.7734009
Cenpf	-2.9605466	0.007427925	40.10604117
Iqcn	3.39065904	0.007891508	20.67642221
Btg1	1.23407144	0.007891508	618.2559305
Tcn2	-0.8434539	0.008432058	439.8151455
Rpl41	0.66890275	0.008706574	2285.556964
Pimreg	-4.8170826	0.008706574	14.463945
Zfp618	1.40088858	0.008845749	122.0173361
Il4ra	-0.7917401	0.008845749	1458.206718
Adam17	-0.7592063	0.008845749	834.4712154
Hhex	1.04940571	0.009092535	300.8873993
Fos	1.05377842	0.009092535	1653.469056
S1pr4	1.14621583	0.009427765	254.299343
Pik3r1	0.75942097	0.009610424	356.4785816
Znhit6	1.23448792	0.009774603	147.428935
Gm48427	5.95463081	0.009774603	9.013922762
Cfd	1.57569649	0.009781775	146.6230348
Tspan11	6.4605178	0.009841224	7.665871165
Cdh23	1.46899977	0.010094759	261.3782026
Tspan2	-0.9994044	0.010201484	297.6469795
Eng	-0.9963214	0.010534558	3785.228475
1700025G04Rik	-1.2380652	0.011293775	404.5354751
Hbb-bt	-1.0279036	0.011726576	15280.21259
Emc7	-1.2402714	0.011726576	248.6373794
Col4a1	-0.8395052	0.011726576	11250.9018
Rbm15	-1.2090576	0.011726576	114.1679717
Rhob	-0.805832	0.011868784	2408.441497
Rpe	-1.6299158	0.011868784	63.15498518
Akap8	0.72278892	0.011868784	520.8081893
Myh11	1.52885633	0.011997709	262.7759162
Axin2	6.14320706	0.012093189	6.156491203
Gm31410	5.68993599	0.012093189	7.522949174
Retnla	1.64778101	0.012093189	202.2594588
C1qtnf6	-2.2178058	0.013248938	69.24059852

Btg2	0.78288376	0.013453464	1033.939244
Prc1	-3.5550751	0.013453464	19.06865757
Cyren	1.01903181	0.013463518	256.2781413
Gm44224	2.56697677	0.013463518	26.68573016
Mgll	-0.6026207	0.01436126	28743.73183
Ift122	-1.5795441	0.014750717	72.3600475
Rgs12	-0.8881793	0.014750717	357.6067664
Pkm	-0.8083663	0.014750717	975.8429733
Egflam	1.19687865	0.016104294	144.5016175
Slc1a1	-0.9662449	0.016104294	148.4169108
9530068E07Rik	-2.3415237	0.016104294	65.75734617
Ccdc88c	0.74370478	0.016909546	718.4473963
Cygb	1.29031241	0.017569606	241.3593488
Plpp1	-0.8498605	0.017936704	2067.581452
Rrad	3.31430408	0.018862282	15.00540759
Fam110a	1.66397165	0.019386288	69.04726704
Chp2	1.52311863	0.019672207	65.88184986
Slc27a3	1.51557108	0.019965485	88.85193307
Zfp467	1.00988749	0.022848794	231.8520191
Bik	1.79736517	0.022848794	48.42575844
Acss2	1.21177694	0.022848794	151.8082534
Pcmtd1	0.68455548	0.022893939	579.983469
Fabp5	-0.9360926	0.022945876	1318.810601
5730414N17Rik	-1.8887203	0.022945876	38.00148489
Rps15	0.680823	0.022945876	1477.633036
Stat5a	1.40825756	0.022962617	91.70806248
5033406O09Rik	-2.2919291	0.022970681	33.64061023
Slc25a37	-1.0169161	0.023252617	289.0805562
Gm42790	1.82758787	0.023262958	38.91798908
Max	-0.9221489	0.023569812	430.0442989
Dusp26	1.15863521	0.023569812	320.9443717
Samd5	0.90222484	0.024039848	359.5667571
Atm	1.00350303	0.024073613	146.7154688
Tob1	0.93959237	0.026148741	212.2025085
Bnip3	-0.9085099	0.026627329	208.9994139
Tbc1d1	-0.8873534	0.026943227	458.024638
Emp1	-1.2440362	0.026943227	317.5742769
Dact2	3.68763483	0.026943227	13.53347033
Cdca8	-3.1634477	0.027280262	22.12845252
Flnb	-0.9785481	0.027349616	1609.47716
H2-Q6	1.3263198	0.027349616	137.1817991
Stat1	0.68429608	0.027349616	757.9138905
Aldoa	-0.6758883	0.027349616	1440.177591
Tshz2	0.65616764	0.027349616	1150.786098
Alkbh7	1.40106615	0.027349616	76.94909255
Slc5a6	2.0422241	0.027349616	29.77263099

Vwa1	-1.2712665	0.027349616	198.5748484
Ptprf	2.54465781	0.028709007	26.96364634
Rpl37a	0.71027966	0.028881675	850.0403863
Lima1	-0.8226228	0.028958618	859.5548394
Snord104	1.38974503	0.029499509	116.5460529
Dgke	0.78440371	0.029586781	491.7182536
Serpine2	1.98144651	0.029749897	58.61377401
Bmpr2	-0.6162555	0.029749897	998.536258
9230101D24Rik	1.4069224	0.031357039	130.052092
Ssr3	-0.8789453	0.031357039	427.2892776
RP24-374N16.7	1.16041041	0.032206373	241.3055516
Sdc3	-0.6721036	0.032337714	1574.941248
Tgfb2	1.16657995	0.033285925	289.946104
Timp4	0.84252024	0.033285925	2613.548561
Lpl	-0.5728868	0.033384827	11693.67219
Zeb2	1.1255312	0.033384827	126.1811019
Cdh13	-0.5052257	0.033384827	3553.275862
Apln	-1.8923368	0.033438761	59.55322451
Maff	-2.0004669	0.034661474	72.71674121
Rassf4	-1.0109588	0.034748292	277.9612774
Trib1	-1.0223926	0.035170798	382.7637309
Gm20661	5.91445154	0.035226802	5.260430994
P4ha2	-1.0513117	0.036026003	169.0640258
Acaa2	0.62174721	0.036095972	804.4231851
Pde1a	3.18812907	0.036203441	23.50905421
Sh2d4b	4.62820449	0.036203441	9.529064502
Itih5	1.09966166	0.036203441	98.64200645
Top2a	-1.4683601	0.036990884	92.96241067
Scn5a	3.46412806	0.037120338	16.03353187
Btbd3	0.82835751	0.037156367	193.861019
Gm14221	1.74167459	0.03844021	54.95057064
Noc3l	2.4235749	0.038544092	21.71120241
Akap7	0.85775484	0.038580361	266.1499041
Fmod	2.21531185	0.039228009	26.41814767
Cd81	-0.542506	0.039487593	7664.761599
Tspan12	-0.8586356	0.039487593	278.0801933
Ramp3	-1.0889859	0.039487593	268.1740944
Plscr3	-0.6856817	0.039487593	493.0357826
Aspm	-3.4815271	0.039574454	18.28802834
St3gal1	-0.7278455	0.040459996	801.2387221
Stk32c	-3.2682746	0.040524247	26.53412133
Cfap20	-2.2958715	0.04078715	26.43104965
Myl9	1.07196066	0.041131549	468.270092
Aldh1l1	1.47390883	0.042095287	77.26551608
Stx3	-0.6479377	0.042801326	556.3444002
Gm47573	5.99456034	0.043818923	5.562236065
Gm45380	1.65325393	0.043918487	50.73313668
Tpp1	-0.6330502	0.04398585	628.4494214
Clic4	-0.6944685	0.044230352	865.6983821
Nuak1	0.95352651	0.044822668	247.4818077
Cmtm8	-0.5394922	0.045437506	1021.132655
Ckb	-0.8067921	0.045721011	453.6178018
Med16	0.92455454	0.045721011	259.2557188
Tbc1d9	-1.2839715	0.045721011	93.59019876
Cd40	-1.6327184	0.045721011	73.11206138
Atf3	1.20262777	0.045721011	210.5442629
A630001G21Rik	-5.3253166	0.045721011	6.274206975
Snca	-2.0787546	0.045721011	30.61624425
Ywhaq	-0.6179138	0.045721011	1536.236949
Rps5	0.60650214	0.045721011	3392.053746
Tmem100	2.3806031	0.046143283	48.38721881
Gm25541	5.84542019	0.046253687	5.015174871
Mef2c	0.63314929	0.046452014	1982.64263
Sirt1	0.96894761	0.046452014	237.717058
Ncam1	3.006658	0.047064523	15.27322517
Spns2	-0.8330825	0.047156654	787.3989183
Vtn	2.17564076	0.047544282	38.32400333
Neurl3	-1.2982992	0.048352344	81.85207848
Eps8l2	0.99082643	0.048633055	290.7483916
Spin4	-2.3588385	0.048644013	29.56860278
Klhl30	5.36814415	0.048851434	6.051313722
Smc1a	0.59479194	0.049284665	2080.026907
Gm42633	1.264962	0.049284665	109.3334649
Isoc2b	-2.243959	0.049284665	24.46662919
Cd34	-0.5791626	0.049284665	1587.280428
Las1l	0.75833312	0.049284665	301.9592054
Gngt2	-0.8329286	0.049284665	793.6716056
Mill2	-0.919378	0.049961576	154.7209524
Angptl4	-0.6792584	0.049968443	2670.910446
Gm15902	2.58418169	0.049968443	31.30301464

Table 20 Differentially regulated genes of AT-MEC in WATi upon chronic cold exposure

Gene Symbol	logFC	adj.P.Val	baseMean
Ifi27l2a	1.925993588	6.93E-12	294.3079721
Ccnd1	-1.174056607	2.01E-07	2461.406276
Slc6a6	-1.52927864	3.91E-07	2694.021672
Mki67	-2.750212047	6.07E-05	77.5439768
Cfd	1.413489219	9.94E-05	800.2159284
Tcim	-1.106030314	0.000288039	1405.285445
ND1	-0.747840133	0.000541652	23863.75829
Hp	2.735478966	0.001267292	42.81232097
D030007L05Rik	-6.763403505	0.008974172	10.40989846
Ccnd2	0.687732452	0.008974172	3759.466579
Ccna2	-2.600358294	0.008974172	43.21232585
Ccnb2	-2.734762278	0.00922452	50.22441468
Top2a	-1.366682717	0.01040012	252.9659307
Plp2	-4.702689825	0.019068064	13.68603894
Tbx3	-0.974349746	0.023264621	1475.611626
Gm3558	6.601017829	0.025169954	8.170936164
Sncg	0.89776479	0.030177216	660.1352761
Plin4	1.533678764	0.030177216	88.56990696
Mmd	-0.934970067	0.030177216	307.3312112
Melk	-4.804219408	0.037879947	14.72579248
Ak1	-1.596753074	0.037879947	139.3223897
Scd1	-0.865594281	0.039041992	1423.151876
Ncaph	-1.911545392	0.043161441	70.39754907

Table 21 Differentially regulated genes of AT-MEC in WATg upon chronic cold exposure

Gene Symbol	logFC	adj.P.Val	baseMean
Me1	-2.4203534	9.17E-12	188.219977
Thrsp	-1.1490979	5.24E-07	1241.08171
Fasn	-1.6811035	1.15E-05	750.58664
Slc6a6	-0.9374423	0.000714944	926.421951
Ifi30	1.46475071	0.001603876	312.193914

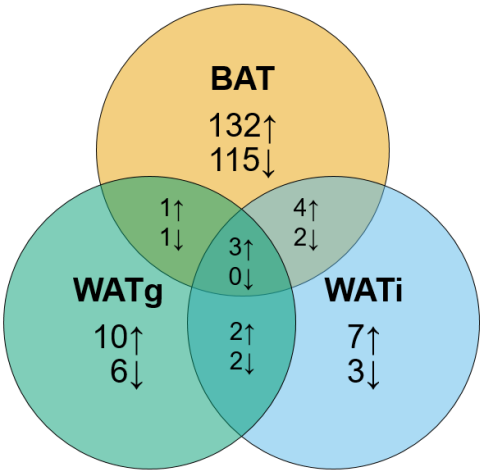

Figure 39 Venn-diagram displaying the number of differentially regulated genes, which were commonly regulated upon sustained cold-exposure in AT-MEC of the three different adipose tissues. Upward pointing arrows indicate upregulation of a certain number of genes and similarly downwards pointing arrows indicate downregulation.

Table 22 List of differentially regulated genes, which were commonly regulated upon sustained cold-exposure in AT-MEC of the three different adipose tissues

Upon 4°C sust. cold:	**BAT ∩ WATi**	**WATi ∩ WATg**	**WATg ∩ BAT**	**BAT ∩ WATi ∩ WATg**
Up-regulated↑	Tbx3	Scd1	Cdh13	Ccnd1
	Mki67	ND1		Slc6a6
	Tcim			Top2a
	Ak1			
Down-regulated↓	Sncg	Hp	Myh11	
	Cfd	Ifi27l2a		

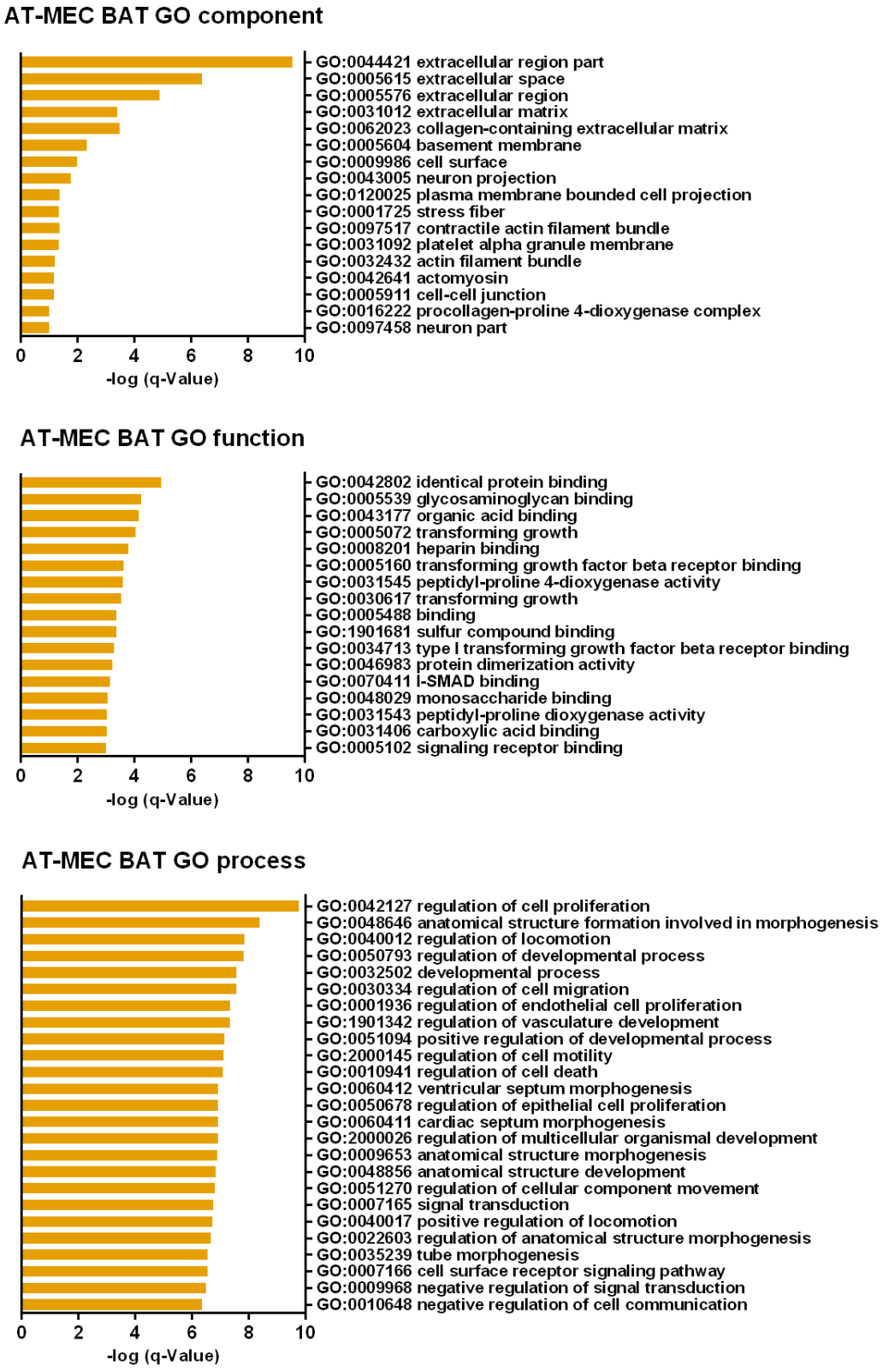

Figure 40 Gene Ontology analysis of the AT-MEC BAT sustained cold-exposure dataset.

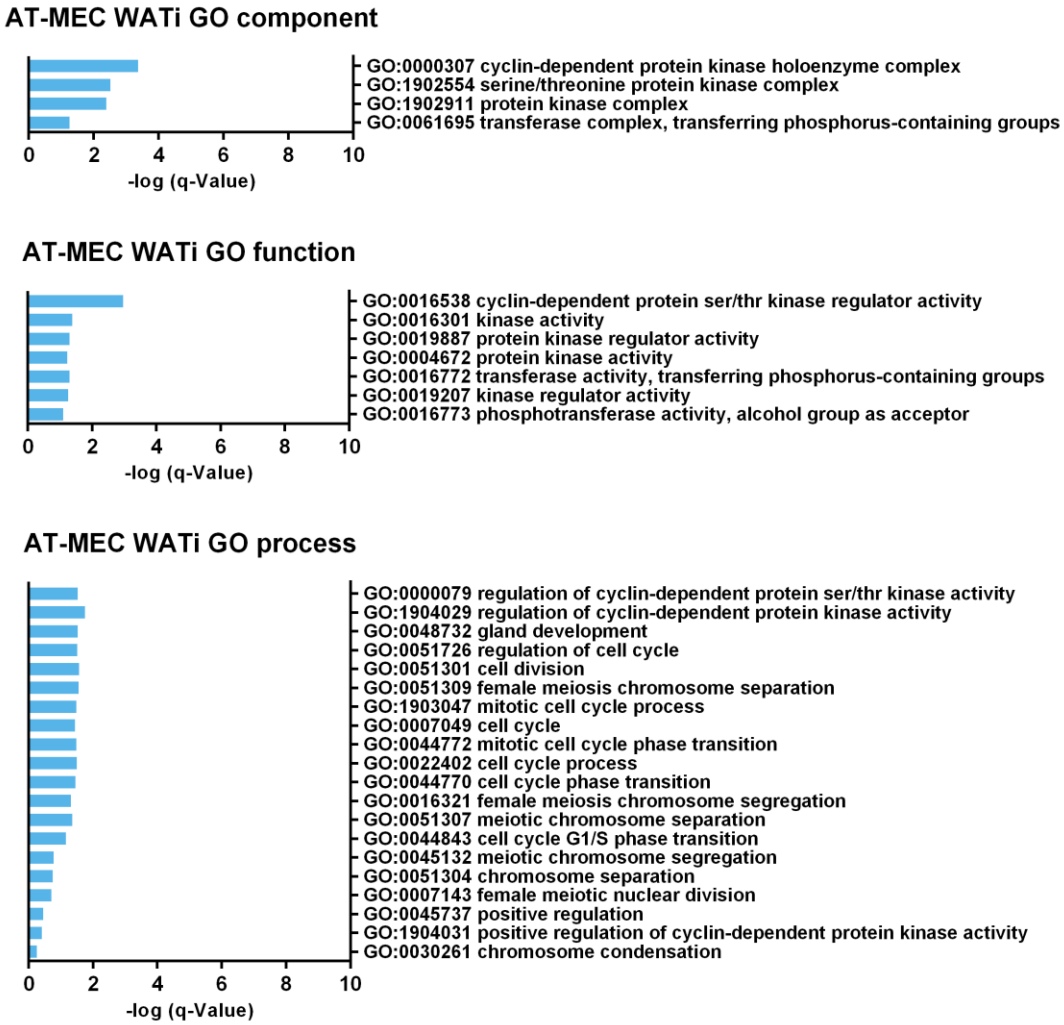

Figure 41 Gene Ontology analysis of the AT-MEC WATi sustained cold-exposure dataset.

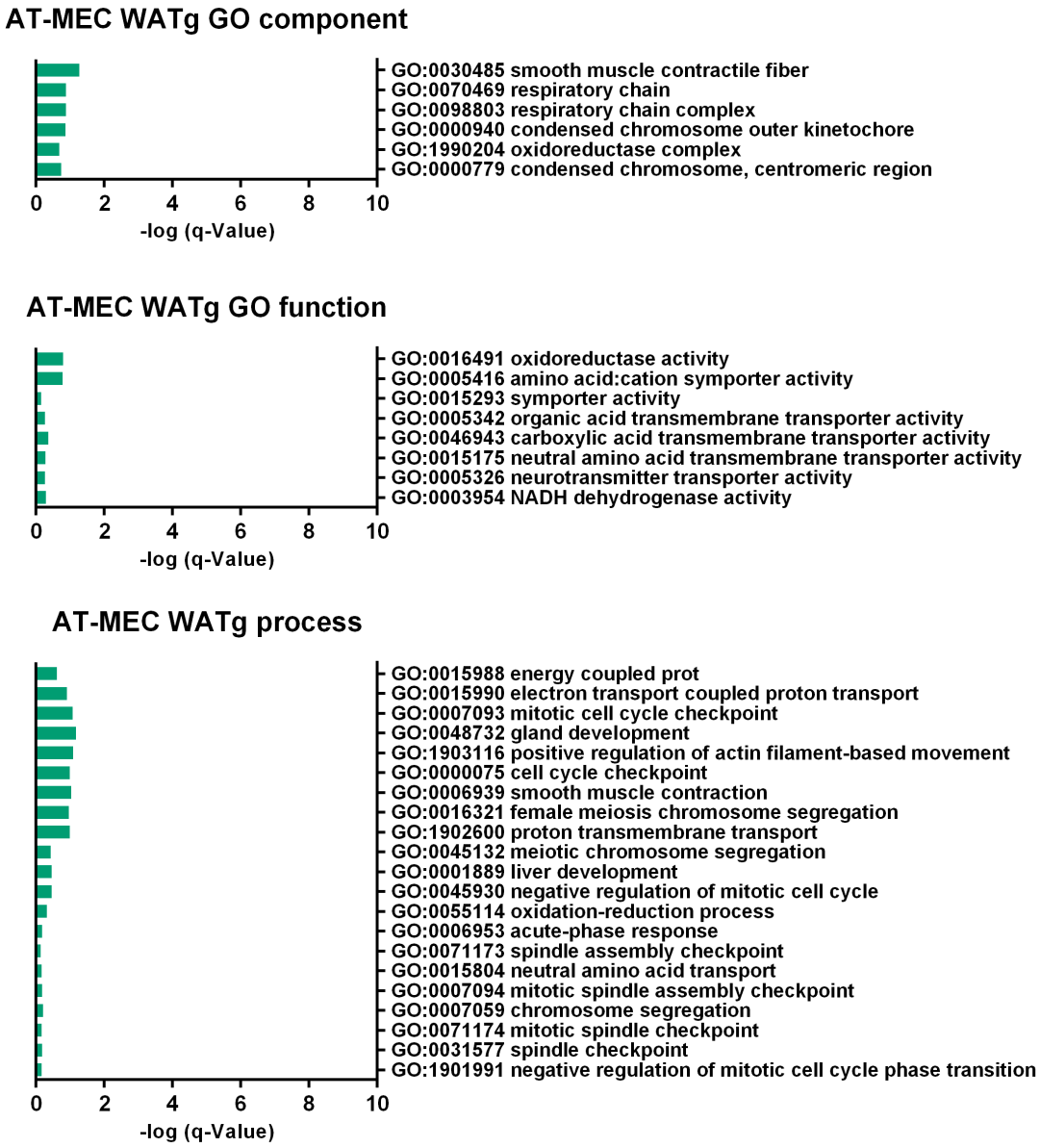

Figure 42 Gene Ontology analysis of the AT-MEC WATg sustained cold-exposure dataset.